3-11-2011

Background and Source Term Identification in Active Neutron Interrogation Methods

David A. Anthony

BACKGROUND AND SOURCE TERM IDENTIFICATION IN ACTIVE NEUTRON INTERROGATION METHODS

THESIS

David A. Anthony, Major, USA

AFIT/GNE/ENP/11-M01

DEPARTMENT OF THE AIR FORCE
AIR UNIVERSITY

AIR FORCE INSTITUTE OF TECHNOLOGY

Wright-Patterson Air Force Base, Ohio

AFIT/GNE/ENP/11-M01

BACKGROUND AND SOURCE TERM IDENTIFICATION IN ACTIVE NEUTRON INTERROGATION METHODS

THESIS

Presented to the Faculty

Department of Engineering Physics

Graduate School of Engineering and Management

Air Force Institute of Technology

Air University

Air Education and Training Command

In Partial Fulfillment of the Requirements for the

Degree of Master of Science in Nuclear Engineering

David A. Anthony, BS

Major, USA

March 2011

AFIT/GNE/ENP/11-M01

BACKGROUND AND SOURCE TERM IDENTIFICATION IN ACTIVE NEUTRON INTERROGATION METHODS

David A. Anthony, BS

Major, USA

Approved:

//SIGNED//	
Maj Benjamin R. Kowash (Chairman)	Date
//SIGNED//	
LTC John W. McClory (Member)	Date
//SIGNED//	
James C. Petrosky, PhD (Member)	Date

Abstract

The detection and tracking of special nuclear material (SNM) is vitally important in order to know where these materials are and prevent them from being used in a harmful manner. Active neutron interrogation is a sought after method for this since the resulting high energy gamma rays produced by inelastic scattering and neutron capture reactions can pass through denser shielding than natural decay gammas, and their energy spectra are unique to each isotope. Using Monte Carlo N Particle (MCNP) simulations, this research investigated the characterization of gamma ray sources created by active neutron interrogation. Ring detector and mesh tallies within MCNP provide the energy and spatial distributions of gamma rays and neutrons associated with the induced background produced by a 14 MeV D-T neutron generator operated for 10 seconds at the Defense Threat Reduction Agency (DTRA) Technical Evaluation Assessment Monitor Site (TEAMS) at Kirtland AFB, NM. Iron (Fe-56), lead (Pb-207), polyethylene (C_2H_4 —> C-12 & H-1), and uranium (U-235 and U-238) were simulated as the target isotopes. Analysis of their corresponding neutron and gamma ray energy spectra provide the target source term. The resulting signal-to-noise ratios for each target demonstrated that while 6,859 cm^3 of Fe-56, H-1, and C-12 were distinguishable from the neutron induced background radiation, the same size of Pb-207 and U-238 and 1.5 kg of U-235 were not. Therefore, a reduction in the induced background radiation is necessary to accurately identify materials at these sizes or smaller, based upon the simulation.

Acknowledgments

I would like to express the sincere appreciation to the faculty advisor, Maj Benjamin Kowash, for his guidance and support throughout the course of this thesis effort. His insight and experience was certainly appreciated. I am also indebted to the following individuals who spent their valuable time explaining the processes and procedures in accessing the Monte Carlo N Particle (MCNP) program via the AFIT Macintosh and cluster computer systems: Dr. Abigail Bickley and 2dLt James Bevins. Special thanks go to my wife for her emotional support during the time spent away from our family completing this project.

David A. Anthony

Table of Contents

Page

List of Figures

Figure Page

Figure Page

List of Tables

BACKGROUND AND SOURCE TERM IDENTIFICATION IN

ACTIVE NEUTRON INTERROGATION METHODS

I. Introduction

General Issue

The importance of controlling special nuclear material (SNM) for both military and peaceful use is recognized by several international treaties. Governments are responsible for protecting against the illegal and harmful uses of SNM as well as overseeing its peaceful, legal use. The need for quick and effective methods of detecting SNM in order to monitor SNM, however, continues to remain an area of intense research. Current passive and low-level gamma detectors work well for finding unshielded sources, but the spatial and energy resolution remains poor. They will neither detect shielded SNM nor provide the spatial resolution needed for determining directionality, especially if the source or detector is moving during the scan. Active neutron interrogation provides the benefit of creating a unique gamma ray spectrum, with the proper detection equipment, that allows for sufficient fidelity for accurately finding SNM within very thick shielding, and can further provide the material location. .

This research project provides an understanding of the induced background and target source terms associated with active neutron interrogation at the TEAMS site. The intent is that effective new detector systems cannot be created and tested unless the environment is accurately modeled. The University of Cincinnati (UC) and Air Force

Institute of Technology have initiated collaborative research to investigate new detector designs that will support active interrogation. They plan to use the active neutron interrogation site at the Defense Threat Reduction Agency (DTRA) Technical Evaluation Assessment Monitor Site (TEAMS) for testing and validation. Before the site is used, the primary source term needs to be modeled as accurately as possible in order to determine the ideal signal-to-noise ratio when considering the expected target source and induced background; target (Fe-56, Pb-207, polyethylene, U-235, or U-238) and earth, road, table, etc.), The isotopes of uranium (U-235 and U-238) were the only SNM isotopes studied in this research. However, analysis of their gamma ray spectra provides insight into identification of SNM using the TEAM site configuration. The use of non-SNM targets (Fe-56, Pb-207, and polyethylene) provides a comparison of gamma ray spectra from SNM, allowing for the determination of efficacy for the TEAMS active neutron interrogation technique in active interrogation. The ambient background (cosmic, natural radiation, etc.) was not simulated.

Figure 1 shows the layout of the DTRA TEAMS active neutron interrogation site. The primary gamma source terms are labeled. For the simulations in this research, the high energy isotropic neutron source (10^8 neutrons/second) was turned on for 10 seconds. During the simulation, most neutrons interact with the on-site materials (earth, concrete road, steel pipe, etc.) and not the target. These interactions (inelastic scattering and neutron capture) provide the gamma rays for the background source terms. Gamma rays created by neutron interactions in the target are the target source term. Interactions take place elsewhere, however, it is the energy spectrum of the gamma rays in the induced

background that dominates, and target source gamma rays that provide the spectrum for identification.

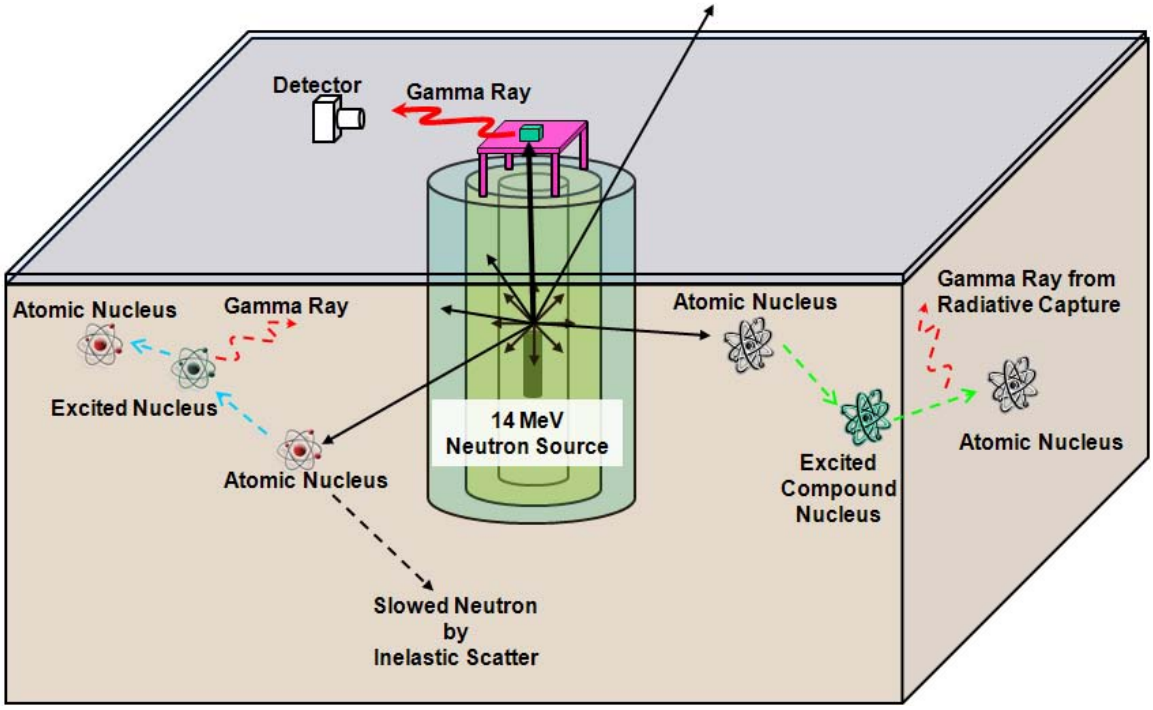

Figure 1. Graphical representation of the TEAMS active interrogation site. An isotropic neutron source emits high-energy neutrons which interact with the surrounding non-target materials: air in center hole, steel pipe, concrete pipe, earth, concrete road, steel table, and aluminum box. The target fills the aluminum box. Inelastic scattering reactions create gamma rays and slow the incident neutrons. Radiative capture removes the incident neutron from the system and creates gamma rays as the compound nucleus de-excites. All gamma rays created within non-target isotopes were considered part of the induced background source term.

Problem Statement

This research investigates the ability to identify materials at the DTRA TEAMS active interrogation site. The modeled gamma rays spectra produced by the inelastic scattering and capture of neutrons at the site were compared to the gamma ray spectrum from the target during a simulated 10s neutron pulse in order to determine if target could

be identified. The low threshold detectable level for the target source term was determined.

Methodology

This research investigated the following hypothesis statement. Based upon an idealized MCNP simulation of the DTRA TEAMS active neutron interrogation system (a 14 MeV isotropic neutron source operating at 10^8 neutrons/s for 10 seconds), a 1.5 kg U-235 sample can be identified using a simulated 10 second neutron pulse, given the added spectrum resulting from neutron interactions in the background material. There are three necessary inputs required to test this hypothesis.

1. The induced background gamma ray source terms produced by inelastic and capture neutrons in the environment surrounding the active interrogation system at the DTRA TEAMS. This provides the quantitative induced background value inherent in the system. The induced background must be known first in order to accurately account for the target source spectrum. The induced background source term was calculated using air as the target.
2. The target source gamma ray spectra for each isotope. This was accomplished in two steps. Initially, a simple model consisting of a neutron source and a target isotope inside a vacuum was simulated in order to provide pure signal gamma ray spectra. These spectra are the ideal target source term absent a background source. Using these spectra as a benchmark, each target isotope was compared to it in simulation of the DTRA TEAMS site.

3. The threshold target source term capable of being detected without the need for detector shielding when using a 14 MeV isotropic neutron source operating at 10^8 neutrons/s for 10 seconds at the DTRA TEAM site. This primarily provides the signal-to-noise ratio (SNR) required for identification.

II. Literature Review

Chapter Overview

This chapter presents a review of the relevant theory pertaining to this thesis. Of specific interest is the creation of gamma rays from inelastic scattering and neutron capture within various materials. Neutron induced fission (while not the focus of this research) is reviewed since fissioning creates a significant low energy gamma ray spectrum. Basic information on the MCNP program utilized to obtain the results is also covered. The expected gamma ray energy spectra from neutron interactions are provided for the targets (Fe-56, Pb-207, polyethylene, U-235, and U-238) as a baseline of comparison for analysis of the simulation results.

Theory

Neutron Interactions

Neutrons primarily react with atomic nuclei. As a neutron interacts with the atomic nucleus, it undergoes many complex reactions. The cross section represents the interaction probability. Because the cross section is element and isotope dependent, theoretical methods are used to predict cross sections and provide empirical information. (Shultis, 2000, 49-50)

For the purposes of this research, the evaluated nuclear data files (ENDF) was used. This database is extensive and there are continuous efforts to fill regions (e.g. resonances) where the data is unreliable. As an example, the results are not reliable at neutron energy range near a relatively large cross section. (Shultis, 2000, 50)

Only three neutron interactions are considered in this research: inelastic scattering, capture, and fission. Neutron interactions are categorized by energy. For neutron energies > 20 MeV, the ultra-high-energy range, secondary particles are created. This is, however, higher than the 14 MeV D-T neutrons created at the DTRA TEAMS site. Neutron interactions below 1 eV (the low-energy to thermal region) can be complicated due to Bragg scattering from the crystal plane and coherent scattering from molecules, but these are not important to active neutron interrogation. The remaining high energy region (1 eV < E < 20 MeV) supports the neutron inelastic scattering, capture, and fission, which is of interest in this research. (Shultis, 2000, 50)

In the high energy region, the most important reaction for neutrons is that of scattering. Elastic scattering is present for all atoms. When the neutron energy is higher than the atomic nucleus' first excited state energy level, inelastic scattering becomes possible and induces the reactions needed for neutron active interrogation. If the neutron energy is above 8 MeV, multiple-particle reactions such as (n, 2n) and (n, n+p) is also possible. Fortunately for these reactions the cross sections are significantly smaller than that of inelastic scattering.

Elastic scattering is always much more probable than inelastic scattering. Elastic scattering (n, n) is the process whereby an incident neutron interacts with but does not excite an atomic nucleus. This reaction does not decrease the energy of the incident neutron.

Inelastic scattering (n, n'), despite its lower probability, becomes the primary means of slowing fast neutrons with energies greater than the threshold energy, E_T. This is related to the atomic mass as

$$E_T = -\frac{A+1}{A}Q\,, \tag{1.1}$$

where A is the atomic mass of the isotope and Q is the value of the reaction equal to

$$Q = \Delta M_o c^2 - W\,, \tag{1.2}$$

where ΔM_o is the change in mass of the neutron and atomic nucleus during the reaction, c is the speed of light, and W is the sum of the nuclear excitation energies in the reaction. In scattering reactions, the neutron and atomic nucleus do not change their mass. Therefore Q is equal to the excitation energy of the final state of the atomic nucleus with respect to the ground state. For elastic scattering, Q is thus zero. With inelastic scattering, some of the kinetic energy of the neutron is transferred to the atomic nucleus in an endothermic reaction. Therefore, the Q value for the inelastic scattering is negative and equal the known excited state values. Table 1 lists the first two excited states and associated threshold energies for the isotopes Fe-56, Pb-207, H-1, C-12, U-235, & U-238 used in this research. (Shultis, 2000, 32-57) The total, elastic, 1st excited state, and 2nd excited state cross sections of these isotopes for energies above 0.1 MeV are shown in Figures 2 through 7.

In neutron capture (n, γ) the incident neutron is absorbed by the target nucleus, and the excess binding energy leaves the daughter nucleus in an excited state.

Within approximately one picosecond after interaction, the compound nucleus deexcites, possibly through several intermediate states, emitting a gamma ray. By way of example, consider the following nuclear reaction.

$$^{1}_{1}H + ^{1}_{0}n \rightarrow ^{2}_{1}H + \gamma + 2.22 \text{ MeV} \tag{1.3}$$

The capture cross section for high energy neutrons is small compared to the elastic scattering cross section,. (Shultis, 2000, 32-57)

H-1 does not have excited states, therefore, it cannot be excited by an inelastically scattered neutron. H-1 can capture a neutron, however, forming a compound nucleus which excites and de-excites creating a gamma ray. Since the binding energy of hydrogen is 2.23 MeV, a gamma ray of this energy is produced as the compound nucleus de-excites. (Caffrey, 1992, 1423)

Although inelastic scatter and neutron capture reactions are the focus of this research, induced fissioning is a possible outcome of active neutron interrogation. Fissioning is started by interaction between the Coulomb and nuclear forces inside of heavy nuclei (thorium and beyond). The total nuclear binding energy within a nucleus increases as the atomic mass of the nucleus increases. The Coulomb repulsion force increases approximately a power of two faster than the binding energy. Because of this, heavy nuclei can be considered to reside inside a potential well with the Coulomb barrier being the energy value at which the nucleus can overcome the binding nuclear forces. When an incident neutron is captured by a heavy nucleus a compound nucleus is formed, much like with radiative neutron capture. The difference with fission is that the added energy of the incident neutron causes the compound nucleus to penetrate the Coulomb barrier. Once the Coulomb repulsion force dominates, the nucleus splits into two to three fission fragments, some of which are neutrons. (Krane, 1988, 478-479) The importance of this is the creation of additional neutrons must be accounted for when isotopes of uranium are the target.

Table 1. Energies of the first and second excited states for select isotopes and their associated inelastic scattering threshold energies, E_T.

Isotope	Excited State [MeV]	E_T [MeV]
Fe-56	1st: 0.847	0.862
	2nd: 2.085	2.122
Pb-207	1st: 0.570	0.573
	2nd: 0.898	0.902
C-12	1st: 4.439	4.809
	2nd: 7.654	8.292
U-235	1st: 7.5×10^{-5}	7.53×10^{-5}
	2nd: 0.013	0.013
U-238	1st: 0.045	0.04519
	2nd: 0.148	0.149

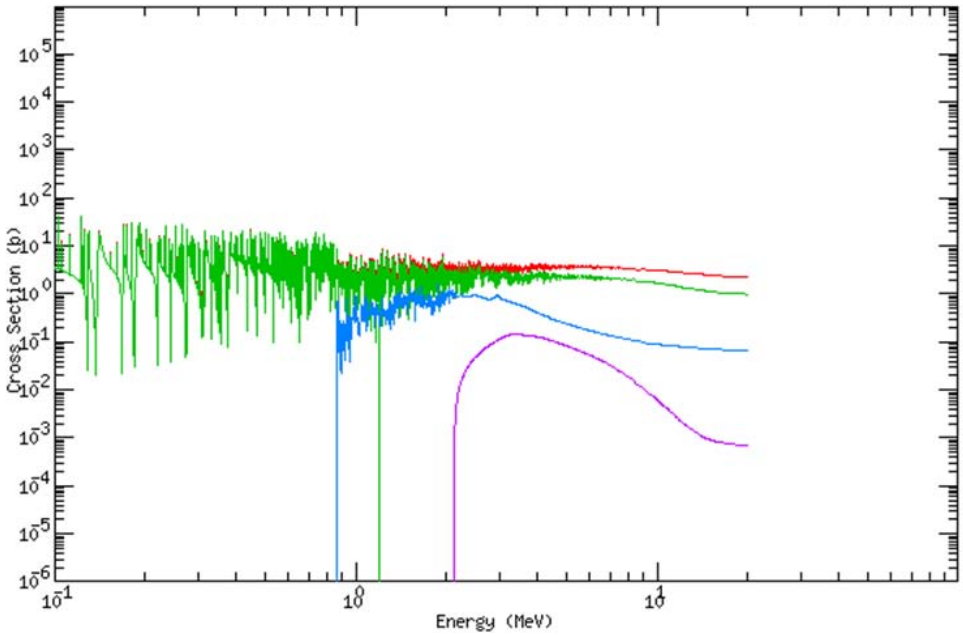

Figure 2. ENDF plot of Fe-56 cross sections between 0.1 and 20 MeV. They are identified by color: total (red), elastic (green), 1st excited state (blue)and 2nd excited state (purple). (Chang, 2000)

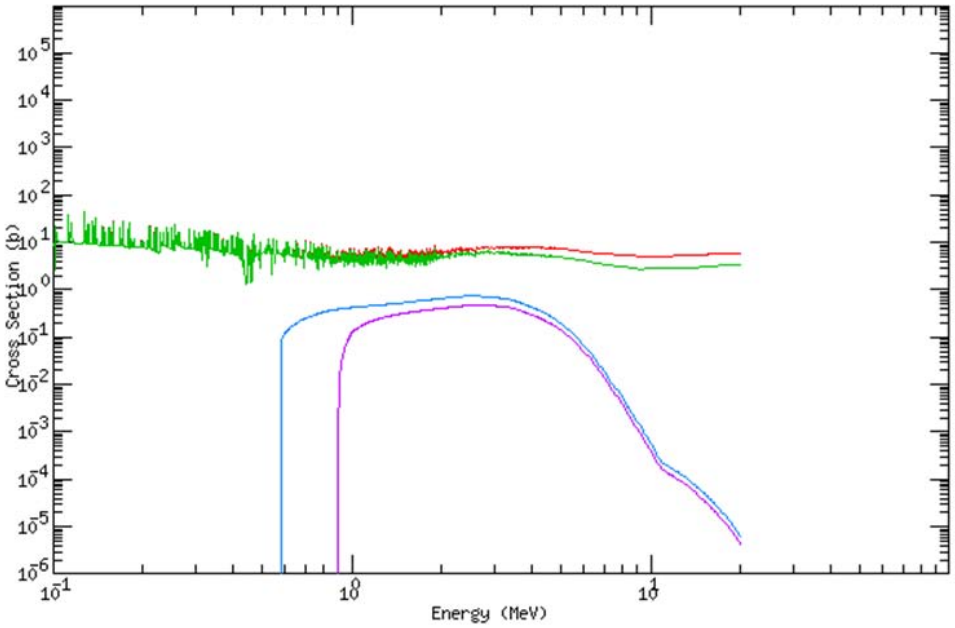

Figure 3. ENDF plot of Pb-207 cross sections between 0.1 and 20 MeV. They are identified by color: total(red), elastic (green), 1st excited state (blue)and 2nd excited state (purple). (Chang, 2000)

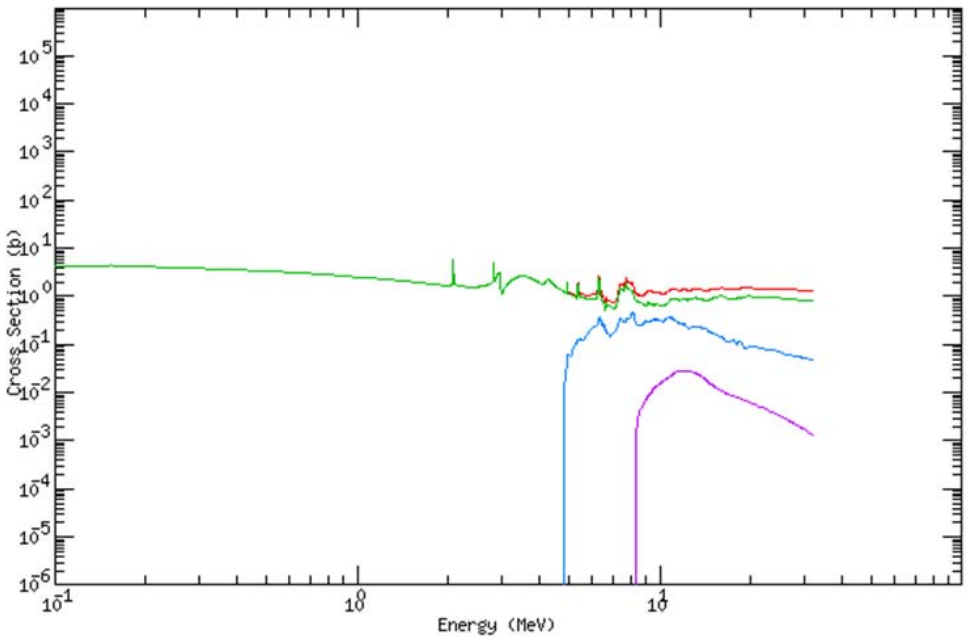

Figure 4. ENDF plot of C-12 cross sections between 0.1 and 20 MeV. They are identified by color: total(red), elastic (green), 1st excited state (blue)and 2nd excited state (purple). (Chang, 2000)

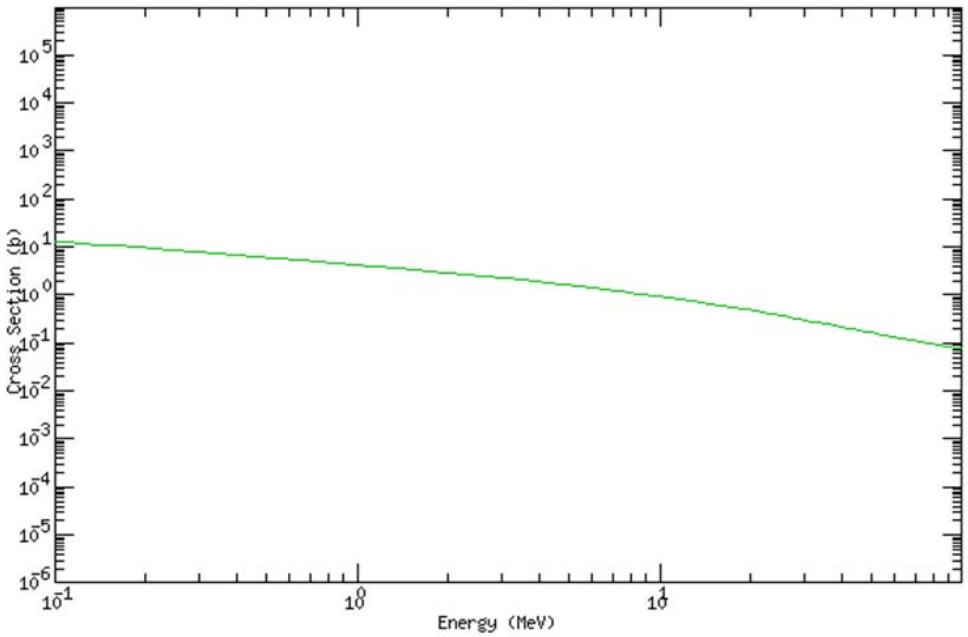

Figure 5. ENDF plot of H-1 cross sections between 0.1 and 100 MeV. They are identified by color: total (red) does not appear separate in this energy range as it is too close to the elastic (green) cross section for fidelity at this scale. (Chang, 2000)

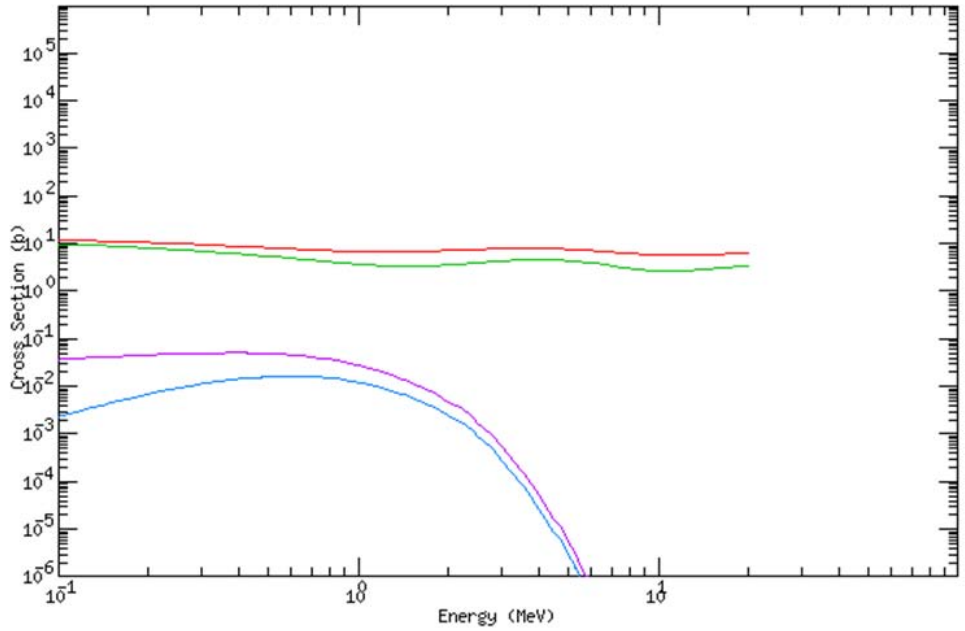

Figure 6. ENDF plot of U-235 cross sections between 0.1 and 20 MeV. They are identified by color: total(red), elastic (green), 1st excited state (blue)and 2nd excited state (purple). (Chang, 2000)

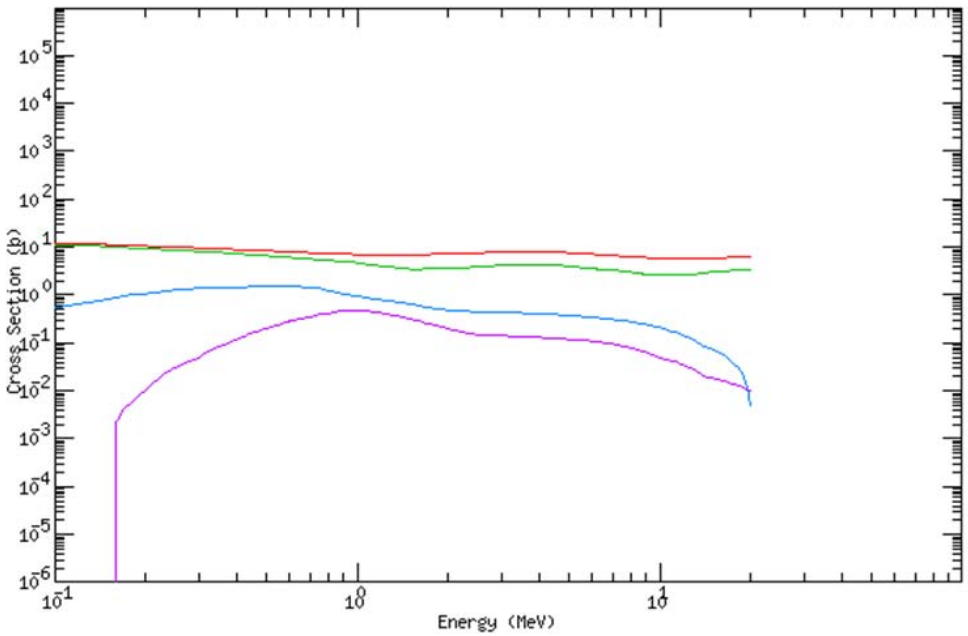

Figure 7. ENDF plot of U-238 cross sections between 0.1 and 20 MeV. They are identified by color: total(red), elastic (green), 1st excited state (blue)and 2nd excited state (purple). (Chang, 2000)

As shown in Table 1, U-235 and U-238 have much lower excited state cross sections than many isotopes with lower atomic numbers. This is due the characteristic of SNM isotopes to fission at low neutron energy. While all isotopes can fission with neutrons of high enough energy, SNM isotopes fission with thermal neutrons. The excitation/de-excitation of the compound nucleus results in fissioning of SNM. These fission events create neutrons which can further interact with atomic nuclei, changing the overall gamma spectrum. Since the probability of a fission event increases as the neutron energy decreases, any inelastic scattering or radiative capture peaks are hidden behind the fission spectra below neutron energies of approximately 2 MeV. As such, SNM isotope gamma ray spectra do not have discrete gamma ray peaks like the isotopes Fe-56, Pb-207, H-1, and C-12. Rather, SNM isotopes have continuous spectra with other unique

features. In the low MeV neutron energy range, the increased numbers of neutrons from scattering, fissioning, and capture interact such that strong, broad spectra of gamma rays are created. Table 2 provides NNDC data on peak gamma ray energies for the target isotopes in this research, except H-1.

Table 2. Peak gamma ray energies in MeV for select nuclides
The energies listed correspond to inelastic scattering and neutron capture. (NNDC, 2010)

Nuclide	Gamma Ray Energy [MeV]
Fe-56	0.846771, 1.238282, 1.810772, 2.113123, 2.52288, 2.95977, 3.5542
Pb-207	0.569702, 0.89778, 1.770237, 2.0537, 2.0927
C-12 (in Polyethylene)	4.43803
U-235	0.564007, 0.61163, 0.6404, 0.74797, 0.76987,0.7794, 0.8059, many more til 1.1422
U-238	0.58355, 0.63519, 0.68699, 0.81806, 0.8494, 0.88546, 0.9055, 1.015, 1.2233

An example of this difference between SNM and non-SNM is the work done by Gozani on non-conventional nuclear signatures. In 2009, Gozani conducted MCNP simulations using targets of iron, lead, C-12 in polyethylene (C_2H_4), U-235, & U-238 in his active neutron interrogation research. A pulsed beam of 8.5 MeV neutrons interrogated various cargo containers, and he determined that SNM could be detected. Gozani's initial MCNP results are provided in Figure 8.

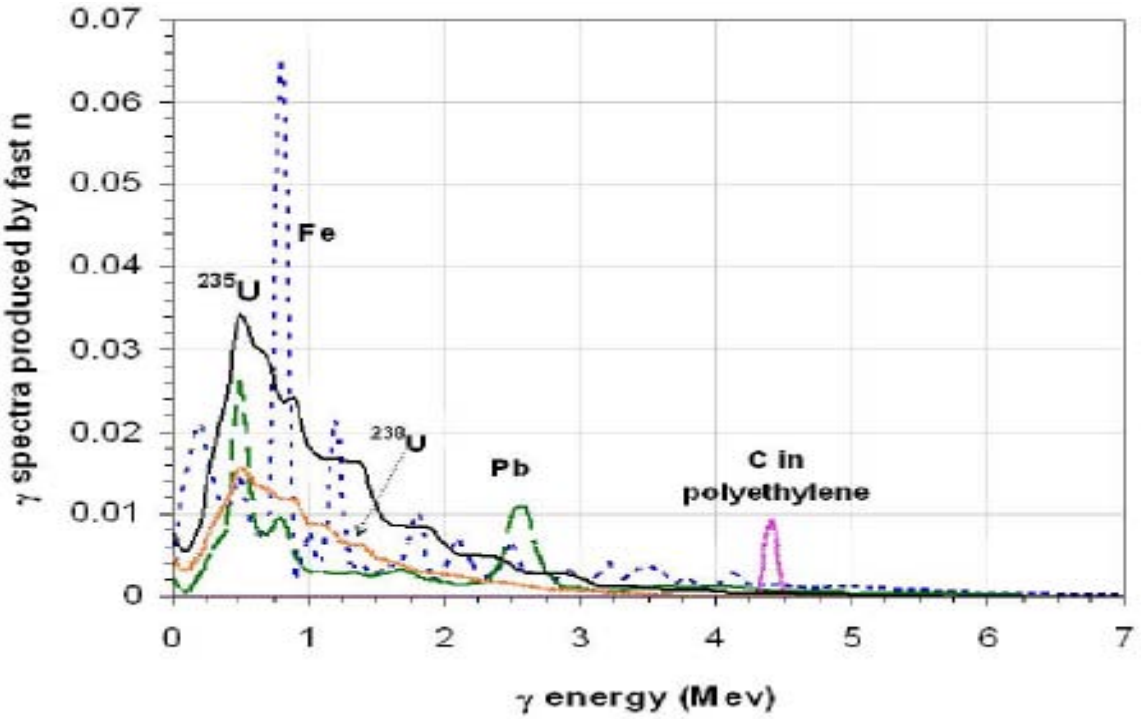

Figure 8. MCNP simulations of gamma production spectra by 8.5 MeV neutrons in 10 cm thick C-12, Fe-56, Pb-207, U-238, and 1 cm thick 235U. (Gozani, 2009, 600).

By further analyzing the simulation results, Gozani determined that SNM isotopes produce gamma ray spectra with characteristically sharper high energy slopes than other isotopes. It is this steep slope, which is used in identifying SNM. Figure 9 provides Gozani's results demonstrating this. His analysis shows that the increased fission cross section and multiplication accounts for an increase in the discrimination ratio of approximately 20% when the 10 cm thick U-238 was replaced by the 1 cm thick U-235. (Gozani, 2009, 600)

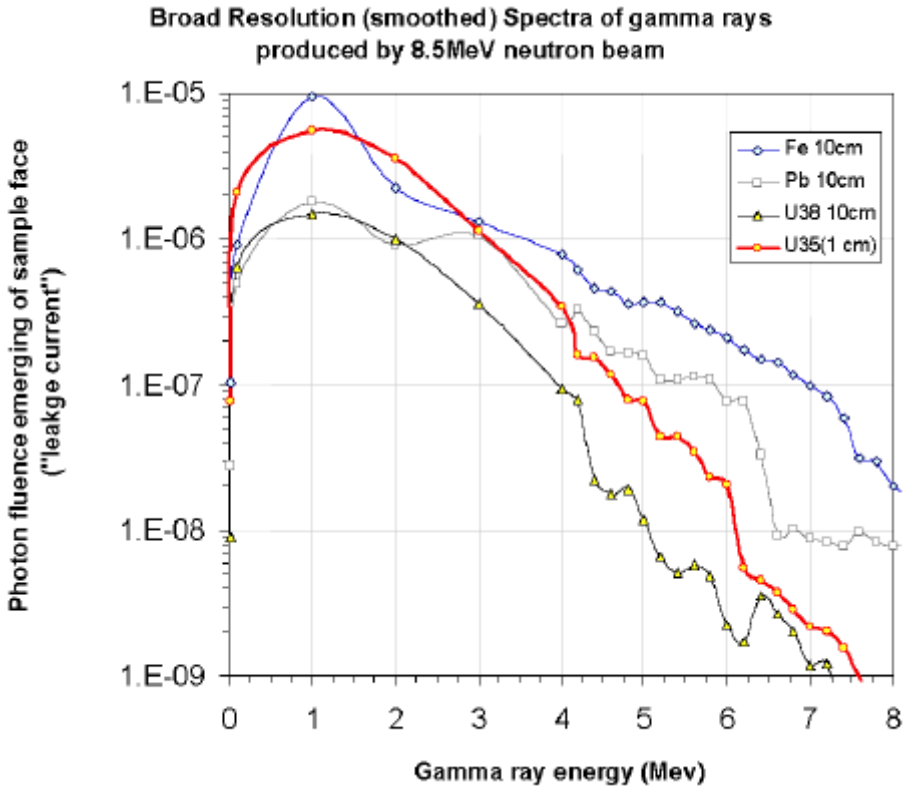

Figure 9. Gamma ray spectra produced by 8.5 MeV neutron interactions. (Gozani, 2009, 601)

Active interrogation using high energy neutrons has proven effective for years. In 1992, scientists at the Idaho National Engineering Laboratory (INL) used a high-purity germanium (HPGe) detector to distinguish between high explosive (HE) compounds and chemical agents. Figure 10 provides the resulting gamma-ray spectra for mustard gas (a chemical agent) and one type of HE from a 155 mm artillery shell. The spectra clearly represent distinct peaks at the expected excitation energies for each of the isotopes present. (Caffrey, 1992, 1425)

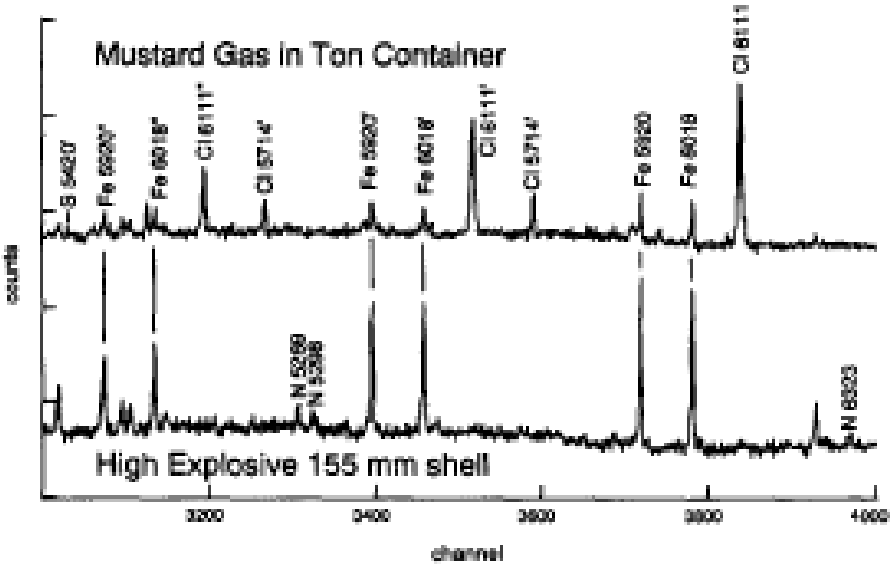

Figure 10. Comparison of HD and HE gamma-ray spectra. (Caffrey, 1992, 1425)

Another example is experimental work done by Gozani et al. in 1992 during the development of a new gamma ray detector. Carbon, oxygen, and nitrogen were the targets and the resulting spectra are provided in Figure 11. Like the work done at INL, plotting gamma ray events versus the channel number clearly showed that the high energy neutrons created distinct gamma rays via neutron capture and inelastic scattering, making it a viable method to identify the isotopes present in a target. The ability to distinguish between various materials is an advantage of the active neutron interrogation technique.

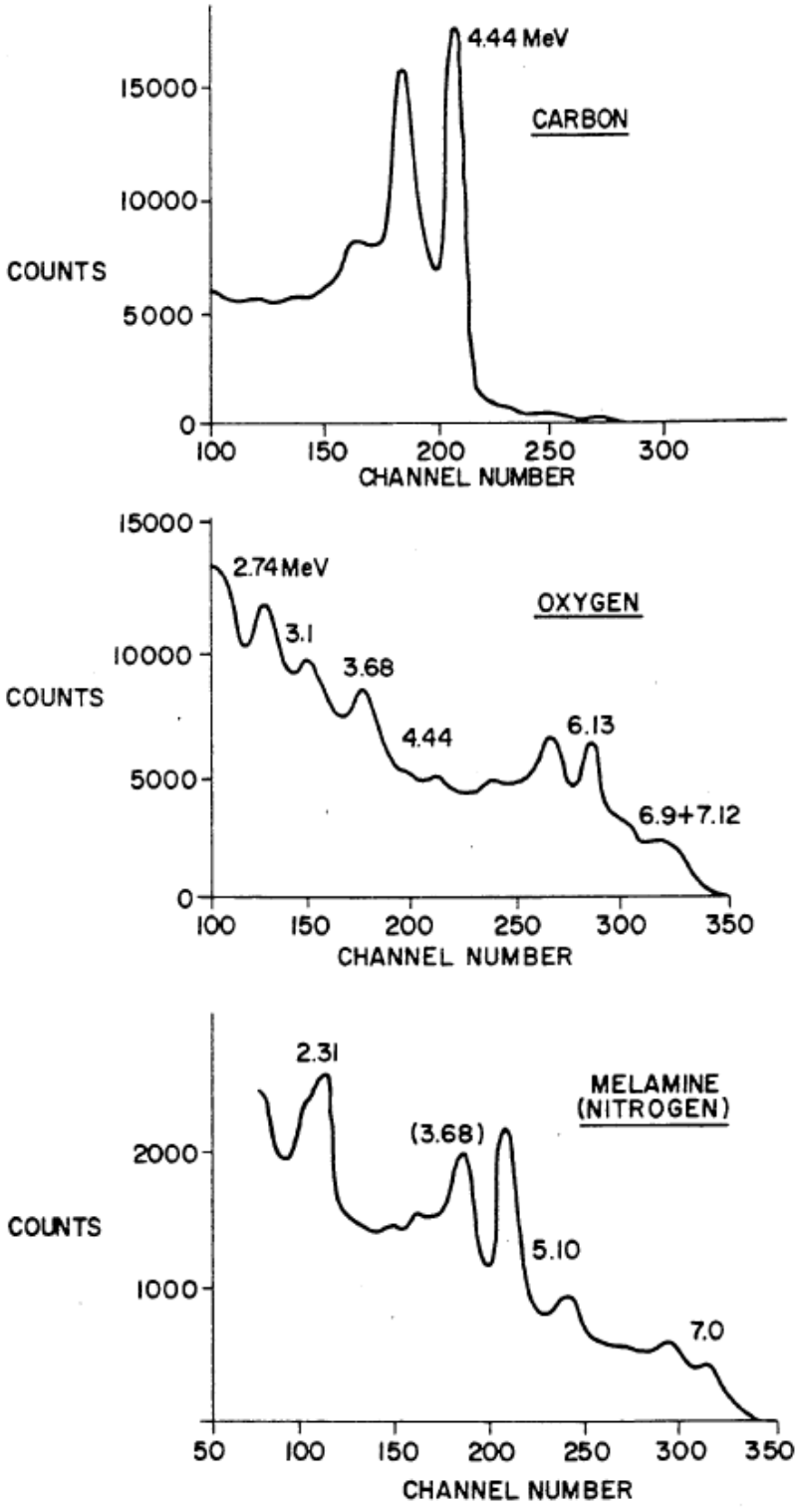

Figure 11. C, O, & N gamma-ray spectra from Gozani et al. work.

Background Sources

For this research, the background source term should not be confused with the ambient background associated with cosmic radiation and the natural decay radioactivity. (Knoll, 2010, 779) The ambient background was not included because it unnecessarily increased computational time and is not expected to dominate. The induced background source term refers to the gamma rays created from neutrons from the TEAMS Site neutron source not interacting with the target. This induced background source term then functions as the induced background in the system when the targets are introduced. As a baseline, the air, earth, steel pipe, concrete pipe, road, steel table, and aluminum box included as part of the environment, and thus induced background source terms. Any neutron scattering and gamma ray creation and/or scattering within these materials was recognized as induced background for the purposes of the research. In this manner, the resulting contribution from each target was separated for analysis and possible use in future MCNP simulations and/or research.

MCNP Functionality

Monte Carlo N Particle (MCNP) is a Monte Carlo transport code that calculates reactions for each particle based upon the corresponding cross section library information. For this research, three specific MCNP tally types were utilized. The surface current tally (f1 – MCNP) calculates the number of particles, represented by the Monte Carlo weight, crossing a surface and provides the resulting data in specified energy bins. Particles are recorded by crossing the surface without concern for direction, therefore a purely outward moving count is not possible with this tally unless the

environment is simulated to prevent backward scattering. (X-5 Monte Carlo Team, 2005, 2-84)

The mesh tally (mesh – MCNP) calculates geometric fluxes using particle track lengths. As the simulation is conducted, MCNP creates a separate output file dedicated to the mesh tally results by providing the flux for each cell. Unlike other tallies within MCNP, the mesh tally only provides the relative error for each result. (X-5 Monte Carlo Team, 2005, 2-83)

In this research, the mesh tally flux results are used to calculate the effective dose, assuming uniform whole body frontal exposure. The frontal exposure position was chosen since it provides the highest effective dose value. The effective dose, H_E, is calculated as

$$H_E = h_E \Phi , \qquad (1.4)$$

where Φ is the fluence in neutrons per cm^2, and h_E is the fluence-to-effective-dose conversion coefficient in Sieverts cm^2. The value for h_E increases with increasing neutron energy from ~10^{-11} at 10^{-2} MeV to ~4×10^{-10} at 10 MeV. (Knoll, 2010, 60) For this research, the highest value of 4×10^{-10} is used in the safety calculations to ensure a worst case scenario limit. In 2008, the International Commission on Radiological Protection (ICRP) reaffirmed its 1990 recommendation that the occupational yearly effective dose should be 5 mSv. (ICRP, 2008, 165) The fluence is calculated by multiplying the flux by the 10^9 neutrons produced by the 14 MeV 10^8 neutron/second neutron source operating for 10s.

The ring detector tally (f5 – MCNP) is a non-fixed point detector tally sampled at multiple locations on a ring. A point detector tally interprets every neutron or photon creation or collision as an event and then calculates the flux involved with that event as if the particle had moved directly to the point detector afterward. When conducting computations for problems that are symmetric about an axis, a ring detector can enhance the efficiency over a point detector tally. The DTRA TEAMS active neutron interrogation setup is an example of symmetry about the z axis. Ring detectors provide average fluences at each point along the ring, and this fluence is constant about the symmetrical axis. (X-5 Monte Carlo Team, 2005, 2-91 – 2-94)

Another reason to use a ring detector instead of a point detector is that ring detectors calculate mean values closer to the true mean for each history. Point detectors tend to group mean results inaccurately due to their inability to sample multiple paths from each event to the detector. Ring detectors are not limited to a single detector location, and calculate many paths from the event location to various points on the ring. In this manner, ring detectors can sample uniformly from all locations in the modeled geometry to provide more accurate fluence values. (X-5 Monte Carlo Team, 2005, 2-96)

All tallies calculated in MCNP are normalized per starting particle and provided with an estimated relative uncertainty, *R*, corresponding to one estimated standard deviation of the mean, S_χ, divided by the estimated mean, χ. *R* is calculated after each Monte Carlo history, resulting in various tally contributions per history. *R* is generally proportional to $-\sqrt{N}$, where *N* is the number of histories. In order to reduce *R by ½*, the total number of histories must increase fourfold.

Using *R*, conclusions can be made about the precision of the results from the confidence intervals about the estimated mean. According to the Central Limit Theorem, as *N* approaches infinity a 68% chance exists that the true result will be in the range $\chi(1 \pm R)$ and a 95% chance in the range $\chi(1 \pm 2R)$. These confidence statements can assist with precision estimates of the calculations and should not be considered the accuracy of the experimental results. Further analysis of all uncertainties (physical data, modeling, sampling techniques, approximations, etc.) is needed to correctly determine the accuracy of the tally results.

Table 3. Guidelines for Interpreting the Relative Error *R for Neutron Simulations (X-5 Monte Carlo Team, 2005, 1-7)**

Range of *R*	Quality of the Tally
0.5 to 1.0	Not meaningful
0.2 to 0.5	Unreliable
0.1 to 0.2	Questionable
< 0.10	Generally reliable
<0.05	Generally reliable for point detectors

***** $R = S_\chi / \chi$ **and represents the estimated relative error. These interpretations of *R* assume that all portions of the problem phase space are being sampled well by the Monte Carlo process.**

The guidelines for interpreting the quality of the confidence interval for various values of *R* are listed in Table 3. In accordance with the Table 3 footnote, care must be taken in designing a simulation in order to ensure proper sampling. One example is the non-sampling of a highly unlikely but important particle, resulting in incorrect tally results with poor confidence intervals. This situation is avoided by not excluding any phase space regions and attempting to sample all problem areas sufficiently. (X-5 Monte Carlo Team, 2005, 1-6 – 1-7)

In this research, sampling uniformly for positions on the ring detector tally determines the fluence at any point on the ring. (X-5 Monte Carlo Team, 2005, 2-94) This means that the probability of each neutron and gamma ray moving from its creation or interaction location to the ring detector without any interactions is calculated and then the mean value for all particles in each energy bin selected in the code is provided. This essentially gives the user a fluence at the location of the ring detector and is very useful when determining the amount of shielding needed for the scintillation detector to block unwanted signatures.

III. Methodology

Chapter Overview

The purpose of this chapter is to provide a detailed accounting of the process by which the research was conducted. First, the work of Gozani is replicated, with detailed steps in creating and running the MCNP code as a means to verify the usage of the program for this research. Next, the work in simulating a model of the neutron activation site at the DTRA TEAMS is discussed. Information regarding the decisions for each input value (cross sections, materials, configurations, tally requests, etc.) is provided.

Test Subjects

Gozani Comparison

Gozani's 2009 work regarding active neutron interrogation was replicated as closely as possible in order to better understand MCNP tallies and their output. It also provided valuable information used in analyzing the results of simulations of the DTRA TEAMS site. Appendix A provides the input MCNP codes and Figure 12 is a graphical representation of the system modeled. The system consists of an 8.5 MeV neutron source and a single target (Fe-56, Pb-207, polyethylene (C_2H_4), U-235, or U-238) during each simulation. In order to eliminate all other neutron and gamma ray sources, the neutron source term and target are placed within a spherical vacuum space 1000 cm in radius. The neutron beam source was coded as an isotropic point source with all of its emitted neutrons, then focused in a single direction (along the z axis from the origin of a Cartesian coordinate system). The target was positioned (arbitrarily) 100 cm away. A

surface current tally (f1 – MCNP) was simulated as a 500 cm radius sphere. 500 cm is halfway between the center of the coordinate system and the edge of the simulated universe. The surface current tally provided the current integrated over the tally surface, also referred to as the number of photons crossing the tally surface. Since the neutron source and target are within a vacuum, the only gamma rays recorded were those from the target source.

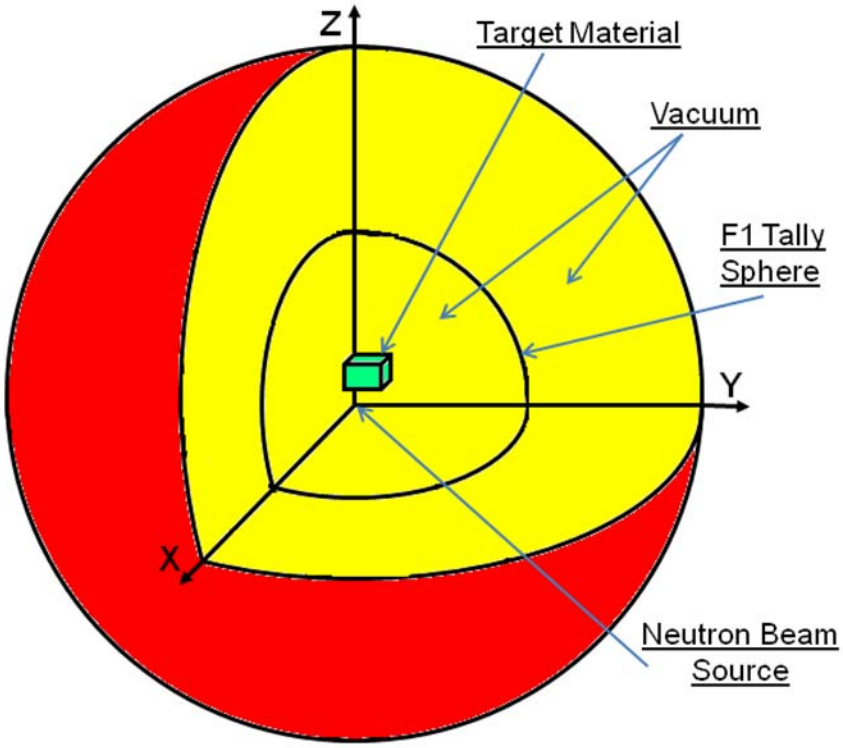

Figure 12. Representation of MCNP simulation layout for Gozani comparison.

Some minor assumptions about Gozani's work were required, due to a lack of modeling data. Gozani provided the thickness of the target (10 cm for the Fe-56, Pb-207,

H-1, C-12, and U-238 and 1 cm for the U-235) but not the size of the surface area perpendicular to the source beam. The decision to use a 10 x 10 cm front surface area for each target in the code was arbitrary since the modeled neutron source was anisotropic, toward the center of the target. Thus the surface area was important, and created a reasonable volume for interactions. Tally results for all energies from 0.05 to 5 MeV in increments of 0.05 MeV were simulated. This was due to the desire to have relatively small energy bins in order to observe as many of the gamma ray peaks as possible without significantly increasing the computational time of the simulations. 5 MeV was the upper energy limit since the neutron cross section above this energy is small. Each simulation started with 10^6 neutron source particles in order to ensure enough neutron interactions occurred to observe gamma ray peaks and not unduly increase simulation time. Not knowing the uranium enrichment modeled by Gozani, pure U-235 was used as a limiting case, even though 100% U-235 is not realistic. Gozani used a pulsed beam of neutrons with a width of one nanosecond, whereas this research assumed a continuous source beam. This was expected to have no effect on the results. Lastly, it was not clear which cross section library Gozani used for the MCNP simulations. Therefore, the default, non-user specified cross section tables from MCNP were used. This is addressed in the results section.

DTRA TEAM Site Modeling

The realistic active neutron interrogation site at DTRA TEAMS (see Figures 1, 13, and 14) was modeled using MCNP. Appendix B contains the MCNP inputs. The model primarily consists of a 12’ deep, 6” diameter hole into which a neutron generator is placed on a stand approximately halfway down the hole. Known physical properties of

the site include a 1” thick steel pipe surrounding the hole and 8” of Portland concrete surrounding the steel pipe. A concrete road covers the pipes and earth at the site. The depth of the road was estimated at 12” thick from online research of similar roads since the exact depth is not known. A steel table and aluminum box were added as a means to hold the target over the neutron source. Figure 15 provides a 2-D graphical representation of the MCNP simulation of the site. Figure 16 provides a 3-D image of the site coded in MCNP, displaying the materials and layout with the exception of the earth, air above earth, and road. A 14 MeV isotropic neutron point source, producing 10^8 neutrons/second, simulated the actual neutron generator 6’ down the hole.

Figure 13. Picture of the DTRA TEAMS active neutron interrogation location at Kirtland AFB, NM (Grumman, 2004). The neutron generator is positioned in the hole below the red arrow.

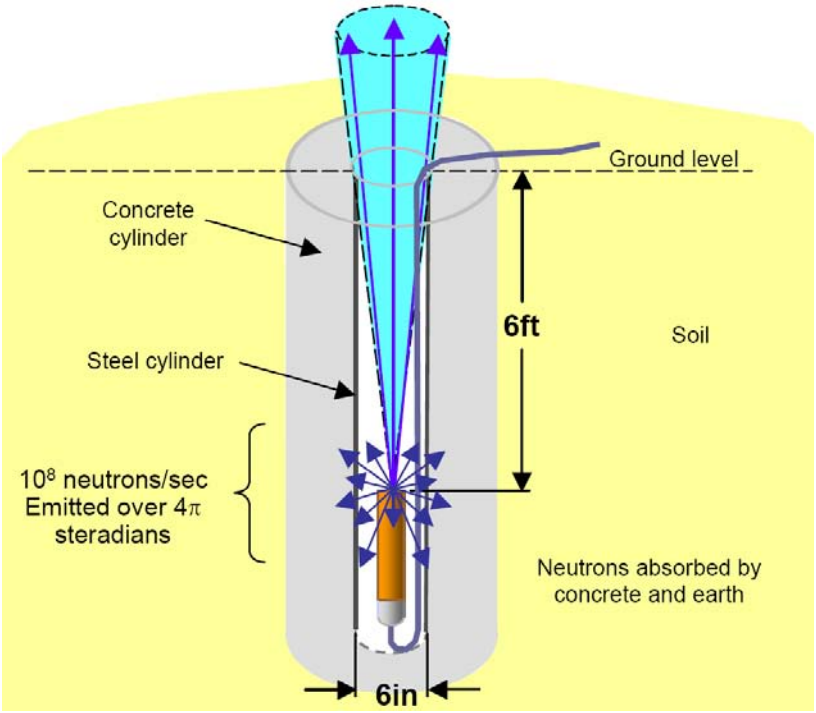

Figure 14. Graphical representation of the DTRA TEAMS neutron generator inside the earth (Grumman, 2004).

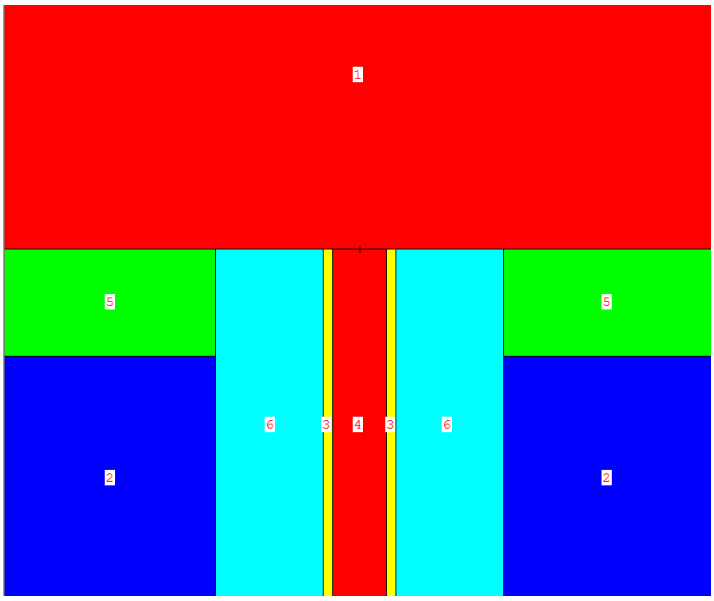

Figure 15. Representation of initial MCNP modeling of the DTRA TEAMS. This picture shows a zoomed in picture of the materials present on site prior to the addition of testing equipment. Red represents air, green represents ordinary concrete, dark blue represents earth/earth, light blue represents Portland concrete, and yellow represents steel.

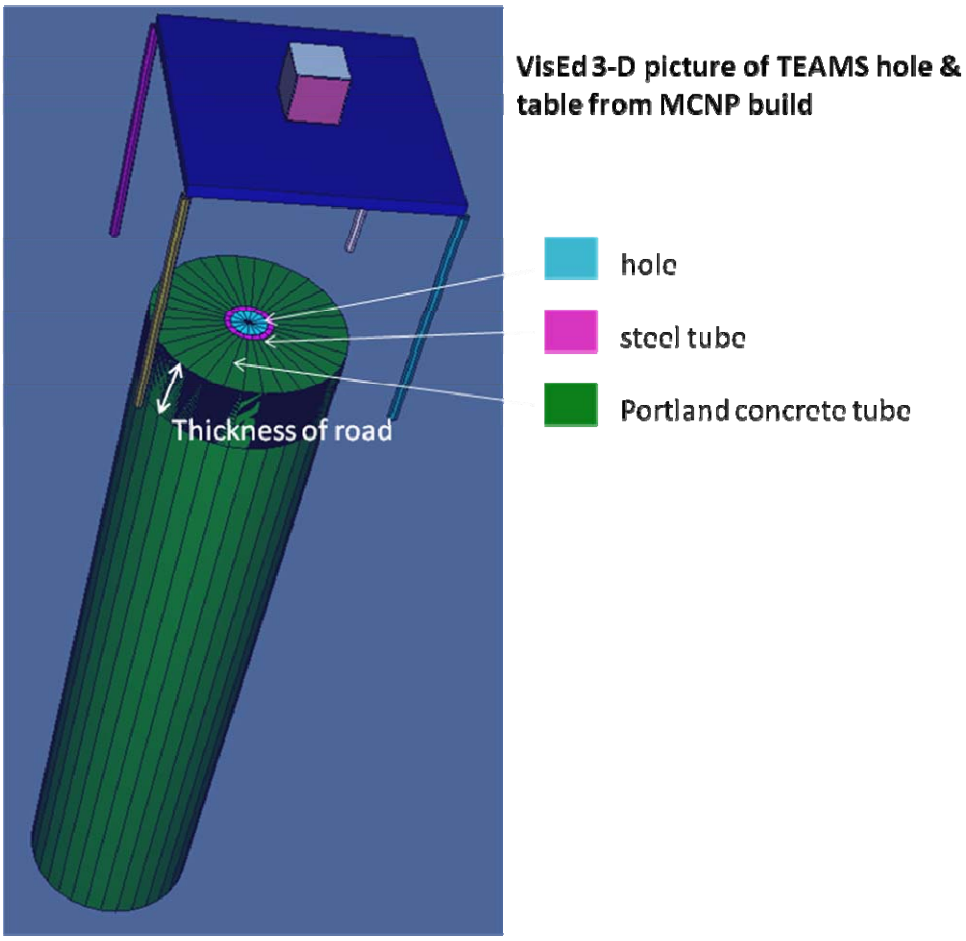

Figure 16. Representation of final MCNP modeling of the DTRA TEAMS. This picture shows a 3-D image of the materials present except for the earth, air above earth, and road. The material inside of the steel box is not shown and changes in accordance with the desired target.

When modeling the earth, the average chemical composition of the earth's continental crust was used (see Tables 5 and 6). (Wikipedia, 2010) These values were used as a reasonable estimate of the actual chemical composition at the DTRA TEAM site without the cost and time required to conduct soil sampling. Estimates of the average density for the upper crust range between 2.69 and 2.74 g/cm^3. The upper value was used as a worst case, since a denser material would create more neutron and photon interactions.

Table 4. Oxide Percent of Continental Crust
Provides information on the average compound structure of earth's crust for use in simulation modeling and analysis of induced background source terms during active neutron interrogation.

Oxide	Percent
SiO_2	60.6
Al_2O_3	15.9
CaO	6.4
MgO	4.7
Na_2O	3.1
Fe	6.7
K_2O	1.8
TiO_2	0.7
P_2O_5	0.1

Table 5. Chemical Properties of Continental Crust
Provides the average amount of each element present in the earth's crust for input into MCNP for use in modeling the DTRA TEAM Site.

Element	Chemical Symbol	Percentage of Total Elements
Oxygen	O	46.60%
Silicon	Si	27.72%
Aluminium	Al	8.13%
Iron	Fe	5.00%
Calcium	Ca	3.63%
Sodium	Na	2.83%
Potassium	K	2.59%
Magnesium	Mg	2.09%
Titanium	Ti	0.44%
Hydrogen	H	0.14%
Phosphorus	P	0.12%
Manganese	Mn	0.10%
Fluorine	F	0.08%
Carbon	C	0.03%
Sulfur	S	0.05%
Vanadium	V	0.01%
Chlorine	Cl	0.05%
Chromium	Cr	0.01%
Rubidium	Rb	0.03%
Copper	Cu	0.01%
Nitrogen	N	0.01%

The materials and dimensions of the table and box were arbitrarily assigned and should not significantly affect the relevancy of the results if other dimensions and/or materials are used. The steel table has four legs 100 cm long of radius 2 cm. The table top is 5 cm thick and is centered directly over the hole. For the targets other than U-235, the aluminum box has outside dimensions of 20 x 20 x 20 cm with 0.5 cm thick walls. For U-235, the box was reduced in size to limit the amount of fissile material and allow the MCNP software to run more efficiently. The box is filled with air initially for the induced background simulations and then one of the targets replaces the air for each simulation. Also, the box is a completely sealed container with no openings. The walls, top, and bottom have seamless connections. The railroad tracks shown in Figure 13 were not included in the model in order to maintain cylindrical symmetry in the simulation model. However, they should be added during more detailed simulations prior to physical experimentation. Also, neither the neutron generator material nor its stand were included, as these would introduce small quantities of materials below the isotropic neutron point source, thus sending any scattered neutrons and created gamma rays laterally or downward which would be of no interest in this research.

For comparison to NNDC data and Gozani results, the MCNP simulations were coded to provide fluence (neutrons or gamma rays per cm^2) for the 10 second neutron generator operation time versus energy (MeV). This was accomplished using a ring detector tally (f5 – MCNP) parallel to the xy plane of the system at a height equal to the center of the aluminum box with an initial radius of 100 cm. Each simulation reflects 720 minutes of computational time.

Each tally provided energy results in increments of 0.05 MeV from 0.05 – 6 MeV. This range was selected in order to bound the detection of most of the inelastic scattering and radiative capture events. By setting the lower limit at 0.05 MeV, all inelastic scattering and radiative capture events are included, with the exception of U-235 reactions for low neutron energy. For U-235, low energy neutrons (thermal neutrons) are more likely to cause fission than inelastic scattering or radiative capture and as such would mask the intended spectra results. The upper limit was set below 8 MeV in order to prevent multiple-particle reactions such as (n, 2n) and (n, n+p) from adversely affecting the resulting fluences. Of note is that the MNCP code created for this research calculated the tally results below 0.05 MeV and over 6 MeV. However, those results were not the focus of this research and as such are not included in the analysis.

As a method of analysis, the signal-to-noise ratio (SNR) for each isotope's gamma ray spectra was calculated. As a reminder, the signal refers to the results from the combined gamma ray spectra (both target and induced background source terms are present) and the noise is the induced background source term. Dividing the signal by the induced background resulted in a quantitative method of analyzing the ability to identify the specific isotope introduced as target. Values greater than 1 represent a signal which is at least partially recognizable.

Once the initial simulations for each target source term were complete, the ring detector location was changed several times to analyze the effect this would have on the SNR. The intent was to investigate whether or not the SNR could be increased by moving only the ring detector tally. This information should be useful for follow-on research, especially if experiments are conducted at the DTRA TEAMS.

The final simulation consisted of identifying the radial distribution of neutrons for the induced background source term in order to better understand where the neutrons were traveling as opposed to their energy levels. To do this, a mesh tally (mesh – MCNP) was used (Appendix C). This tally created cylindrical boundaries, parallel to the z axis of the system, within the center of the air inside the hole (3.81 cm radius), the steel pipe (8.89 cm radius), the Portland concrete pipe (25.4 cm radius), and the earth (70.32 cm radius). These new boundaries are visualized using Figures 1 and 16 and extending the displayed cylinders upward above the top of the road approximately 12 ft. When simulated, the mesh tally used these columns of air to create a results file showing the average neutron flux (neutrons per cm^2) across each column's boundary versus the height in centimeters. The results of this tally were initially normalized, but the 14 MeV 10^8 neutrons/second neutron source operating for 10s provided the necessary results for analysis and the dose calculations.

Summary

The MCNP simulation coding techniques were the most important aspect of this research. Replicating published work provided a baseline for understanding the expected output from active neutron interrogation in which inelastic scattering / radiative capture. Simulating of the active neutron interrogation system at the DTRA TEAM Site provided the induced background and target source terms from Fe-56, Pb-207, H-1, C-12, U-235, and U-238 need to answer the research questions and test the research hypothesis stated in the introduction.

IV. Analysis and Results

Chapter Overview

The purpose of this chapter is to provide the results of the MCNP simulations and conduct an analysis of those results using the expected/known data provided in the theory section above.

Results of Simulations

Starting with simulations to replicate the results of Gozani, MCNP models were successfully completed using the target isotopes of Fe-56, Pb-207, H-1, C-12, U-235, & U-238. Figure 17 presents the surface current tally (f1 – MCNP) results for each isotope. Figure 18 uses the same data as Figure 17 in a log/lin plot in order to better compare the surface currents. Appendix D. MCNP Tally Results for Gozani Comparison contains the numerical surface tally results for these simulations. The blank spaces in the U-235 data represent those energy values where no gamma rays were created by neutron interactions. The simulations used 10^6 initial neutrons from the neutron beam source. Those neutrons inelastically scattered and slowed down increasing the probability of further interactions. With each interaction, the neutrons either lost energy or neutrons with less energy were created, continuing to increase the probability of interactions at lower energies. Starting with a higher number of neutrons from the neutron beam source increased the probability of interactions resulting in more gamma rays above 2 MeV. However, in this research the U-235 gamma ray spectrum data of most interest is below the 2 MeV level.

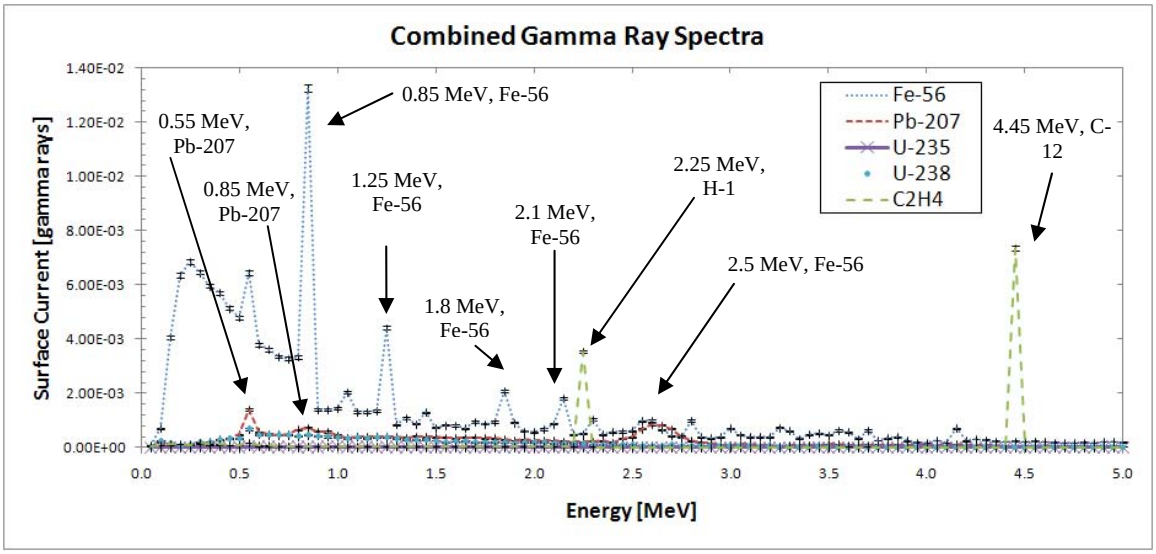

Figure 17. MCNP calculated gamma ray spectra from inelastic scattering of 8.5 MeV neutrons in 10 cm thick Fe-56, Pb-207, H-1, C-12, and U-238. Also included is the gamma ray spectra for 1 cm thick U-235. All error bars represent absolute uncertainties.

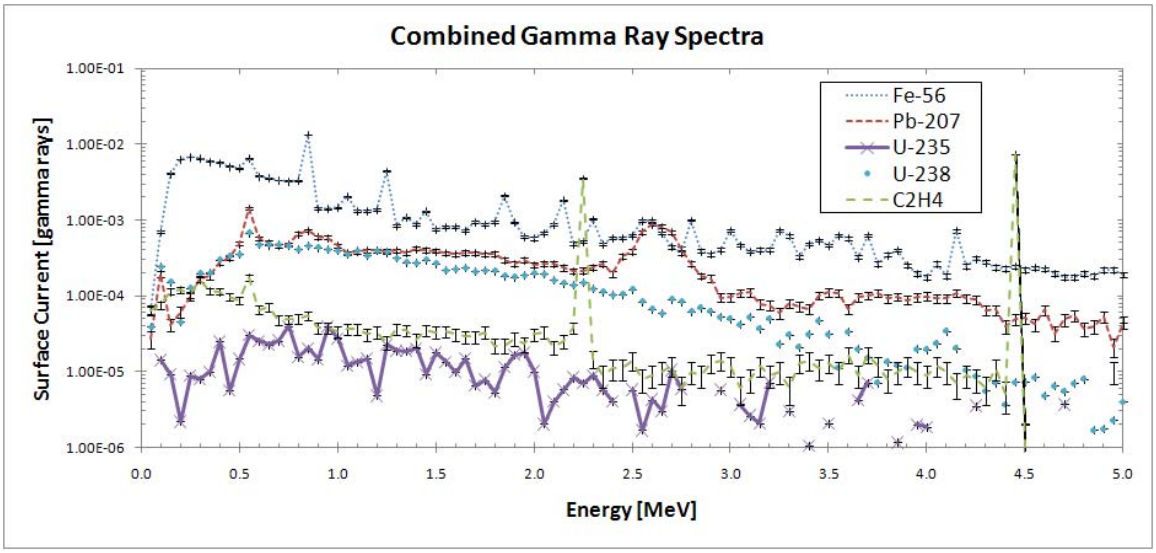

Figure 18. MCNP calculated gamma ray spectra from inelastic scattering of 8.5 MeV neutrons in 10 cm thick Fe-56, Pb-207, H-1, C-12, and U-238. Also included is the gamma ray spectra for 1 cm thick U-235. All error bars represent absolute uncertainties.

The results of this comparison study of Gozani's work provided valuable information, which was used in analyzing the results of the DTRA TEAMS site. Due to

the number of unknowns from Gozani's work and assumptions made to complete this research, the gamma ray spectra (specifically the fluences) in Figures 17 and 18 were not expected to match the Gozani results provided in the theory section. However, the gamma ray energy peaks for each non-SNM isotope and the gamma ray spectrum continua for the uranium isotopes should have corresponded within approximately 0.05 MeV since that was the lowest energy bin established in the simulations for this research. With the exception of the ~0.55 MeV and ~2.65 MeV gamma ray peaks on the Fe-56 and Pb-207 spectra respectively, the results for the non-SNM gamma ray spectra match those from Gozani's work and provide a pure target source spectra (no background source) for use in future analysis of the non-SNM targets.

As for the SNM targets (U-235 and U238), the Gozani comparisons had mixed results. The resulting U-238 gamma ray spectra clearly represent the expected large continuous peak approximately over the 0.5 – 2 MeV range with an almost linear decrease in fluence levels as the energy increases. Use of the 0.05 MeV energy bins was not good enough to fully create the expected continua gamma ray spectra for U-235. Below 2 MeV the probability of inelastic scattering and neutron capture within the U-235 target increased, just as with the other targets. However, due to the fissile nature of U-235 the increased probability of fissions at the lower energy levels was not taken into account when creating the energy bins. The size of the bins caused each peak formed within each bin structure decreased at each boundary between the bins, creating the jagged spectra observed instead of the expected continuous spectra provided in Gozani's work. Despite this concern with the energy bins, though, the lack of time to change the bin structure and conduct more simulations plus the relatively accurate results for the

other targets allowed the research to move on modeling the active neutron interrogation system at the DTRA TEAM site.

Unlike with the Gozani comparison work, which was only pure target source term, modeling the DTRA TEAM Site primarily consisted of background materials. Prior to introducing any target isotopes, the induced background needed to be known. This was accomplished by conducting simulations with only non-target materials (pipes, road, table, box, earth, and air) in place and then setting the result as the induced background source term. The neutron and gamma ray tally results plotted in Figures 19 and 20 represent these induced background source terms.

As noted in the theory section, ring detector tallies (f5 – MCNP) provided both neutron and photon fluences [particles/cm^2] as functions of their energies. Figure 19 represents the tally results concerning only collided neutrons since uncollided neutrons by definition did not interact with any background materials, which made them unimportant for the analysis of the results. Figure 20 represents gamma rays which were both collided, those gamma rays which interacted with background materials enroute to the detector, and uncollided, those gamma rays which moved essentially straight from creation to the detector without any other interactions. For the purposes of this research the collided and uncollided gamma ray spectra are combined for the induced background (and later on for the target isotopes) in order to create a single gamma ray spectra for analysis purposes from each simulation run.

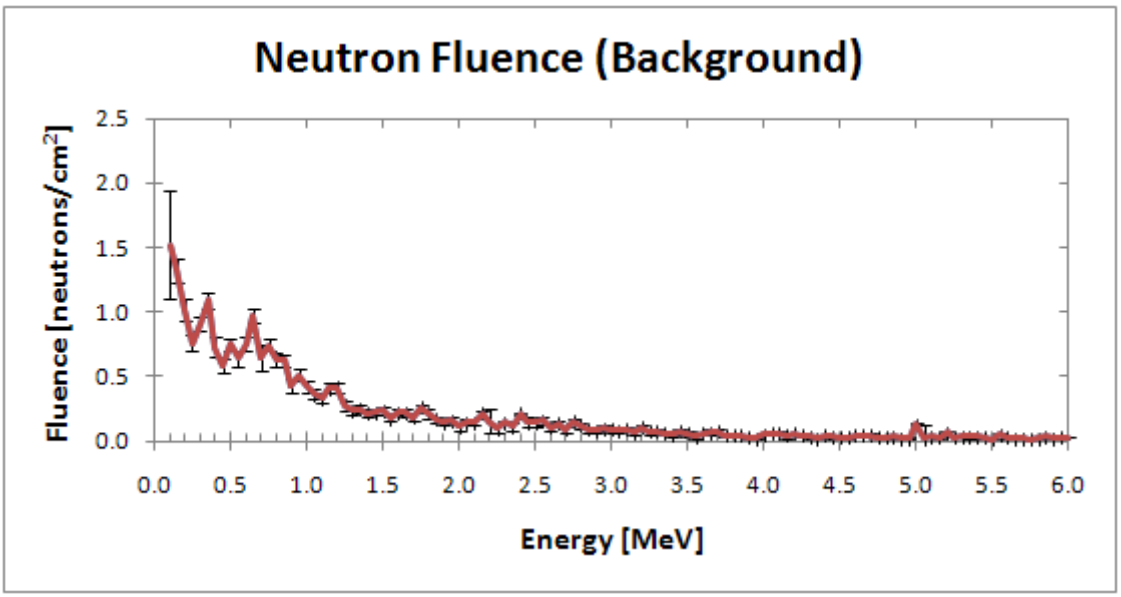

Figure 19. The neutron background results from ring detector tally (f5 – MCNP) set into energy bins 0.05 MeV wide, for the collided neutrons in the induced background created by 10^8 neutrons/second source after 10 seconds. All error bars represent absolute uncertainties.

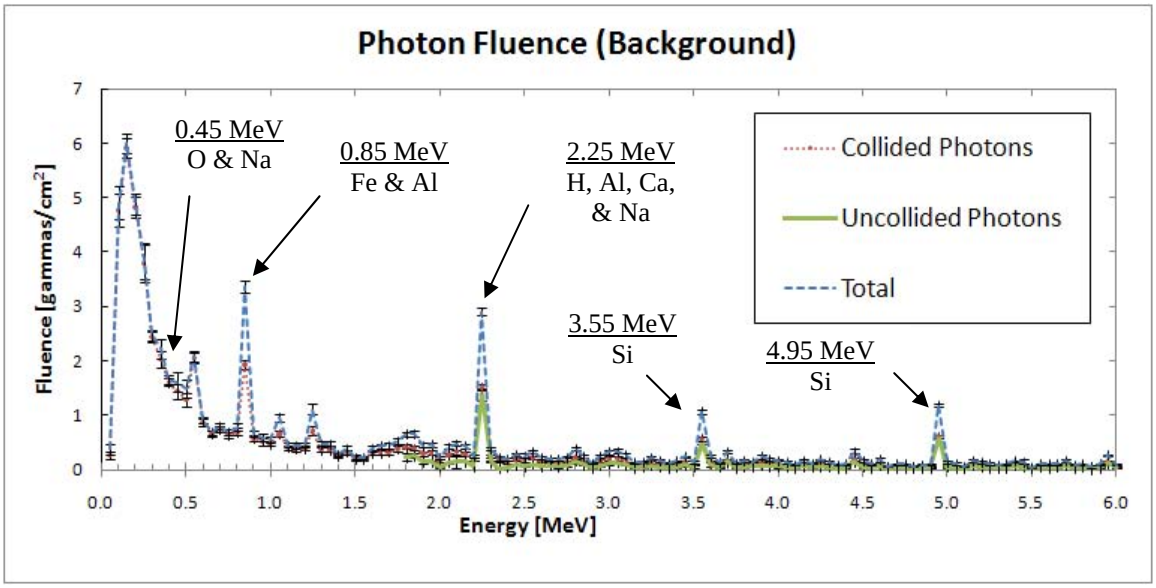

Figure 20. The gamma ray background results from ring detector tally (f5 – MCNP) set into energy bins 0.05 MeV wide, for gamma rays in the induced background created by 10^8 neutrons/second source after 10 seconds. The arrows show the peak locations (within 0.05 meV) for the isotopes most abundant in the background materials. All error bars represent absolute uncertainties.

The importance of modeling the induced background source term first is that it then became the lowest possible detectable value. Regardless of the material or isotope used, if the target source term does not at least provide fluences statistically above the induced background then it will not be distinguishable as its own signal. For the case of using non-SNM target isotopes, individual gamma ray peaks are expected to appear above the induced background at the energy values specific to each isotope as mentioned previously. For the SNM targets, the overall gamma ray spectra from at least 0.5 – 2 MeV should be raised above the induced background. The two methods of comparing the induced background to each of the target source terms are visual (not always accurate but can provide information either for or against the expected result) and using calculated SNRs.

Simulations using the non-SNM target isotopes were conducted next. Fe-56 and Pb-207 were introduced individually, with H-1 and C-12 together in the form of polyethylene (C_2H_4). Table 6 provides the expected NNDC gamma ray peak energy with the corresponding simulation fluence results for each isotope. As will be discussed shortly, these peak energies were not directly observed due to the 0.05 MeV energy bins used in the ring detector tally but they are presented here as the actual peaks for reference. Figures 21 through 23 show the combined fluence spectra of collided and uncollided gamma rays for Fe-56, Pb-207, H-1, and C-1.

Table 6. Gamma Ray Spectra for Target Source Terms

Isotope	Peak Energy [MeV]	Total Fluence [gamma rays/cm^2]	Background Fluence [gamma rays/cm^2]
Fe-56	0.846	6.533	3.355
	1.238	1.895	1.120
	1.810	0.980	0.663
	2.113	0.596	0.436
	2.522	0.425	0.328
	2.959	0.374	0.248
	3.554	1.210	1.066
Pb-207	0.569	2.500	2.096
	0.897	3.877	3.355
	1.770	0.711	0.657
	2.053	0.460	0.422
	2.092	0.603	0.476
H-1	2.230	7.162	2.910
C-12	4.438	2.077	0.348

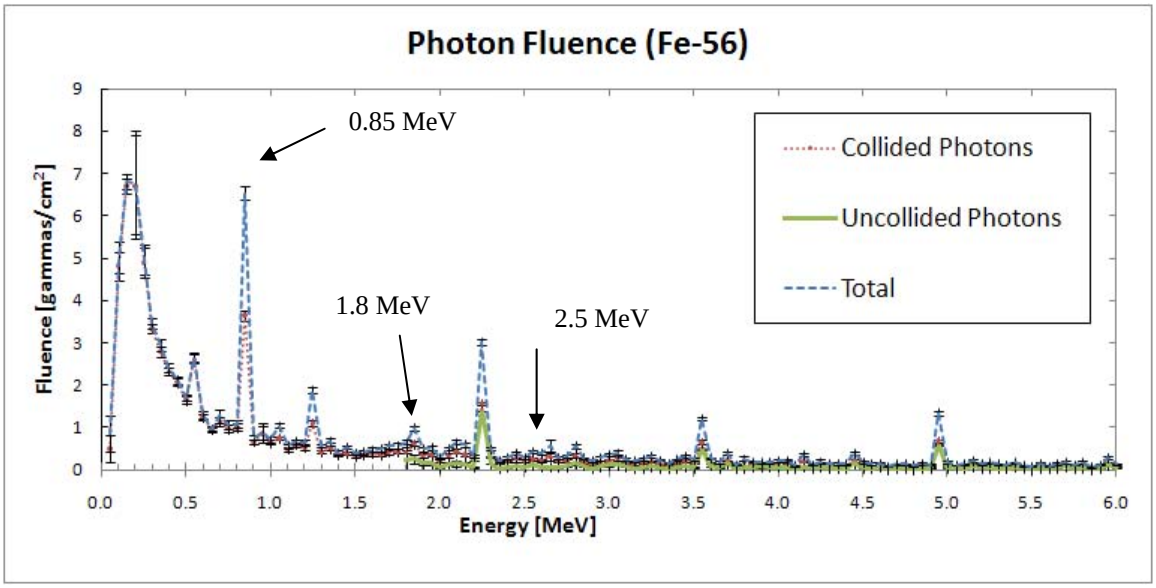

Figure 21. Total gamma ray fluence with Fe-56 target source created by 10^8 neutrons/second source after 10 seconds as provided by the ring detector tally (f5 – MCNP). The arrows provide the locations of the visible isotope specific peaks. All error bars represent absolute uncertainties.

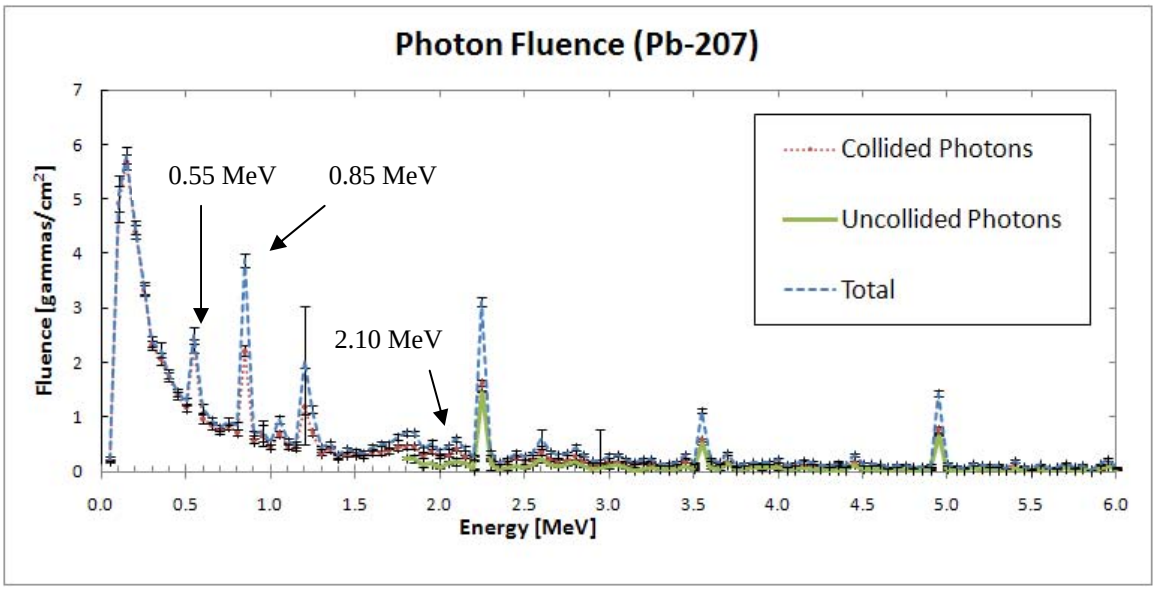

Figure 22. Total gamma ray fluence with Pb-207 target source created by 10^8 neutrons/second source after 10 seconds as provided by the ring detector tally (f5 – MCNP). The arrows provide the locations of the visible isotope specific peaks. All error bars represent absolute uncertainties.

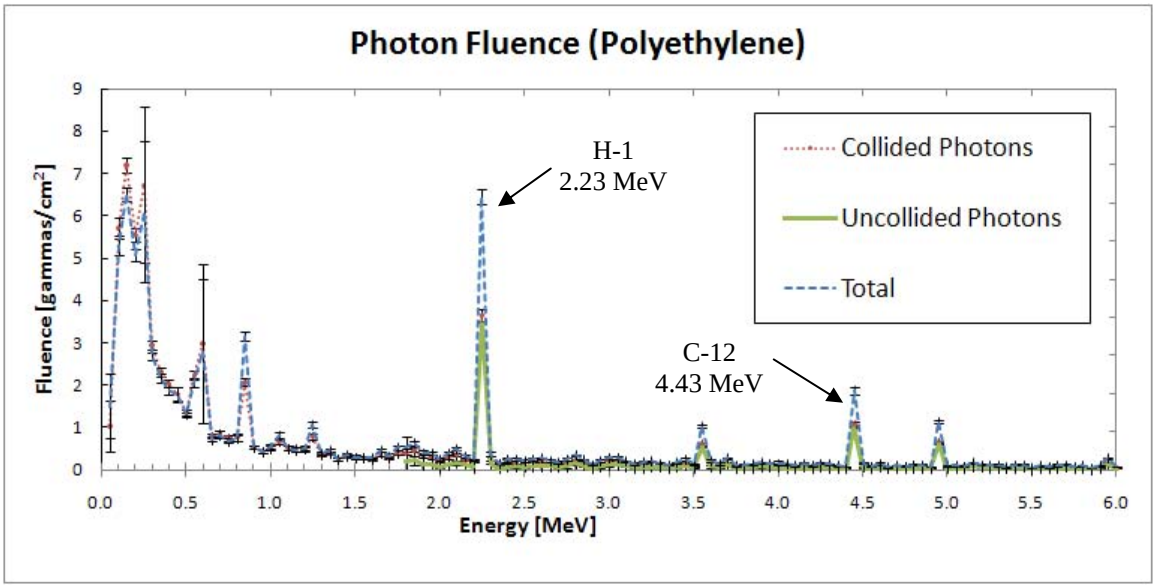

Figure 23. Total gamma ray fluence with C-12 and H-1 target sources created by 10^8 neutrons/second source after 10 seconds as provided by the ring detector tally (f5 – MCNP). The arrows provide the locations of the visible isotope specific peaks. All error bars represent absolute uncertainties.

Visual inspections of these results compared to the induced background spectrum clearly indicate that the induced background source term dominated most of the spectra but some distinctions were observed. The gamma ray results for Fe-56 visibly show increases in the prominent Fe-56 peaks at 0.846 MeV, 1.810 MeV, and 2.52 MeV; but the induced background masked the peaks at 1.238 MeV, 2.113 MeV, 2.959 MeV, and 3.554 MeV. The simulation results for Pb-207 also display the strongest visual peaks at 0.569 MeV, 0.897 MeV, and 2.092 MeV; while the induced background appeared to block the 1.770 MeV and 2.053 MeV peaks. The C-12 and H-1 results provide the best case where the prominent H-1 (2.23 MeV) and C-12 (4.438 MeV) peaks are both clearly distinguishable from the induced background.

Since Fe-56, H-1, and C-12 are all present in the background materials a more exact method was needed to determine if their target source gamma ray spectra was distinguishable from the induced background. Calculating the SNR for each target isotopes results provides the level of detail necessary. The SNR is calculated by dividing the total fluence from the target isotope simulations by the induced background fluence. Any result > 1 refers to those energy levels at which the target source term can provide enough of a signal to overcome the induced background source term. However, as the SNR approaches 1, the harder it is to distinguish between the two values, therefore the absolute uncertainties are used to provide a threshold for each gamma ray peak energy below which the SNR is determined to be inadequate to make a distinction between the induced background and the target source terms. For this research, double the absolute uncertainty of the total fluence plus the absolute uncertainty of the induced background fluence were added to the baseline SNR value of 1. Any resulting gamma ray peak SNR

having a value smaller than this calculated value was determined to be indistinguishable from the induced background.

Table 7 provides SNR data for the expected gamma ray peaks of Fe-56, Pb-207, C-12, and H-1. The uranium targets are discussed later. Note that in Table 7 the values of the energy peaks have changed from the experimental results to the energy bin values calculated by MCNP during the simulations. This is done in order to provide easier reference to the visual spectra in Figure 21 through 23. Appendix E provides the complete SNR results for all targets used in this research.

Using the SNRs as references, Fe-56, H-1, and C-12 were distinguishable from the induced background. The Fe-56 peaks in the 0.85, 1.2, 2.1, and 2.95 MeV energy bins and both polyethylene peaks had SNR values sufficient to support the use of this neutron activation interrogation technique. The Pb-207 results, however, do not since all but one of the peaks were within the uncertainty range established to preclude target isotope distinction.

Table 7. SNR Results for the Expected Gamma Ray Peaks

Isotope	MCNP Peak Energy [MeV]	SNRs	SNR Abs Uncert.	(Total Fluence Abs Uncert. x 2) + Bkgd Fluence Abs Uncert. + 1
Fe-56	0.85	1.947	0.079	1.424
	1.2	1.400	0.203	1.243
	1.8	1.000	0.092	1.169
	2.1	1.381	0.159	1.127
	2.5	1.083	0.247	1.104
	2.95	1.113	0.230	1.111
	3.55	1.135	0.062	1.140
Pb-207	0.55	1.193	0.094	1.415
	0.85	1.156	0.051	1.343
	1.8	1.082	0.102	1.138
	2.05	1.090	0.131	1.110
	2.1	1.266	0.139	1.126
H-1	2.25	2.461	0.090	1.458
C-12	4.45	5.962	0.625	1.237

The uranium isotopes were analyzed next. Figures 24 and 25 present the gamma ray fluences for U-235 and U-238, respectively. For the cases involving SNM, the gamma ray fluences decrease from 0.1 to 2.0 MeV. As the target in the induced background source term is air, any target denser than air will increase the probability of neutron and gamma ray interactions. Increased interactions further slow down and/or completely attenuate the neutrons and gamma rays such that the number of gamma rays in energy bins above 0.1 MeV is decreased from that of air. Fewer gamma rays above 0.1 MeV result in the continuous spectra having steeper slopes for increased target atomic mass, with special nuclear materials being recognizable by their extremely steep slopes.

Visual comparisons to the induced background do not reveal this slope change for higher overall gamma ray fluences, which were expected from the fissions created by the lower energy neutrons. From a SNR perspective (Appendix E), the SNR values for neither U-235 nor U-238 are high enough to distinguish from the induced background.

Combining these results with those of the non-SNM results provided support to the need for induced background reduction in order to positively identify the target isotope.

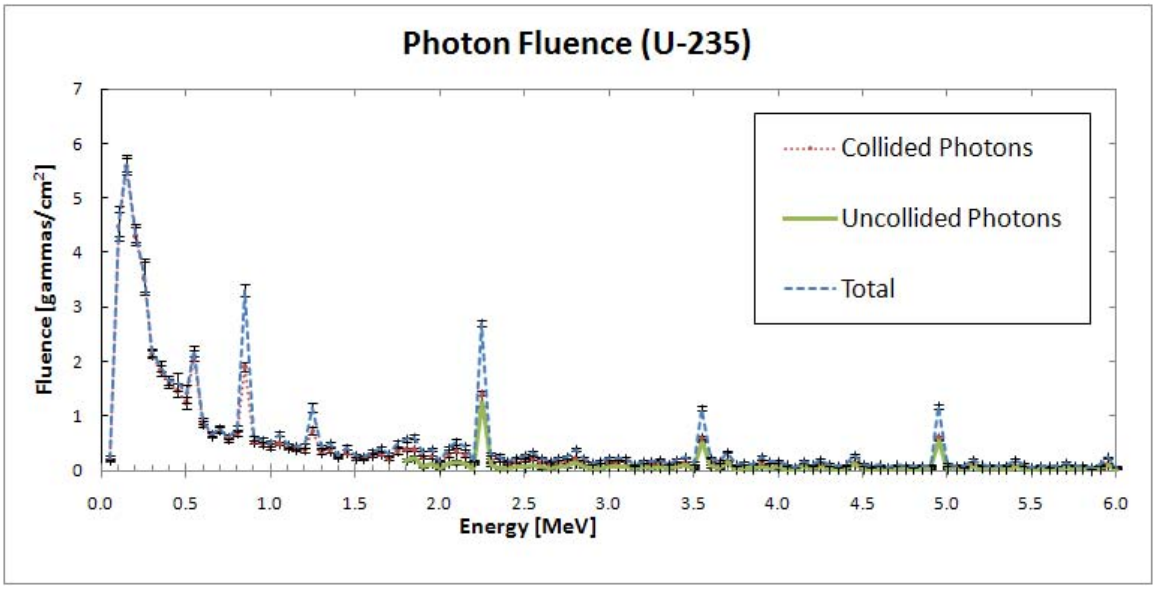

Figure 24. Total gamma ray fluence with U-235 target source created by 10^8 neutrons/second source after 10 seconds as provided by the ring detector tally (f5 – MCNP). The arrows provide the locations of the visible isotope specific peaks. All error bars represent absolute uncertainties.

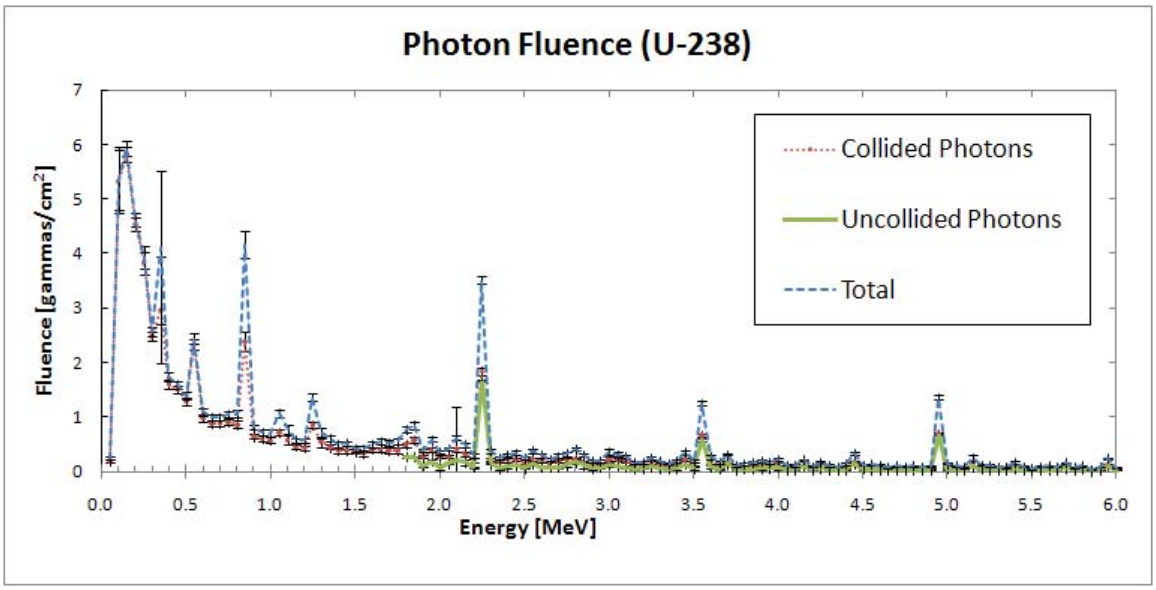

Figure 25. Total gamma ray fluence with U-238 target source created by 10^8 neutrons/second source after 10 seconds as provided by the ring detector tally (f5 – MCNP). The arrows provide the locations of the visible isotope specific peaks. All error bars represent absolute uncertainties.

With the SNR being the determining factor in either support for or against the research hypothesis, the location of the ring detector tally was investigated in order to determine how the SNRs were affected by the tally positioning. The initial ring detector tally position was arbitrarily located to be level with the target and 1 m away. Four alternate positions were chosen to increase the horizontal and vertical distance from the target for analysis. The induced background was simulated each time since it was needed as the baseline measurement. For efficiency, only Pb-207 was simulated in this analysis.

Figure 26 presents the updated SNRs for the four ring positions. Figure 27 presents the updated SNRs as the vertical height of the ring detector tally changed. As the ring location moved farther from the target source term, the corresponding gamma ray fluence decreased as expected. It was unknown as to whether or not the induced background would decrease and if so, would it do so more than the target source term.

As the ring radius and height increased, the amount of background material through which the gamma rays traveled increased, thereby increasing the number of possible interactions and overall attenuation.

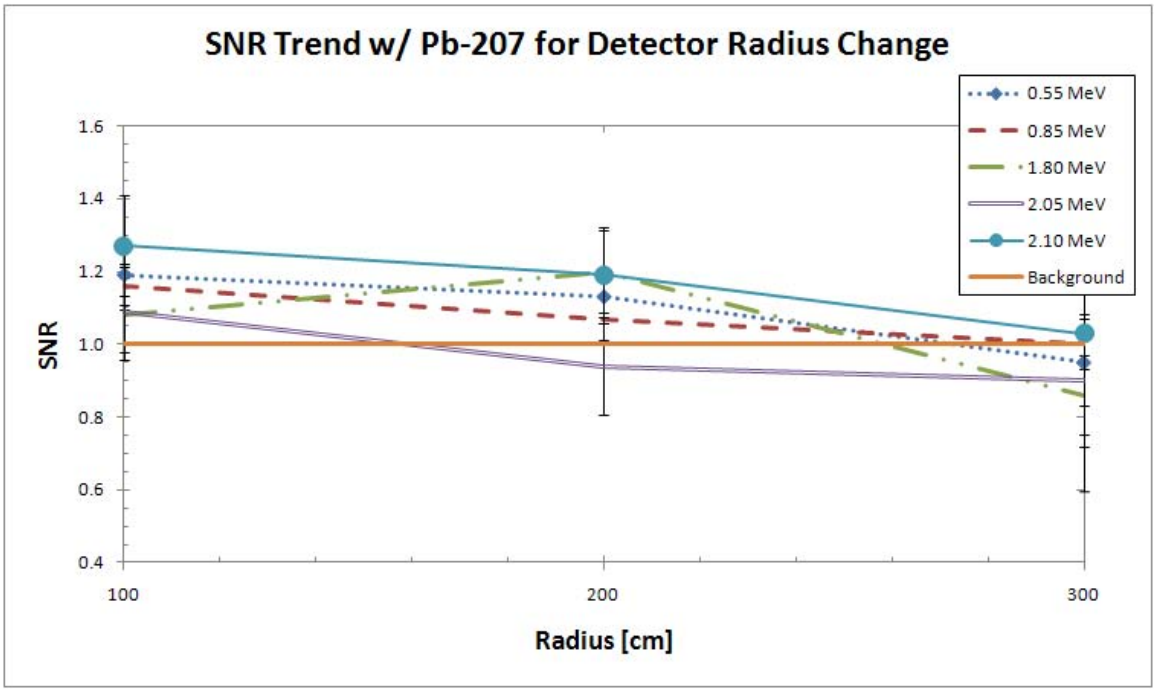

Figure 26. SNR trend results as ring detector radius changes.
The SNR of the gamma ray fluencies with Pb-207 as the target isotope. The energy values plotted refer to the gamma ray peaks for Pb-207. The height of the ring detector is 110 cm above the concrete road. All error bars represent absolute uncertainties.

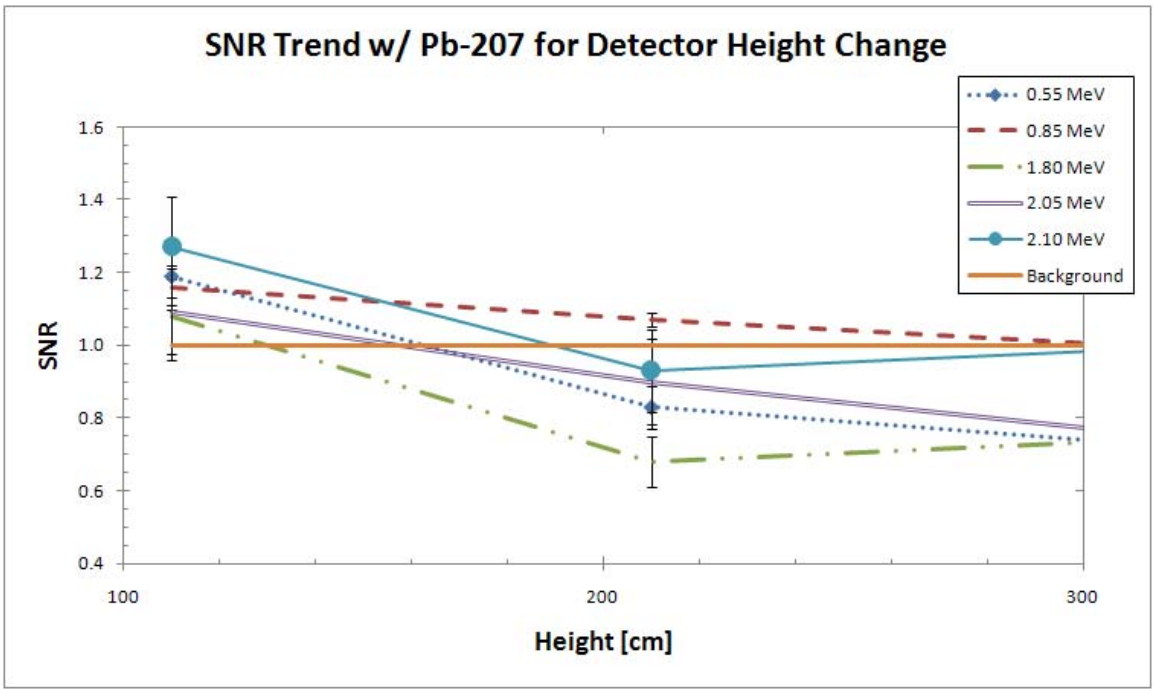

Figure 27. SNR trend results as ring detector height changes. The SNR of the gamma ray fluencies with Pb-207 as the target isotope. The energy values plotted refer to the gamma ray peaks for Pb-207. The radius of the ring detector is 100 cm. All error bars represent absolute uncertainties.

Tables 8 and 9 provide the tabulated data from Figures 26 and 27 for each Pb-207 gamma ray peak energy. Position 1 refers to the location of the ring detector tally used in the original DTRA TEAMS simulations. Positions 2 and 3 expand the radius of the ring detector tally to 200 and 300 cm, respectively. Positions 4 and 5 raise the height of the ring detector tally to 210 and 310 cm, respectively. The expected reduction in the induced background was calculated, but the Pb-207 target source term decreased much faster. The single exception was the 1.8 MeV gamma ray peak when the ring detector tally had a 200 cm radius. As such, the SNR values decreased. Increasing the radius provided better results than increasing the height, despite the ring detector being closer to the background materials. This may be useful information for future experimentation to

save operators time in determining detector setup locations. Of note is that the ring detector tally was not moved closer to the target, which would have clearly increased the SNR value, since this research is in support of efforts to detect SNM and the requirement to be less than one meter from the target source is unrealistic.

Table 8. SNRs for Various Ring Detector Radii

Detector Tally Position	Gamma Ray Energy Bin [MeV]	Horizontal Distance from Target Isotope to Ring Tally [cm]	SNR	SNR Abs. Uncert.
1	0.55	100	1.19	0.094
2	0.55	200	1.13	0.074
3	0.55	300	0.95	0.352
1	0.85	100	1.16	0.051
2	0.85	200	1.07	0.057
3	0.85	300	1	0.070
1	1.8	100	1.08	0.102
2	1.8	200	1.2	0.112
3	1.8	300	0.86	0.110
1	2.05	100	1.09	0.131
2	2.05	200	0.94	0.134
3	2.05	300	0.9	0.183
1	2.1	100	1.27	0.139
2	2.1	200	1.19	0.133
3	2.1	300	1.03	0.198

Table 9. SNRs for Various Ring Detector Heights

Detector Tally Position	Gamma Ray Energy Bin [MeV]	Vertical Distance from Ground Level to Ring Tally [cm]	SNR	SNR Abs. Uncert.
1	0.55	110	1.19	0.094
4	0.55	210	0.83	0.058
5	0.55	310	0.73	0.080
1	0.85	110	1.16	0.051
4	0.85	210	0.68	0.021
5	0.85	310	0.67	0.022
1	1.8	110	1.08	0.102
4	1.8	210	0.68	0.069
5	1.8	310	0.74	0.077
1	2.05	110	1.09	0.131
4	2.05	210	0.9	0.116
5	2.05	310	0.76	0.115
1	2.1	110	1.27	0.139
4	2.1	210	0.93	0.115
5	2.1	310	0.99	0.116

Although not the focus of this research, the results of the gamma ray spectra warranted additional analysis concerning the collided neutron spectra. The intent was to determine if using neutron spectra the target source terms were more distinguishable from the induced background source term. Figures 28 through 32 present the total neutron fluence for each target isotope. The purpose behind these tally results is more than just showing that as neutrons interact with matter they lose energy in inelastic collisions, neutron capture, and/or fission. In these figures, the slopes of the neutron spectra from approximately 0.5 – 2 MeV are compared in order to determine the SNM or non-SNM nature of the target isotope. This method does not provide identification of the target isotope like gamma ray spectra analysis, but it should be able to identify the presence of SNM.

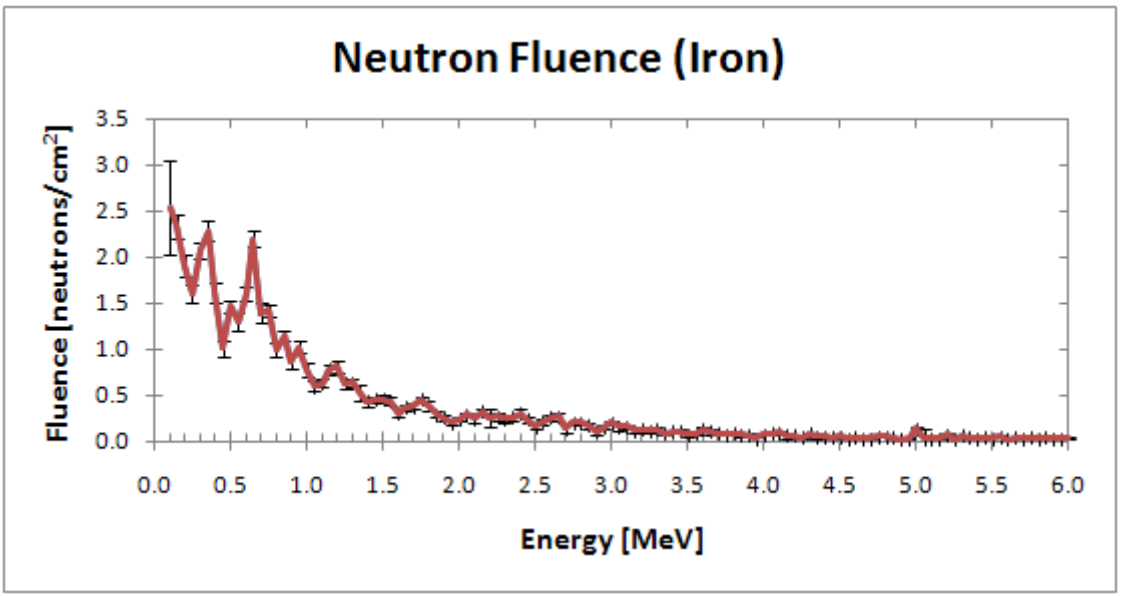

Figure 28. Collided neutron fluence for Fe-56 created by the 10^8 neutrons/second source after 10 seconds as provided by the ring detector tally (f5 – MCNP). All error bars represent absolute uncertainties.

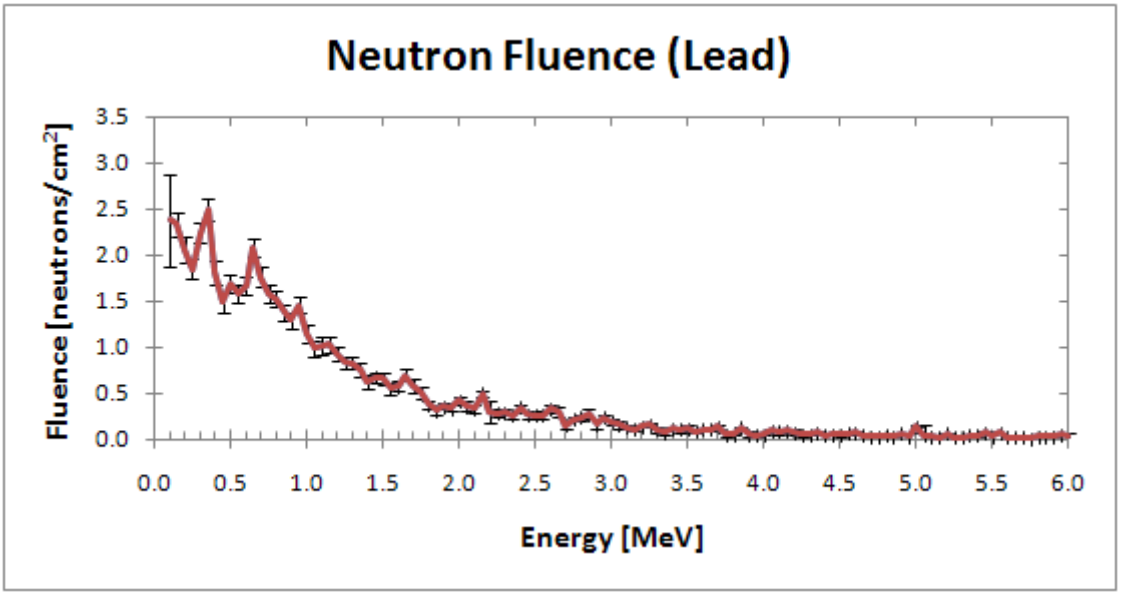

Figure 29. Collided neutron fluence for Pb-207 created by the 10^8 neutrons/second source after 10 seconds as provided by the ring detector tally (f5 – MCNP). All error bars represent absolute uncertainties.

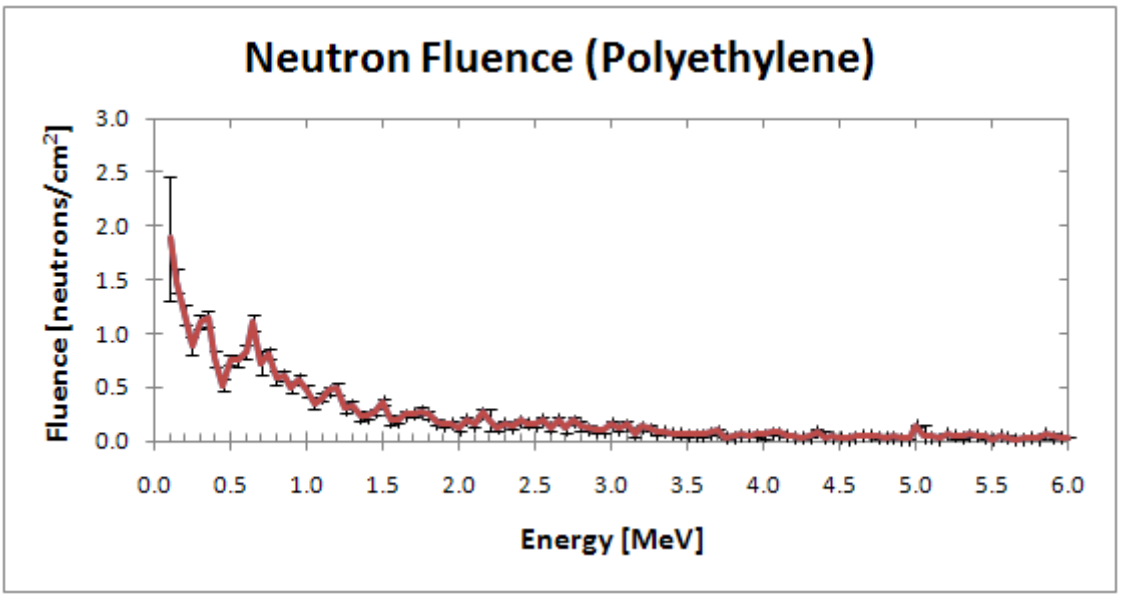

Figure 30. Collided neutron fluences for C-12 and H-1 created by the 10^8 neutrons/second source after 10 seconds as provided by the ring detector tally (f5 – MCNP). All error bars represent absolute uncertainties.

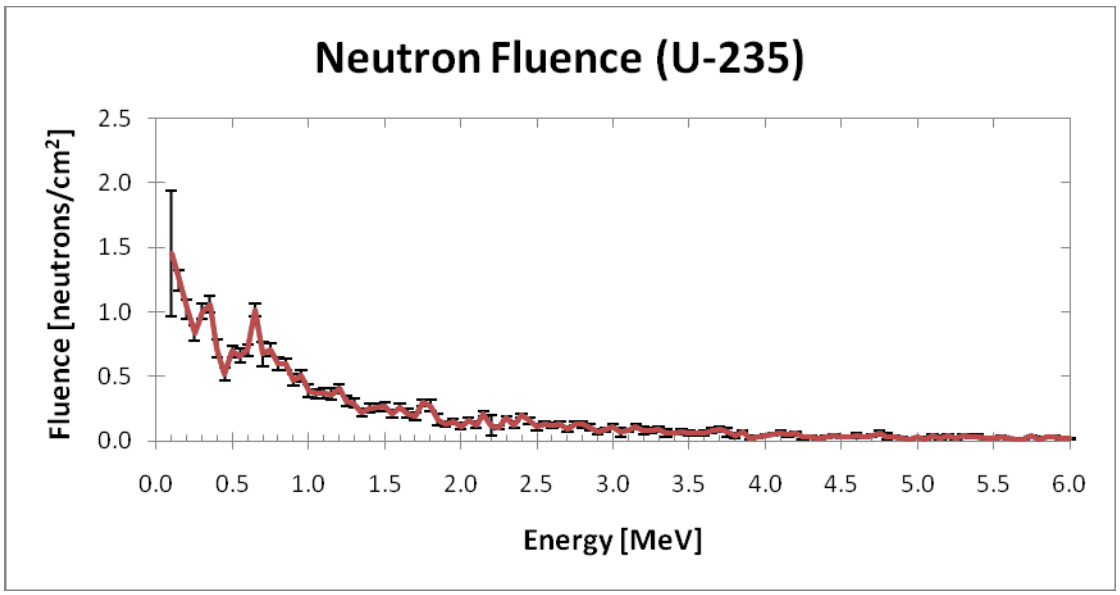

Figure 31. Collided neutron fluence for U-235 created by the 10^8 neutrons/second source after 10 seconds as provided by the ring detector tally (f5 – MCNP). All error bars represent absolute uncertainties.

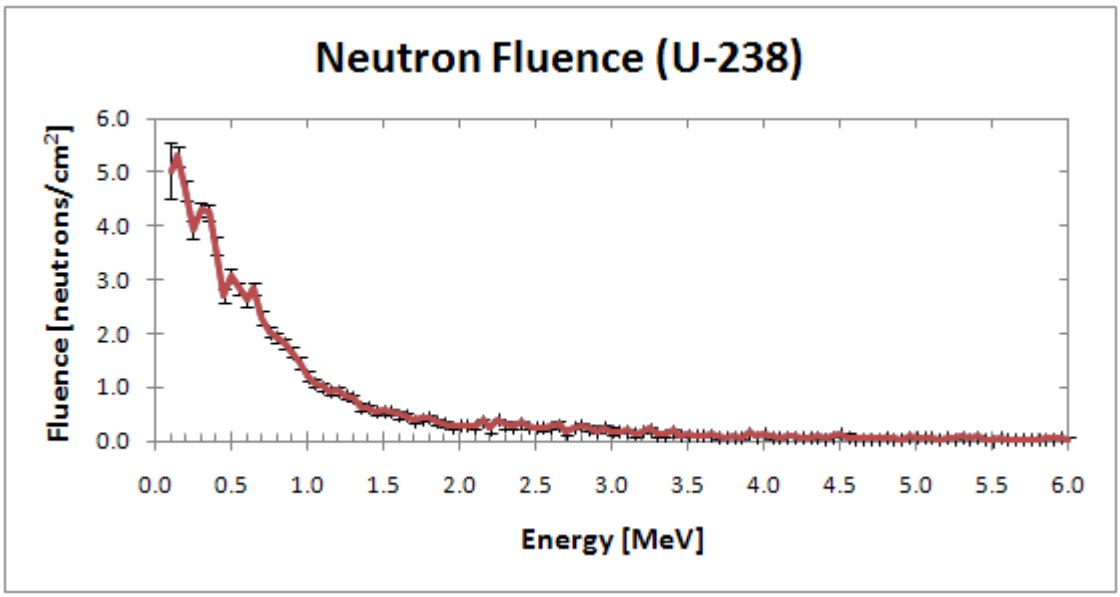

Figure 32. Collided neutron fluence for U-238 created by the 10^8 neutrons/second source after 10 seconds as provided by the ring detector tally (f5 – MCNP). All error bars represent absolute uncertainties.

Disregarding the uncertainties for the initial value for now, the neutron fluencies for the Fe-56, Pb-207, H-1, and C-12 appear similar. This is not unexpected since the target volumes are relatively small (6,859 cm^3) compared to the rest of the simulated model's volume (4.19 x 10^9 cm^3) within which neutron interactions can occur. The uranium targets, though, should have increased neutron fluencies as the energy levels become below 2 MeV. This is because the neutrons can cause fission in addition to the inelastic scattering and neutron capture, creating additional neutrons. The inclusion of U-235 appears not to change the induced background. This may be due to the small volumeU-235 (81 cm^3) as compared to the other target isotopes. The U-238 was more massive and produced 2 times more added neutron fluence. From these results, the SNM were more distinguishable when comparing neutron spectra than gamma ray spectra.

However, the inability of this method to identify the specific isotope or provide reliable results for the U-235 do not make it more viable as a SNM identification technique.

Ring detector tallies are non-fixed point detector tallies situated on a ring. They calculate the average flux of neutrons or gamma rays moving to the detector after an event without interactions, where an event refers to the creation or interaction of a neutron or gamma ray. When using detector tallies the distance an event occurs from the detector factors into the flux strength. For example, if a neutron is inelastically scattered inside of a material 100 m from the detector, it will have a lower probability of reaching the detector without further interactions with the surrounding material than a neutron with the same mass/energy inside of the same material but only 1 cm from the detector. (X-5 Monte Carlo Team, 2005, 2-91 – 2-94)

In most cases this weighting function simulates realistic behavior. However, as the distance from the event to the detector approaches zero, the flux approaches infinity. As a means to prevent a few events near the detector from adversely affecting the calculated average flux at the detector, a vacuum space can be simulated around the detector. In this research, though, the intent was to model the DTRA TEAM site which does not have vacuum space. Therefore, such events were minimalized by ensuring the ring detector tallies were located in air, the least dense material in the model, and a small exclusion zone of 0.5 cm radius around the detector tally was added in MCNP. Any event occurring inside the exclusion zone was omitted from the tally calculations. (X-5 Monte Carlo Team, 2005, 2-91 – 2-94) While these did not guarantee an event near the ring detector tally from artificially raising the calculated average fluence, inspection of the MCNP output data for each simulation did not reveal such an event. As such, the

conclusion was made that only the relative uncertainties of the ring detector tally results affect their accuracy.

Thus far, the analysis has focused on utilizing the gamma ray and neutron spectra calculated for the induced background and each of the targets in order to determine if the active neutron interrogation technique being used in this research can identify SNM under the specific simulation conditions presented. In this final section of analysis, the spatial distribution of the induced background neutrons is addressed. This provided the track length estimate of the neutron flux across cylindrical boundaries at various heights from ~6' to ~12' above the surface of the concrete road. The results of the mesh tally used to generate Figures 33 and 34 also allowed for calculation of estimated radiation dose rates for each of the cylindrical zones created by the tally.

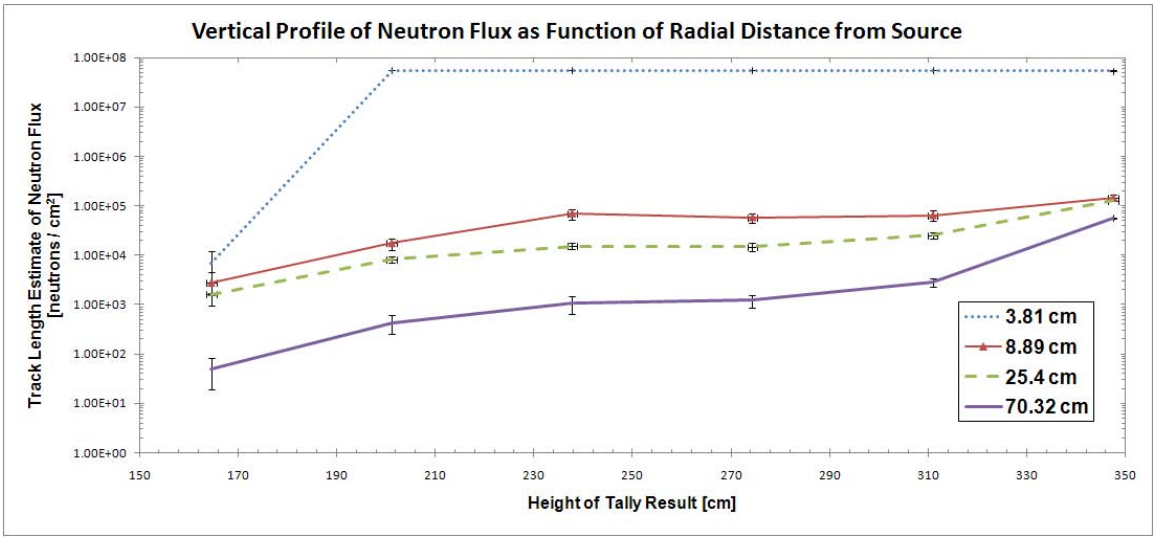

Figure 33. Radial distribution of neutron background source at DTRA TEAMS shown as log/lin plot. The lines represent the neutron flux from the 10^8 neutron/second source after 10 seconds of irradiation at various radial distances from the z axis. All error bars represent absolute uncertainties.

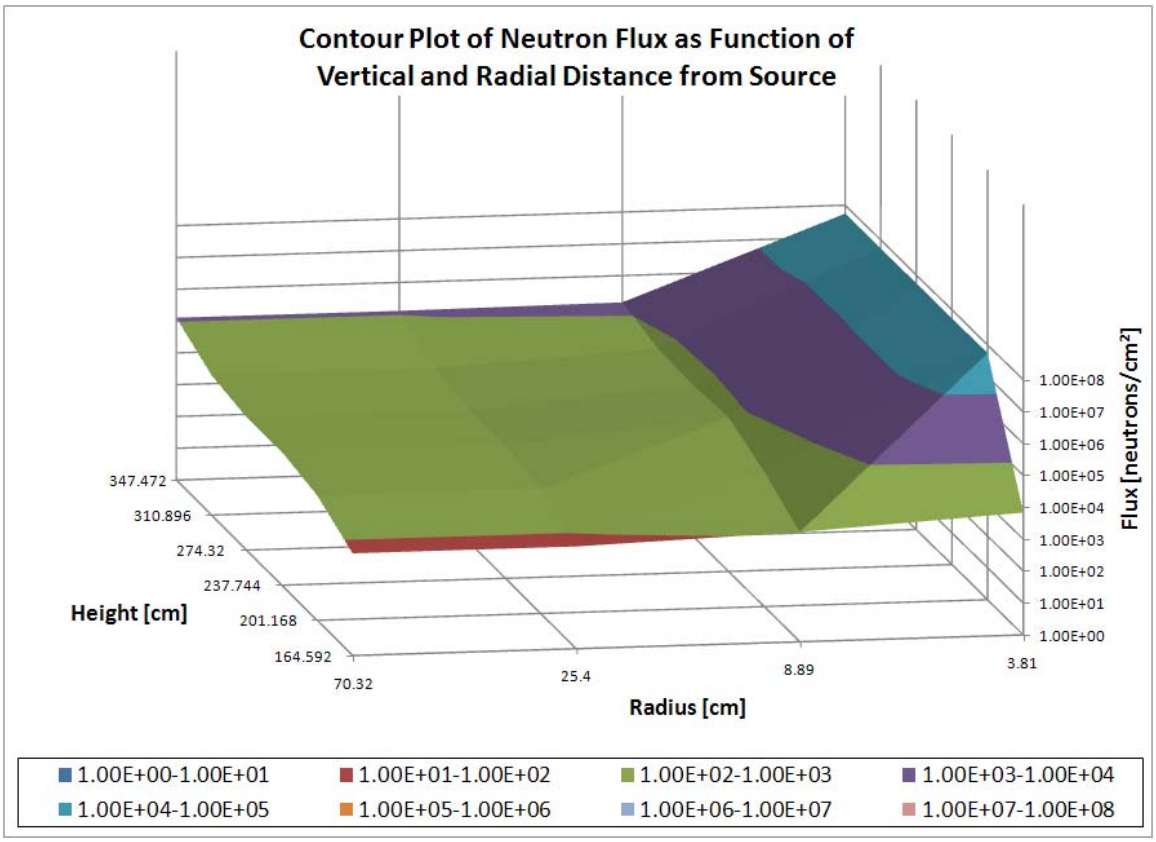

Figure 34. 3-D contour plot of radial distribution of neutron background at DTRA TEAMS shown with the respective fluxes in log format. The contour surface of the neutron flux is calculated from the 10^8 neutron/second source after 10 seconds of irradiation at various radial distances from the z axis.

Each line in Figure 33 represents a distance radially from the z axis (neutron beam line) and the corresponding average neutron flux versus height. The results provided range in height from 150 – 350 cm in order to cover the upper body of personnel working at the site. The 3.81 cm radius line, representing those neutrons that interact with only air, the steel table, and aluminum box has the highest flux, as expected, since the air and small amount of material in the table and box resulted in fewer interactions with the high-energy neutrons and thus fewer neutrons were slowed to below 6 MeV. Along the

remaining lines, the flux continues to decrease as the radial distance from the z axis increases.

The radial distances (3.81, 8.89, 25.4, and 70.32 cm) were not randomly chosen, but rather the center of the radii of the hole, steel pipe, and Portland concrete pipe, as well as an arbitrary radius for the earth. Analysis of the results suggests that as the height increases the relatively small distinctions between the radial distances become insignificant. The increase in flux observed for the wider radial distances suggests that many of the neutrons which were initially in the 3.81 cm group are interacting more and changing directions so as to disperse among the other groups at higher altitudes.

While this research is computational, follow-on research may include experimentation that would require maintaining radiation safety. To that end, utilizing the flux results of the mesh tally, effective dose rates were estimated at the radial distances simulated. Using equation 1.4 with the highest possible fluence-to-effective-dose conversion coefficient, h_E, (~4×10^{-10}), the largest flux for each radial distance, and a 10s neutron generator run time, the effective dose rates were calculated (see Table 10). These rates correspond only to the specific conditions simulated in this research. For example, a 10s exposure for someone working greater than one meter from the center of the hole would likely result in ≤ 0.0576 mSv, which is far below the yearly limit.

Table 10. Effective Dose for 10s Exposure at Various Radial Distances

Radial Distance [cm] from z axis	Effective Dose [mSv]
3.81	22
8.89	0.0576
25.4	0.0512
70.32	0.0223

V. Conclusions and Recommendations

Chapter Overview

The purpose of this chapter is draw informative conclusions from the research.

Conclusions of Research

Based upon the scope of this research, the hypothesis was disproven. The simulated background source term dominated the gamma spectrum at the locations simulated and the SNM target materials could not be uniquely identified. With the exception of Fe-56, H-1, and C-12 (which also exist in the background materials) the target source terms were indistinguishable from the induced background. In hindsight this should have been expected. Based upon the model's geometry and the isotropic nature of the 10^9 neutrons generated by the neutron source in 10 seconds only ~ 434,000 neutrons will exit the hole through the opening. With the amount of dense materials surrounding the neutron generator, the ~ 434,000 neutrons passing through air have higher probabilities of interacting with the target isotopes than those which interact first in the steel, Portland concrete, concrete, or earth. With the vast majority of the neutrons not interacting with the target isotopes, the induced gamma background should dominate. To this end, either adding shielding around the ring detectors or focusing the neutron generator output should have been simulated early on in the research. The relative uncertainties of the fluences remain above the desired 10%, but with the effect of the induced background masking most of the source terms, this was not a concern. It is unknown how much of an effect the use of undetermined cross section libraries had upon the DTRA TEAMS simulations, but the early results in replicating Gozani's work

suggest that any effect was minimal. The end result is that while the research provided some useful information and output data, the hypothesis was disproven for the simulated conditions and the U-235 was not distinguishable from the induced background.

Significance of Research

This research supports a UC/AFIT research grant proposal to "Design of a Novel, Multi-Element Scintillation Detector Exhibiting Improved Energy and Spatial Resolution for Measuring Low Photon Energy Emitting Radioactive Materials". Overall, the objectives of the project are that "a novel, multi-element scintillation detector array will be designed having enhanced energy and spatial resolution compared to conventional radiation detectors for monitoring the safety and security of uranium- and plutonium-bearing materials or weapons stockpile components that emit low energy photons (E < 200 keV). If the induced background and source terms are properly simulated and documented, follow-on research can begin testing various neutron and gamma ray detector materials, such as phoswich scintillators, to further improve energy and spatial resolution toward the overarching project's goal.

Recommendations for Action

Several actions can be undertaken to further refine this research. First, the induced background source term needs to be reduced without significantly decreasing the target source term. One method of doing this is to add shielding around the ring detectors to block as much of the induced background as possible, while still leaving enough of an opening to allow gamma rays from the target to enter. This method has the disadvantage of possibly blocking part of the target source term as well. Another method is to change

the isotropic neutron generator into a beam type source. This can be done by moderating the neutrons, except for those initially traveling toward the target. This method is most likely to provide better SNRs since it is significantly lowering the possibility of neutron interactions with materials other than the target and does not have the possibility of blocking the target source term from the detector. Second, variance reduction techniques need to be implemented for each of the target isotope codes in order to reduce the relative uncertainties. Third, a MESH card should be added to provide more detailed information on where the neutrons and gamma rays are being created and scattered/captured in order to better shield the detector and assist with safely executing physical testing. The MESH tally only does this radially, whereas a MESH card would record 3-D positioning of target particles. If a MESH card is not possible then at least simulate a mesh tally for gamma rays and neutrons with the induced background and each target isotope. These actions were not conducted during this research due to time constraints in coding and simulation execution.

Recommendations for Future Research

Once additional simulations are made using these previous recommendations, the SNRs should improve such that U-235 can be consistently identified. With successful U-235 identification possible for the specific conditions simulated, more research into the affect of detector positioning on the SNR should be completed. With the conclusion of these simulations, detectors can begin to be modeled and scintillator material testing eventually conducted.

Appendix A. MCNP Input Codes for Gozani Comparison

Iron Code

```
MAJ Anthony - Gozani Comparison for Iron - f1 tally used
C    Cell Cards
1    1  -7.874  1 -2 3 -4 5 -6  imp:n,p 1  $ Iron Target
2    0         #1 #3 -100      imp:n,p 1  $ empty space
3    0         #1 -7           imp:n,p 1  $ empty space
100  0          100            imp:n,p 0  $ void - outside of universe

C    Surface Cards
1    pz  100  $ bottom of target slab
2    pz  110  $ top of target slab
3    px  -5   $ back side of target
4    px  5    $ front side of target
5    py  -5   $ left side of target
6    py  5    $ right side of target
7    so  500  $ f1 tally sphere
100  so  1000  $ edge of universe

C    Data Cards
C    Material Cards
m1   26000 1.00 $ Iron
C    Source Cards
mode n p
sdef pos=0 0 0  dir=1  vec=0 0 1  par=1  erg=8.5  $ beam source up z axis
C    Tally Cards
f1:p 3   $ surface current tally
e1   0 0.05 0.1 0.15 0.2 0.25 0.3 0.35 0.4 0.45 0.5 0.55 0.6 0.65
     0.7 0.75 0.8 0.85 0.9 0.95
     1 1.05 1.1 1.15 1.2 1.25 1.3 1.35 1.4 1.45 1.5 1.55 1.6 1.65
     1.7 1.75 1.8 1.85 1.9 1.95
     2 2.05 2.1 2.15 2.2 2.25 2.3 2.35 2.4 2.45 2.5 2.55 2.6 2.65
     2.7 2.75 2.8 2.85 2.9 2.95
     3 3.05 3.1 3.15 3.2 3.25 3.3 3.35 3.4 3.45 3.5 3.55 3.6 3.65
     3.7 3.75 3.8 3.85 3.9 3.95
     4 4.05 4.1 4.15 4.2 4.25 4.3 4.35 4.4 4.45 4.5 4.55 4.6 4.65
     4.7 4.75 4.8 4.85 4.9 4.95 5
nps  1e6
```

Lead Code

```
MAJ Anthony - Gozani Comparison for Lead - f1 tally used
C    Cell Cards
1    1  -11.35  1 -2 3 -4 5 -6  imp:n,p 1  $ lead Target
2    0         #1 #3 -100      imp:n,p 1  $ empty space
3    0         #1 -7           imp:n,p 1  $ empty space
100  0          100            imp:n,p 0  $ void - outside of universe

C    Surface Cards
1    pz  100  $ bottom of target slab
2    pz  110  $ top of target slab
3    px  -5   $ back side of target
```

```
4    px  5    $ front side of target
5    py  -5   $ left side of target
6    py  5    $ right side of target
7    so  500  $ f1 tally sphere
100  so  1000  $ edge of universe

C    Data Cards
C    Material Cards
m1   82000 1.00 $ Lead
C    Source Cards
mode n p
sdef pos=0 0 0  dir=1  vec=0 0 1  par=1  erg=8.5  $ beam source up z axis
C    Tally Cards
f1:p 3   $ surface current tally
e1   0 0.05 0.1 0.15 0.2 0.25 0.3 0.35 0.4 0.45 0.5 0.55 0.6 0.65
     0.7 0.75 0.8 0.85 0.9 0.95
     1 1.05 1.1 1.15 1.2 1.25 1.3 1.35 1.4 1.45 1.5 1.55 1.6 1.65
     1.7 1.75 1.8 1.85 1.9 1.95
     2 2.05 2.1 2.15 2.2 2.25 2.3 2.35 2.4 2.45 2.5 2.55 2.6 2.65
     2.7 2.75 2.8 2.85 2.9 2.95
     3 3.05 3.1 3.15 3.2 3.25 3.3 3.35 3.4 3.45 3.5 3.55 3.6 3.65
     3.7 3.75 3.8 3.85 3.9 3.95
     4 4.05 4.1 4.15 4.2 4.25 4.3 4.35 4.4 4.45 4.5 4.55 4.6 4.65
     4.7 4.75 4.8 4.85 4.9 4.95 5
nps  1e6
```

Polyethylene Code

```
MAJ Anthony - Gozani Comparison for Polyethylene - f1 tally used
C    Cell Cards
1    1  -0.930  1 -2 3 -4 5 -6  imp:n,p 1  $ polyethylene target
2    0         #1 #3 -100      imp:n,p 1  $ empty space
3    0         #1 -7           imp:n,p 1  $ empty space
100  0          100            imp:n,p 0  $ void - outside of universe

C    Surface Cards
1    pz  100  $ bottom of target slab
2    pz  110  $ top of target slab
3    px  -5   $ back side of target
4    px  5    $ front side of target
5    py  -5   $ left side of target
6    py  5    $ right side of target
7    so  500  $ f1 tally sphere
100  so  1000  $ edge of universe

C    Data Cards
C    Material Cards
m1   01001 -0.143716  06012 -0.856284  $ Polyethylene
C    Source Cards
mode n p
sdef pos=0 0 0  dir=1  vec=0 0 1  par=1  erg=8.5  $ beam source up z axis
C    Tally Cards
f1:p 3   $ surface current tally
e1   0 0.05 0.1 0.15 0.2 0.25 0.3 0.35 0.4 0.45 0.5 0.55 0.6 0.65
```

```
    0.7 0.75 0.8 0.85 0.9 0.95
    1 1.05 1.1 1.15 1.2 1.25 1.3 1.35 1.4 1.45 1.5 1.55 1.6 1.65
    1.7 1.75 1.8 1.85 1.9 1.95
    2 2.05 2.1 2.15 2.2 2.25 2.3 2.35 2.4 2.45 2.5 2.55 2.6 2.65
    2.7 2.75 2.8 2.85 2.9 2.95
    3 3.05 3.1 3.15 3.2 3.25 3.3 3.35 3.4 3.45 3.5 3.55 3.6 3.65
    3.7 3.75 3.8 3.85 3.9 3.95
    4 4.05 4.1 4.15 4.2 4.25 4.3 4.35 4.4 4.45 4.5 4.55 4.6 4.65
    4.7 4.75 4.8 4.85 4.9 4.95 5
nps  1e6
```

U-235 Code

```
MAJ Anthony - Gozani Comparison for U235 - f1 tally used
C    Cell Cards
1    1  -18.95  1 -2 3 -4 5 -6  imp:n,p 1  $ U235 target
2    0         #1 #3 -100      imp:n,p 1  $ empty space
3    0         #1 -7           imp:n,p 1  $ empty space
100  0          100            imp:n,p 0  $ void - outside of universe

C    Surface Cards
1    pz  100  $ bottom of target slab
2    pz  101  $ top of target slab
3    px  -5   $ back side of target
4    px  5    $ front side of target
5    py  -5   $ left side of target
6    py  5    $ right side of target
7    so  500  $ f1 tally sphere
100  so  1000  $ edge of universe

C    Data Cards
C    Material Cards
m1   92235 1.00 $ U-235
C    Source Cards
mode n p
sdef pos=0 0 0  dir=1  vec=0 0 1  par=1  erg=8.5  $ beam source up z axis
C    Tally Cards
f1:p 3   $ surface current tally
e1   0 0.05 0.1 0.15 0.2 0.25 0.3 0.35 0.4 0.45 0.5 0.55 0.6 0.65
    0.7 0.75 0.8 0.85 0.9 0.95
    1 1.05 1.1 1.15 1.2 1.25 1.3 1.35 1.4 1.45 1.5 1.55 1.6 1.65
    1.7 1.75 1.8 1.85 1.9 1.95
    2 2.05 2.1 2.15 2.2 2.25 2.3 2.35 2.4 2.45 2.5 2.55 2.6 2.65
    2.7 2.75 2.8 2.85 2.9 2.95
    3 3.05 3.1 3.15 3.2 3.25 3.3 3.35 3.4 3.45 3.5 3.55 3.6 3.65
    3.7 3.75 3.8 3.85 3.9 3.95
    4 4.05 4.1 4.15 4.2 4.25 4.3 4.35 4.4 4.45 4.5 4.55 4.6 4.65
    4.7 4.75 4.8 4.85 4.9 4.95 5
nps  1e6
```

U-238 Code

```
MAJ Anthony - Gozani Comparison for U238 - f1 tally used
C    Cell Cards
```

```
1    1  -19.10  1 -2 3 -4 5 -6  imp:n,p 1  $ U238 target
2    0          #1 #3 -100      imp:n,p 1  $ empty space
3    0          #1 -7           imp:n,p 1  $ empty space
100  0           100             imp:n,p 0  $ void - outside of universe

C    Surface Cards
1    pz  100  $ bottom of target slab
2    pz  110  $ top of target slab
3    px  -5   $ back side of target
4    px  5    $ front side of target
5    py  -5   $ left side of target
6    py  5    $ right side of target
7    so  500  $ f1 tally sphere
100  so  1000  $ edge of universe

C    Data Cards
C    Material Cards
m1   92238 1.00 $ U238
C    Source Cards
mode n p
sdef pos=0 0 0  dir=1  vec=0 0 1  par=1  erg=8.5  $ beam source up z axis
C    Tally Cards
f1:p 3   $ surface current tally
e1   0 0.05 0.1 0.15 0.2 0.25 0.3 0.35 0.4 0.45 0.5 0.55 0.6 0.65
     0.7 0.75 0.8 0.85 0.9 0.95
     1 1.05 1.1 1.15 1.2 1.25 1.3 1.35 1.4 1.45 1.5 1.55 1.6 1.65
     1.7 1.75 1.8 1.85 1.9 1.95
     2 2.05 2.1 2.15 2.2 2.25 2.3 2.35 2.4 2.45 2.5 2.55 2.6 2.65
     2.7 2.75 2.8 2.85 2.9 2.95
     3 3.05 3.1 3.15 3.2 3.25 3.3 3.35 3.4 3.45 3.5 3.55 3.6 3.65
     3.7 3.75 3.8 3.85 3.9 3.95
     4 4.05 4.1 4.15 4.2 4.25 4.3 4.35 4.4 4.45 4.5 4.55 4.6 4.65
     4.7 4.75 4.8 4.85 4.9 4.95 5
nps  1e6
```

Appendix B. MCNP Input Codes for DTRA TEAMS Modeling

Background Code

```
MAJ Anthony - DTRA TEAMS - w/ table and container
C    Cell Cards
1    1  -0.001205  1 -100 #7 #8 #9 #10 #11 #12 #13
                #14 #15 #16 #17 #18   imp:n,p 1 $ air above ground
2    2  -2.74      -5 -100 #3 #4 #6   imp:n,p 1    $ ground
3    3  -7.82      -1 2 3 -4   imp:n,p 1       $ steel tube
4    1  -0.001205  -1 2 -3     imp:n,p 1       $ air inside hole
5    4  -2.3       -1 5 -100 #3 #4 #6   imp:n,p 1  $ concrete road
6    5  -2.3       -1 2 4 -6   imp:n,p 1       $ concrete tube
7    3  -7.82      8 -9 10 -11 12 -13   imp:n,p 1   $ steel table top
8    3  -7.82      -8 1 -14  imp:n,p 1     $ table leg 1
9    3  -7.82      -8 1 -15  imp:n,p 1     $ table leg 2
10   3  -7.82      -8 1 -16  imp:n,p 1     $ table leg 3
11   3  -7.82      -8 1 -17  imp:n,p 1     $ table leg 4
12   6  -2.6989    -23 28 19 -24 21 -22  imp:n,p 1  $ back of Al box
13   6  -2.6989    -23 28 25 -20 21 -22  imp:n,p 1  $ front of Al box
14   6  -2.6989    -23 28 24 -25 21 -26  imp:n,p 1  $ left of Al box
15   6  -2.6989    -23 28 24 -25 27 -22  imp:n,p 1  $ right of Al box
16   6  -2.6989    23 -18 19 -20 21 -22  imp:n,p 1  $ top of Al box
17   6  -2.6989    9 -28 19 -20 21 -22  imp:n,p 1  $ bottom of Al box
18   1  -0.001205  -23 24 -25 26 -27 28  imp:n,p 1  $ air inside box
100  0            100         imp:n,p 0       $ void

C    Surface Cards
1    pz  0        $ ground level
2    pz  -365.76   $ bottom of hole, 12' deep
3    cz  7.62      $ inside of steel tube, 3" radius
4    cz  10.16     $ outside of steel tube, 4" radius
5    pz  -30.48    $ thickness of road, 12" deep
6    cz  40.64     $ outside of concrete tube, 12" thick
7    pz  -182.88   $ plane for source
8    pz  100       $ bottom of table
9    pz  105       $ top of table
10   px  -50       $ back of table
11   px  50        $ front of table
12   py  -50       $ left side of table
13   py  50        $ right side of table
14   c/z  -50 -50 2  $ table leg 1, 2cm radius
15   c/z  -50 50 2   $ table leg 2, 2cm radius
16   c/z  50 -50 2   $ table leg 3, 2cm radius
17   c/z  50 50 2    $ table leg 4, 2cm radius
18   pz  125       $ top of container, outside
```

```
19   px  -10       $ back of container, outside
20   px  10        $ front of container, outside
21   py  -10       $ left side of container, outside
22   py  10        $ right side of container, outside
23   pz  124.5     $ top of container, inside
24   px  -9.5      $ back of container, inside
25   px  9.5       $ front of container, inside
26   py  -9.5      $ left side of container, inside
27   py  9.5       $ right side of container, inside
28   pz  105.5     $ bottom of container, inside
100  so  1000      $ edge of void

C    Data Cards
C    Material Cards
m1   06012 1.51e-4  07014 0.784437  08016 0.210750  $ air
     18040 4.671e-3
m2   08016 0.4660  14028 0.2772  13027 0.0813  $ ground
     26000 0.0500  20040 0.0363  11023 0.0283
     19039 0.0259  12024 0.0209  22048 0.0044
     01001 0.0014  15031 0.0012  25055 0.0010
     09019 0.0008  06012 0.0003  16032 0.0005
     23051 0.0001  17035 0.0005  24052 0.0001
     37085 0.0003  29000 0.0001  07014 5.0e-5
m3   06012 0.022831  26000 0.977170  $ steel
m4   01001 0.304245  06012 0.002870  08016 0.498628  $ ordinary concrete
     11023 0.009179  12000 7.17e-4  13027 0.010261
     14000 0.150505  19000 0.007114  20000 0.014882
     26000 0.001599
m5   01001 0.168759  06012 0.001416  08016 0.562522  $ Portland concrete
     11023 0.011838  12000 0.001400  13027 0.021354
     14000 0.204115  19000 0.005656  20000 0.018674
     26000 0.004264
m6   13027 1.0000    $ aluminum
C    Source Cards
mode n p
sdef pos=0 0 -182.88  par=1  erg=14  $ point source
C    Tally Cards
f35z:n 110 100 0.5 $ neutron ring detector: level with target w/ 100 cm radius
E35  0 0.05 0.1 0.15 0.2 0.25 0.3 0.35 0.4 0.45 0.5 0.55 0.6 0.65
     0.7 0.75 0.8 0.85 0.9 0.95
     1 1.05 1.1 1.15 1.2 1.25 1.3 1.35 1.4 1.45 1.5 1.55 1.6 1.65
     1.7 1.75 1.8 1.85 1.9 1.95
     2 2.05 2.1 2.15 2.2 2.25 2.3 2.35 2.4 2.45 2.5 2.55 2.6 2.65
     2.7 2.75 2.8 2.85 2.9 2.95
     3 3.05 3.1 3.15 3.2 3.25 3.3 3.35 3.4 3.45 3.5 3.55 3.6 3.65
```

```
    3.7 3.75 3.8 3.85 3.9 3.95
    4 4.05 4.1 4.15 4.2 4.25 4.3 4.35 4.4 4.45 4.5 4.55 4.6 4.65
    4.7 4.75 4.8 4.85 4.9 4.95
    5 5.05 5.1 5.15 5.2 5.25 5.3 5.35 5.4 5.45 5.5 5.55 5.6 5.65
    5.7 5.75 5.8 5.85 5.9 5.95 6
f45z:p 110 100 0.5 $ photon ring detector: level with target w/ 100 cm radius
E45  0 0.05 0.1 0.15 0.2 0.25 0.3 0.35 0.4 0.45 0.5 0.55 0.6 0.65
    0.7 0.75 0.8 0.85 0.9 0.95
    1 1.05 1.1 1.15 1.2 1.25 1.3 1.35 1.4 1.45 1.5 1.55 1.6 1.65
    1.7 1.75 1.8 1.85 1.9 1.95
    2 2.05 2.1 2.15 2.2 2.25 2.3 2.35 2.4 2.45 2.5 2.55 2.6 2.65
    2.7 2.75 2.8 2.85 2.9 2.95
    3 3.05 3.1 3.15 3.2 3.25 3.3 3.35 3.4 3.45 3.5 3.55 3.6 3.65
    3.7 3.75 3.8 3.85 3.9 3.95
    4 4.05 4.1 4.15 4.2 4.25 4.3 4.35 4.4 4.45 4.5 4.55 4.6 4.65
    4.7 4.75 4.8 4.85 4.9 4.95
    5 5.05 5.1 5.15 5.2 5.25 5.3 5.35 5.4 5.45 5.5 5.55 5.6 5.65
    5.7 5.75 5.8 5.85 5.9 5.95 6
ctme 720
```

Iron

```
MAJ Anthony - DTRA TEAMS - w/ Iron in container
C    Cell Cards
1    1  -0.001205  1 -100 #7 #8 #9 #10 #11 #12 #13
                #14 #15 #16 #17 #18   imp:n,p 1 $ air above ground
2    2  -2.74      -5 -100 #3 #4 #6   imp:n,p 1    $ ground
3    3  -7.82      -1 2 3 -4   imp:n,p 1       $ steel tube
4    1  -0.001205  -1 2 -3     imp:n,p 1       $ air inside hole
5    4  -2.3       -1 5 -100 #3 #4 #6   imp:n,p 1  $ concrete road
6    5  -2.3       -1 2 4 -6   imp:n,p 1       $ concrete tube
7    3  -7.82      8 -9 10 -11 12 -13   imp:n,p 1   $ steel table top
8    3  -7.82      -8 1 -14  imp:n,p 1     $ table leg 1
9    3  -7.82      -8 1 -15  imp:n,p 1     $ table leg 2
10   3  -7.82      -8 1 -16  imp:n,p 1     $ table leg 3
11   3  -7.82      -8 1 -17  imp:n,p 1     $ table leg 4
12   6  -2.6989    -23 28 19 -24 21 -22  imp:n,p 1  $ back of Al box
13   6  -2.6989    -23 28 25 -20 21 -22  imp:n,p 1  $ front of Al box
14   6  -2.6989    -23 28 24 -25 21 -26  imp:n,p 1  $ left of Al box
15   6  -2.6989    -23 28 24 -25 27 -22  imp:n,p 1  $ right of Al box
16   6  -2.6989    23 -18 19 -20 21 -22  imp:n,p 1  $ top of Al box
17   6  -2.6989    9 -28 19 -20 21 -22   imp:n,p 1  $ bottom of Al box
18   7  -7.874     -23 24 -25 26 -27 28  imp:n,p 1  $ iron inside box
100  0            100         imp:n,p 0       $ void
```

```
C    Surface Cards
1    pz  0         $ ground level
2    pz  -365.76   $ bottom of hole, 12' deep
3    cz  7.62      $ inside of steel tube, 3" radius
4    cz  10.16     $ outside of steel tube, 4" radius
5    pz  -30.48    $ thickness of road, 12" deep
6    cz  40.64     $ outside of concrete tube, 12" thick
7    pz  -182.88   $ plane for source
8    pz  100       $ bottom of table
9    pz  105       $ top of table
10   px  -50       $ back of table
11   px  50        $ front of table
12   py  -50       $ left side of table
13   py  50        $ right side of table
14   c/z  -50 -50 2  $ table leg 1, 2cm radius
15   c/z  -50 50 2   $ table leg 2, 2cm radius
16   c/z  50 -50 2   $ table leg 3, 2cm radius
17   c/z  50 50 2    $ table leg 4, 2cm radius
18   pz  125       $ top of container, outside
19   px  -10       $ back of container, outside
20   px  10        $ front of container, outside
21   py  -10       $ left side of container, outside
22   py  10        $ right side of container, outside
23   pz  124.5     $ top of container, inside
24   px  -9.5      $ back of container, inside
25   px  9.5       $ front of container, inside
26   py  -9.5      $ left side of container, inside
27   py  9.5       $ right side of container, inside
28   pz  105.5     $ bottom of container, inside
100  so  1000      $ edge of void

C    Data Cards
C    Material Cards
m1   06012 1.51e-4  07014 0.784437  08016 0.210750  $ air
     18040 4.671e-3
m2   08016 0.4660  14028 0.2772  13027 0.0813  $ ground
     26000 0.0500  20040 0.0363  11023 0.0283
     19039 0.0259  12024 0.0209  22048 0.0044
     01001 0.0014  15031 0.0012  25055 0.0010
     09019 0.0008  06012 0.0003  16032 0.0005
     23051 0.0001  17035 0.0005  24052 0.0001
     37085 0.0003  29000 0.0001  07014 5.0e-5
m3   06012 0.022831  26000 0.977170  $ steel
m4   01001 0.304245  06012 0.002870  08016 0.498628  $ ordinary concrete
     11023 0.009179  12000 7.17e-4  13027 0.010261
```

```
    14000 0.150505  19000 0.007114  20000 0.014882
    26000 0.001599
m5   01001 0.168759  06012 0.001416  08016 0.562522  $ Portland concrete
    11023 0.011838  12000 0.001400  13027 0.021354
    14000 0.204115  19000 0.005656  20000 0.018674
    26000 0.004264
m6   13027 1.0000    $ aluminum
m7   26000 1.0000    $ iron
C    Source Cards
mode n p
sdef pos=0 0 -182.88  par=1  erg=14  $ point source
C    Tally Cards
f35z:n 110 100 0.5 $ neutron ring detector: level with target w/ 100 cm radius
E35  0 0.05 0.1 0.15 0.2 0.25 0.3 0.35 0.4 0.45 0.5 0.55 0.6 0.65
    0.7 0.75 0.8 0.85 0.9 0.95
    1 1.05 1.1 1.15 1.2 1.25 1.3 1.35 1.4 1.45 1.5 1.55 1.6 1.65
    1.7 1.75 1.8 1.85 1.9 1.95
    2 2.05 2.1 2.15 2.2 2.25 2.3 2.35 2.4 2.45 2.5 2.55 2.6 2.65
    2.7 2.75 2.8 2.85 2.9 2.95
    3 3.05 3.1 3.15 3.2 3.25 3.3 3.35 3.4 3.45 3.5 3.55 3.6 3.65
    3.7 3.75 3.8 3.85 3.9 3.95
    4 4.05 4.1 4.15 4.2 4.25 4.3 4.35 4.4 4.45 4.5 4.55 4.6 4.65
    4.7 4.75 4.8 4.85 4.9 4.95
    5 5.05 5.1 5.15 5.2 5.25 5.3 5.35 5.4 5.45 5.5 5.55 5.6 5.65
    5.7 5.75 5.8 5.85 5.9 5.95 6
f45z:p 110 100 0.5 $ photon ring detector: level with target w/ 100 cm radius
E45  0 0.05 0.1 0.15 0.2 0.25 0.3 0.35 0.4 0.45 0.5 0.55 0.6 0.65
    0.7 0.75 0.8 0.85 0.9 0.95
    1 1.05 1.1 1.15 1.2 1.25 1.3 1.35 1.4 1.45 1.5 1.55 1.6 1.65
    1.7 1.75 1.8 1.85 1.9 1.95
    2 2.05 2.1 2.15 2.2 2.25 2.3 2.35 2.4 2.45 2.5 2.55 2.6 2.65
    2.7 2.75 2.8 2.85 2.9 2.95
    3 3.05 3.1 3.15 3.2 3.25 3.3 3.35 3.4 3.45 3.5 3.55 3.6 3.65
    3.7 3.75 3.8 3.85 3.9 3.95
    4 4.05 4.1 4.15 4.2 4.25 4.3 4.35 4.4 4.45 4.5 4.55 4.6 4.65
    4.7 4.75 4.8 4.85 4.9 4.95
    5 5.05 5.1 5.15 5.2 5.25 5.3 5.35 5.4 5.45 5.5 5.55 5.6 5.65
    5.7 5.75 5.8 5.85 5.9 5.95 6
ctme 720
```

Lead

```
MAJ Anthony - DTRA TEAMS - w/ Lead in container
C    Cell Cards
1    1  -0.001205  1 -100 #7 #8 #9 #10 #11 #12 #13
```

```
                #14 #15 #16 #17 #18   imp:n,p 1 $ air above ground
2    2  -2.74      -5 -100 #3 #4 #6   imp:n,p 1    $ ground
3    3  -7.82      -1 2 3 -4   imp:n,p 1       $ steel tube
4    1  -0.001205  -1 2 -3     imp:n,p 1       $ air inside hole
5    4  -2.3       -1 5 -100 #3 #4 #6   imp:n,p 1  $ concrete road
6    5  -2.3       -1 2 4 -6   imp:n,p 1       $ concrete tube
7    3  -7.82      8 -9 10 -11 12 -13   imp:n,p 1   $ steel table top
8    3  -7.82      -8 1 -14  imp:n,p 1     $ table leg 1
9    3  -7.82      -8 1 -15  imp:n,p 1     $ table leg 2
10   3  -7.82      -8 1 -16  imp:n,p 1     $ table leg 3
11   3  -7.82      -8 1 -17  imp:n,p 1     $ table leg 4
12   6  -2.6989    -23 28 19 -24 21 -22  imp:n,p 1  $ back of Al box
13   6  -2.6989    -23 28 25 -20 21 -22  imp:n,p 1  $ front of Al box
14   6  -2.6989    -23 28 24 -25 21 -26  imp:n,p 1  $ left of Al box
15   6  -2.6989    -23 28 24 -25 27 -22  imp:n,p 1  $ right of Al box
16   6  -2.6989    23 -18 19 -20 21 -22  imp:n,p 1  $ top of Al box
17   6  -2.6989    9 -28 19 -20 21 -22   imp:n,p 1  $ bottom of Al box
18   7  -11.35     -23 24 -25 26 -27 28  imp:n,p 1  $ lead inside box
100  0            100         imp:n,p 0       $ void

C    Surface Cards
1    pz  0        $ ground level
2    pz  -365.76   $ bottom of hole, 12' deep
3    cz  7.62      $ inside of steel tube, 3" radius
4    cz  10.16     $ outside of steel tube, 4" radius
5    pz  -30.48    $ thickness of road, 12" deep
6    cz  40.64     $ outside of concrete tube, 12" thick
7    pz  -182.88   $ plane for source
8    pz  100       $ bottom of table
9    pz  105       $ top of table
10   px  -50       $ back of table
11   px  50        $ front of table
12   py  -50       $ left side of table
13   py  50        $ right side of table
14   c/z  -50 -50 2  $ table leg 1, 2cm radius
15   c/z  -50 50 2   $ table leg 2, 2cm radius
16   c/z  50 -50 2   $ table leg 3, 2cm radius
17   c/z  50 50 2    $ table leg 4, 2cm radius
18   pz  125       $ top of container, outside
19   px  -10       $ back of container, outside
20   px  10        $ front of container, outside
21   py  -10       $ left side of container, outside
22   py  10        $ right side of container, outside
23   pz  124.5     $ top of container, inside
24   px  -9.5      $ back of container, inside
```

```
25   px  9.5       $ front of container, inside
26   py  -9.5      $ left side of container, inside
27   py  9.5       $ right side of container, inside
28   pz  105.5     $ bottom of container, inside
100  so  1000      $ edge of void

C    Data Cards
C    Material Cards
m1   06012 1.51e-4  07014 0.784437  08016 0.210750  $ air
     18040 4.671e-3
m2   08016 0.4660  14028 0.2772  13027 0.0813  $ ground
     26000 0.0500  20040 0.0363  11023 0.0283
     19039 0.0259  12024 0.0209  22048 0.0044
     01001 0.0014  15031 0.0012  25055 0.0010
     09019 0.0008  06012 0.0003  16032 0.0005
     23051 0.0001  17035 0.0005  24052 0.0001
     37085 0.0003  29000 0.0001  07014 5.0e-5
m3   06012 0.022831  26000 0.977170  $ steel
m4   01001 0.304245  06012 0.002870  08016 0.498628  $ ordinary concrete
     11023 0.009179  12000 7.17e-4  13027 0.010261
     14000 0.150505  19000 0.007114  20000 0.014882
     26000 0.001599
m5   01001 0.168759  06012 0.001416  08016 0.562522  $ Portland concrete
     11023 0.011838  12000 0.001400  13027 0.021354
     14000 0.204115  19000 0.005656  20000 0.018674
     26000 0.004264
m6   13027 1.0000    $ aluminum
m7   82000 1.0000    $ lead
C    Source Cards
mode n p
sdef pos=0 0 -182.88  par=1  erg=14  $ point source
C    Tally Cards
f35z:n 110 100 0.5 $ neutron ring detector: level with target w/ 100 cm radius
E35  0 0.05 0.1 0.15 0.2 0.25 0.3 0.35 0.4 0.45 0.5 0.55 0.6 0.65
     0.7 0.75 0.8 0.85 0.9 0.95
     1 1.05 1.1 1.15 1.2 1.25 1.3 1.35 1.4 1.45 1.5 1.55 1.6 1.65
     1.7 1.75 1.8 1.85 1.9 1.95
     2 2.05 2.1 2.15 2.2 2.25 2.3 2.35 2.4 2.45 2.5 2.55 2.6 2.65
     2.7 2.75 2.8 2.85 2.9 2.95
     3 3.05 3.1 3.15 3.2 3.25 3.3 3.35 3.4 3.45 3.5 3.55 3.6 3.65
     3.7 3.75 3.8 3.85 3.9 3.95
     4 4.05 4.1 4.15 4.2 4.25 4.3 4.35 4.4 4.45 4.5 4.55 4.6 4.65
     4.7 4.75 4.8 4.85 4.9 4.95
     5 5.05 5.1 5.15 5.2 5.25 5.3 5.35 5.4 5.45 5.5 5.55 5.6 5.65
     5.7 5.75 5.8 5.85 5.9 5.95 6
```

```
f45z:p 110 100 0.5 $ photon ring detector: level with target w/ 100 cm radius
E45  0 0.05 0.1 0.15 0.2 0.25 0.3 0.35 0.4 0.45 0.5 0.55 0.6 0.65
     0.7 0.75 0.8 0.85 0.9 0.95
     1 1.05 1.1 1.15 1.2 1.25 1.3 1.35 1.4 1.45 1.5 1.55 1.6 1.65
     1.7 1.75 1.8 1.85 1.9 1.95
     2 2.05 2.1 2.15 2.2 2.25 2.3 2.35 2.4 2.45 2.5 2.55 2.6 2.65
     2.7 2.75 2.8 2.85 2.9 2.95
     3 3.05 3.1 3.15 3.2 3.25 3.3 3.35 3.4 3.45 3.5 3.55 3.6 3.65
     3.7 3.75 3.8 3.85 3.9 3.95
     4 4.05 4.1 4.15 4.2 4.25 4.3 4.35 4.4 4.45 4.5 4.55 4.6 4.65
     4.7 4.75 4.8 4.85 4.9 4.95
     5 5.05 5.1 5.15 5.2 5.25 5.3 5.35 5.4 5.45 5.5 5.55 5.6 5.65
     5.7 5.75 5.8 5.85 5.9 5.95 6
ctme 720
```

Polyethylene

```
MAJ Anthony - DTRA TEAMS - TEAME w/ Lead in container
C    Cell Cards
1    1  -0.001205  1 -100 #7 #8 #9 #10 #11 #12 #13
                #14 #15 #16 #17 #18   imp:n,p 1 $ air above ground
2    2  -2.74      -5 -100 #3 #4 #6   imp:n,p 1    $ ground
3    3  -7.82      -1 2 3 -4   imp:n,p 1       $ steel tube
4    1  -0.001205  -1 2 -3     imp:n,p 1       $ air inside hole
5    4  -2.3       -1 5 -100 #3 #4 #6   imp:n,p 1  $ concrete road
6    5  -2.3       -1 2 4 -6   imp:n,p 1       $ concrete tube
7    3  -7.82      8 -9 10 -11 12 -13   imp:n,p 1   $ steel table top
8    3  -7.82      -8 1 -14  imp:n,p 1     $ table leg 1
9    3  -7.82      -8 1 -15  imp:n,p 1     $ table leg 2
10   3  -7.82      -8 1 -16  imp:n,p 1     $ table leg 3
11   3  -7.82      -8 1 -17  imp:n,p 1     $ table leg 4
12   6  -2.6989    -23 28 19 -24 21 -22  imp:n,p 1  $ back of Al box
13   6  -2.6989    -23 28 25 -20 21 -22  imp:n,p 1  $ front of Al box
14   6  -2.6989    -23 28 24 -25 21 -26  imp:n,p 1  $ left of Al box
15   6  -2.6989    -23 28 24 -25 27 -22  imp:n,p 1  $ right of Al box
16   6  -2.6989    23 -18 19 -20 21 -22  imp:n,p 1  $ top of Al box
17   6  -2.6989    9 -28 19 -20 21 -22   imp:n,p 1  $ bottom of Al box
18   7  -0.930     -23 24 -25 26 -27 28  imp:n,p 1  $ Poly inside box
100  0            100         imp:n,p 0       $ void

C    Surface Cards
1    pz  0         $ ground level
2    pz  -365.76   $ bottom of hole, 12' deep
3    cz  7.62      $ inside of steel tube, 3" radius
4    cz  10.16     $ outside of steel tube, 4" radius
```

```
5    pz  -30.48    $ thickness of road, 12" deep
6    cz  40.64     $ outside of concrete tube, 12" thick
7    pz  -182.88   $ plane for source
8    pz  100       $ bottom of table
9    pz  105       $ top of table
10   px  -50       $ back of table
11   px  50        $ front of table
12   py  -50       $ left side of table
13   py  50        $ right side of table
14   c/z  -50 -50 2  $ table leg 1, 2cm radius
15   c/z  -50 50 2   $ table leg 2, 2cm radius
16   c/z  50 -50 2   $ table leg 3, 2cm radius
17   c/z  50 50 2    $ table leg 4, 2cm radius
18   pz  125       $ top of container, outside
19   px  -10       $ back of container, outside
20   px  10        $ front of container, outside
21   py  -10       $ left side of container, outside
22   py  10        $ right side of container, outside
23   pz  124.5     $ top of container, inside
24   px  -9.5      $ back of container, inside
25   px  9.5       $ front of container, inside
26   py  -9.5      $ left side of container, inside
27   py  9.5       $ right side of container, inside
28   pz  105.5     $ bottom of container, inside
100  so  1000      $ edge of void

C    Data Cards
C    Material Cards
m1   06012 1.51e-4  07014 0.784437  08016 0.210750  $ air
     18040 4.671e-3
m2   08016 0.4660  14028 0.2772  13027 0.0813  $ ground
     26000 0.0500  20040 0.0363  11023 0.0283
     19039 0.0259  12024 0.0209  22048 0.0044
     01001 0.0014  15031 0.0012  25055 0.0010
     09019 0.0008  06012 0.0003  16032 0.0005
     23051 0.0001  17035 0.0005  24052 0.0001
     37085 0.0003  29000 0.0001  07014 5.0e-5
m3   06012 0.022831  26000 0.977170  $ steel
m4   01001 0.304245  06012 0.002870  08016 0.498628  $ ordinary concrete
     11023 0.009179  12000 7.17e-4  13027 0.010261
     14000 0.150505  19000 0.007114  20000 0.014882
     26000 0.001599
m5   01001 0.168759  06012 0.001416  08016 0.562522  $ Portland concrete
     11023 0.011838  12000 0.001400  13027 0.021354
     14000 0.204115  19000 0.005656  20000 0.018674
```

```
     26000 0.004264
m6   13027 1.0000    $ aluminum
m7   01001 -0.143716  06012 -0.856284  $ polyethylene
C    Source Cards
mode n p
sdef pos=0 0 -182.88  par=1  erg=14  $ point source
C    Tally Cards
f35z:n 110 100 0.5 $ neutron ring detector: level with target w/ 100 cm radius
E35  0 0.05 0.1 0.15 0.2 0.25 0.3 0.35 0.4 0.45 0.5 0.55 0.6 0.65
     0.7 0.75 0.8 0.85 0.9 0.95
     1 1.05 1.1 1.15 1.2 1.25 1.3 1.35 1.4 1.45 1.5 1.55 1.6 1.65
     1.7 1.75 1.8 1.85 1.9 1.95
     2 2.05 2.1 2.15 2.2 2.25 2.3 2.35 2.4 2.45 2.5 2.55 2.6 2.65
     2.7 2.75 2.8 2.85 2.9 2.95
     3 3.05 3.1 3.15 3.2 3.25 3.3 3.35 3.4 3.45 3.5 3.55 3.6 3.65
     3.7 3.75 3.8 3.85 3.9 3.95
     4 4.05 4.1 4.15 4.2 4.25 4.3 4.35 4.4 4.45 4.5 4.55 4.6 4.65
     4.7 4.75 4.8 4.85 4.9 4.95
     5 5.05 5.1 5.15 5.2 5.25 5.3 5.35 5.4 5.45 5.5 5.55 5.6 5.65
     5.7 5.75 5.8 5.85 5.9 5.95 6
f45z:p 110 100 0.5 $ photon ring detector: level with target w/ 100 cm radius
E45  0 0.05 0.1 0.15 0.2 0.25 0.3 0.35 0.4 0.45 0.5 0.55 0.6 0.65
     0.7 0.75 0.8 0.85 0.9 0.95
     1 1.05 1.1 1.15 1.2 1.25 1.3 1.35 1.4 1.45 1.5 1.55 1.6 1.65
     1.7 1.75 1.8 1.85 1.9 1.95
     2 2.05 2.1 2.15 2.2 2.25 2.3 2.35 2.4 2.45 2.5 2.55 2.6 2.65
     2.7 2.75 2.8 2.85 2.9 2.95
     3 3.05 3.1 3.15 3.2 3.25 3.3 3.35 3.4 3.45 3.5 3.55 3.6 3.65
     3.7 3.75 3.8 3.85 3.9 3.95
     4 4.05 4.1 4.15 4.2 4.25 4.3 4.35 4.4 4.45 4.5 4.55 4.6 4.65
     4.7 4.75 4.8 4.85 4.9 4.95
     5 5.05 5.1 5.15 5.2 5.25 5.3 5.35 5.4 5.45 5.5 5.55 5.6 5.65
     5.7 5.75 5.8 5.85 5.9 5.95 6
ctme 720
```

U-235

```
MAJ Anthony - DTRA TEAMS - w/ 9x9x1 cm container & U-235
C    Cell Cards
1    1  -0.001205  1 -100 #7 #8 #9 #10 #11 #12 #13
                 #14 #15 #16 #17 #18   imp:n,p 1 $ air above ground
2    2  -2.74      -5 -100 #3 #4 #6   imp:n,p 1    $ ground
3    3  -7.82      -1 2 3 -4   imp:n,p 1       $ steel tube
4    1  -0.001205  -1 2 -3     imp:n,p 1       $ air inside hole
5    4  -2.3       -1 5 -100 #3 #4 #6   imp:n,p 1  $ concrete road
```

```
6    5  -2.3       -1 2 4 -6   imp:n,p 1       $ concrete tube
7    3  -7.82      8 -9 10 -11 12 -13   imp:n,p 1   $ steel table top
8    3  -7.82      -8 1 -14  imp:n,p 1     $ table leg 1
9    3  -7.82      -8 1 -15  imp:n,p 1     $ table leg 2
10   3  -7.82      -8 1 -16  imp:n,p 1     $ table leg 3
11   3  -7.82      -8 1 -17  imp:n,p 1     $ table leg 4
12   6  -2.6989    -23 28 19 -24 21 -22  imp:n,p 1  $ back of Al box
13   6  -2.6989    -23 28 25 -20 21 -22  imp:n,p 1  $ front of Al box
14   6  -2.6989    -23 28 24 -25 21 -26  imp:n,p 1  $ left of Al box
15   6  -2.6989    -23 28 24 -25 27 -22  imp:n,p 1  $ right of Al box
16   6  -2.6989    23 -18 19 -20 21 -22  imp:n,p 1  $ top of Al box
17   6  -2.6989    9 -28 19 -20 21 -22   imp:n,p 1  $ bottom of Al box
18   7  -18.95     -23 24 -25 26 -27 28  imp:n,p 1  $ u-235 inside box
100  0            100         imp:n,p 0       $ void

C    Surface Cards
1    pz  0         $ ground level
2    pz  -365.76   $ bottom of hole, 12' deep
3    cz  7.62      $ inside of steel tube, 3" radius
4    cz  10.16     $ outside of steel tube, 4" radius
5    pz  -30.48    $ thickness of road, 12" deep
6    cz  40.64     $ outside of concrete tube, 12" thick
7    pz  -182.88   $ plane for source
8    pz  100       $ bottom of table
9    pz  105       $ top of table
10   px  -50       $ back of table
11   px  50        $ front of table
12   py  -50       $ left side of table
13   py  50        $ right side of table
14   c/z  -50 -50 2  $ table leg 1, 2cm radius
15   c/z  -50 50 2   $ table leg 2, 2cm radius
16   c/z  50 -50 2   $ table leg 3, 2cm radius
17   c/z  50 50 2    $ table leg 4, 2cm radius
18   pz  107       $ top of container, outside
19   px  -5        $ back of container, outside
20   px  5         $ front of container, outside
21   py  -5        $ left side of container, outside
22   py  5         $ right side of container, outside
23   pz  106.5     $ top of container, inside
24   px  -4.5      $ back of container, inside
25   px  4.5       $ front of container, inside
26   py  -4.5      $ left side of container, inside
27   py  4.5       $ right side of container, inside
28   pz  105.5     $ bottom of container, inside
100  so  1000      $ edge of void
```

```
C    Data Cards
C    Material Cards
m1   06012 1.51e-4  07014 0.784437  08016 0.210750  $ air
     18040 4.671e-3
m2   08016 0.4660  14028 0.2772  13027 0.0813  $ ground
     26000 0.0500  20040 0.0363  11023 0.0283
     19039 0.0259  12024 0.0209  22048 0.0044
     01001 0.0014  15031 0.0012  25055 0.0010
     09019 0.0008  06012 0.0003  16032 0.0005
     23051 0.0001  17035 0.0005  24052 0.0001
     37085 0.0003  29000 0.0001  07014 5.0e-5
m3   06012 0.022831  26000 0.977170  $ steel
m4   01001 0.304245  06012 0.002870  08016 0.498628  $ ordinary concrete
     11023 0.009179  12000 7.17e-4  13027 0.010261
     14000 0.150505  19000 0.007114  20000 0.014882
     26000 0.001599
m5   01001 0.168759  06012 0.001416  08016 0.562522  $ Portland concrete
     11023 0.011838  12000 0.001400  13027 0.021354
     14000 0.204115  19000 0.005656  20000 0.018674
     26000 0.004264
m6   13027 1.0000    $ aluminum
m7   92235 1.0000    $ U-235
C    Source Cards
mode n p
sdef pos=0 0 -182.88  par=1  erg=14  $ point source
C    Tally Cards
f35z:n 110 100 0.5 $ neutron ring detector: level with target w/ 100 cm radius
E35  0 0.05 0.1 0.15 0.2 0.25 0.3 0.35 0.4 0.45 0.5 0.55 0.6 0.65
     0.7 0.75 0.8 0.85 0.9 0.95
     1 1.05 1.1 1.15 1.2 1.25 1.3 1.35 1.4 1.45 1.5 1.55 1.6 1.65
     1.7 1.75 1.8 1.85 1.9 1.95
     2 2.05 2.1 2.15 2.2 2.25 2.3 2.35 2.4 2.45 2.5 2.55 2.6 2.65
     2.7 2.75 2.8 2.85 2.9 2.95
     3 3.05 3.1 3.15 3.2 3.25 3.3 3.35 3.4 3.45 3.5 3.55 3.6 3.65
     3.7 3.75 3.8 3.85 3.9 3.95
     4 4.05 4.1 4.15 4.2 4.25 4.3 4.35 4.4 4.45 4.5 4.55 4.6 4.65
     4.7 4.75 4.8 4.85 4.9 4.95
     5 5.05 5.1 5.15 5.2 5.25 5.3 5.35 5.4 5.45 5.5 5.55 5.6 5.65
     5.7 5.75 5.8 5.85 5.9 5.95 6
f45z:p 110 100 0.5 $ photon ring detector: level with target w/ 100 cm radius
E45  0 0.05 0.1 0.15 0.2 0.25 0.3 0.35 0.4 0.45 0.5 0.55 0.6 0.65
     0.7 0.75 0.8 0.85 0.9 0.95
     1 1.05 1.1 1.15 1.2 1.25 1.3 1.35 1.4 1.45 1.5 1.55 1.6 1.65
     1.7 1.75 1.8 1.85 1.9 1.95
```

2 2.05 2.1 2.15 2.2 2.25 2.3 2.35 2.4 2.45 2.5 2.55 2.6 2.65
2.7 2.75 2.8 2.85 2.9 2.95
3 3.05 3.1 3.15 3.2 3.25 3.3 3.35 3.4 3.45 3.5 3.55 3.6 3.65
3.7 3.75 3.8 3.85 3.9 3.95
4 4.05 4.1 4.15 4.2 4.25 4.3 4.35 4.4 4.45 4.5 4.55 4.6 4.65
4.7 4.75 4.8 4.85 4.9 4.95
5 5.05 5.1 5.15 5.2 5.25 5.3 5.35 5.4 5.45 5.5 5.55 5.6 5.65
5.7 5.75 5.8 5.85 5.9 5.95 6
ctme 720

U-238

MAJ Anthony - DTRA TEAMS - w/ U-238 in container

```
C    Cell Cards
1    1  -0.001205  1 -100 #7 #8 #9 #10 #11 #12 #13
                #14 #15 #16 #17 #18   imp:n,p 1 $ air above ground
2    2  -2.74      -5 -100 #3 #4 #6   imp:n,p 1    $ ground
3    3  -7.82      -1 2 3 -4   imp:n,p 1       $ steel tube
4    1  -0.001205  -1 2 -3     imp:n,p 1       $ air inside hole
5    4  -2.3       -1 5 -100 #3 #4 #6   imp:n,p 1  $ concrete road
6    5  -2.3       -1 2 4 -6   imp:n,p 1       $ concrete tube
7    3  -7.82      8 -9 10 -11 12 -13   imp:n,p 1   $ steel table top
8    3  -7.82      -8 1 -14  imp:n,p 1     $ table leg 1
9    3  -7.82      -8 1 -15  imp:n,p 1     $ table leg 2
10   3  -7.82      -8 1 -16  imp:n,p 1     $ table leg 3
11   3  -7.82      -8 1 -17  imp:n,p 1     $ table leg 4
12   6  -2.6989    -23 28 19 -24 21 -22  imp:n,p 1  $ back of Al box
13   6  -2.6989    -23 28 25 -20 21 -22  imp:n,p 1  $ front of Al box
14   6  -2.6989    -23 28 24 -25 21 -26  imp:n,p 1  $ left of Al box
15   6  -2.6989    -23 28 24 -25 27 -22  imp:n,p 1  $ right of Al box
16   6  -2.6989    23 -18 19 -20 21 -22  imp:n,p 1  $ top of Al box
17   6  -2.6989    9 -28 19 -20 21 -22   imp:n,p 1  $ bottom of Al box
18   7  -19.10     -23 24 -25 26 -27 28  imp:n,p 1  $ u-238 inside box
100  0            100         imp:n,p 0       $ void

C    Surface Cards
1    pz  0         $ ground level
2    pz  -365.76   $ bottom of hole, 12' deep
3    cz  7.62      $ inside of steel tube, 3" radius
4    cz  10.16     $ outside of steel tube, 4" radius
5    pz  -30.48    $ thickness of road, 12" deep
6    cz  40.64     $ outside of concrete tube, 12" thick
7    pz  -182.88   $ plane for source
8    pz  100       $ bottom of table
9    pz  105       $ top of table
```

```
10   px  -50       $ back of table
11   px  50        $ front of table
12   py  -50       $ left side of table
13   py  50        $ right side of table
14   c/z  -50 -50 2  $ table leg 1, 2cm radius
15   c/z  -50 50 2   $ table leg 2, 2cm radius
16   c/z  50 -50 2   $ table leg 3, 2cm radius
17   c/z  50 50 2    $ table leg 4, 2cm radius
18   pz  125       $ top of container, outside
19   px  -10       $ back of container, outside
20   px  10        $ front of container, outside
21   py  -10       $ left side of container, outside
22   py  10        $ right side of container, outside
23   pz  124.5     $ top of container, inside
24   px  -9.5      $ back of container, inside
25   px  9.5       $ front of container, inside
26   py  -9.5      $ left side of container, inside
27   py  9.5       $ right side of container, inside
28   pz  105.5     $ bottom of container, inside
100  so  1000      $ edge of void

C    Data Cards
C    Material Cards
m1   06012 1.51e-4  07014 0.784437  08016 0.210750  $ air
     18040 4.671e-3
m2   08016 0.4660  14028 0.2772  13027 0.0813  $ ground
     26000 0.0500  20040 0.0363  11023 0.0283
     19039 0.0259  12024 0.0209  22048 0.0044
     01001 0.0014  15031 0.0012  25055 0.0010
     09019 0.0008  06012 0.0003  16032 0.0005
     23051 0.0001  17035 0.0005  24052 0.0001
     37085 0.0003  29000 0.0001  07014 5.0e-5
m3   06012 0.022831  26000 0.977170  $ steel
m4   01001 0.304245  06012 0.002870  08016 0.498628  $ ordinary concrete
     11023 0.009179  12000 7.17e-4  13027 0.010261
     14000 0.150505  19000 0.007114  20000 0.014882
     26000 0.001599
m5   01001 0.168759  06012 0.001416  08016 0.562522  $ Portland concrete
     11023 0.011838  12000 0.001400  13027 0.021354
     14000 0.204115  19000 0.005656  20000 0.018674
     26000 0.004264
m6   13027 1.0000    $ aluminum
m7   92238 1.0000    $ U-238
C    Source Cards
mode n p
```

```
sdef pos=0 0 -182.88  par=1  erg=14  $ point source
C    Tally Cards
f35z:n 110 100 0.5 $ neutron ring detector: level with target w/ 100 cm radius
E35  0 0.05 0.1 0.15 0.2 0.25 0.3 0.35 0.4 0.45 0.5 0.55 0.6 0.65
     0.7 0.75 0.8 0.85 0.9 0.95
     1 1.05 1.1 1.15 1.2 1.25 1.3 1.35 1.4 1.45 1.5 1.55 1.6 1.65
     1.7 1.75 1.8 1.85 1.9 1.95
     2 2.05 2.1 2.15 2.2 2.25 2.3 2.35 2.4 2.45 2.5 2.55 2.6 2.65
     2.7 2.75 2.8 2.85 2.9 2.95
     3 3.05 3.1 3.15 3.2 3.25 3.3 3.35 3.4 3.45 3.5 3.55 3.6 3.65
     3.7 3.75 3.8 3.85 3.9 3.95
     4 4.05 4.1 4.15 4.2 4.25 4.3 4.35 4.4 4.45 4.5 4.55 4.6 4.65
     4.7 4.75 4.8 4.85 4.9 4.95
     5 5.05 5.1 5.15 5.2 5.25 5.3 5.35 5.4 5.45 5.5 5.55 5.6 5.65
     5.7 5.75 5.8 5.85 5.9 5.95 6
f45z:p 110 100 0.5 $ photon ring detector: level with target w/ 100 cm radius
E45  0 0.05 0.1 0.15 0.2 0.25 0.3 0.35 0.4 0.45 0.5 0.55 0.6 0.65
     0.7 0.75 0.8 0.85 0.9 0.95
     1 1.05 1.1 1.15 1.2 1.25 1.3 1.35 1.4 1.45 1.5 1.55 1.6 1.65
     1.7 1.75 1.8 1.85 1.9 1.95
     2 2.05 2.1 2.15 2.2 2.25 2.3 2.35 2.4 2.45 2.5 2.55 2.6 2.65
     2.7 2.75 2.8 2.85 2.9 2.95
     3 3.05 3.1 3.15 3.2 3.25 3.3 3.35 3.4 3.45 3.5 3.55 3.6 3.65
     3.7 3.75 3.8 3.85 3.9 3.95
     4 4.05 4.1 4.15 4.2 4.25 4.3 4.35 4.4 4.45 4.5 4.55 4.6 4.65
     4.7 4.75 4.8 4.85 4.9 4.95
     5 5.05 5.1 5.15 5.2 5.25 5.3 5.35 5.4 5.45 5.5 5.55 5.6 5.65
     5.7 5.75 5.8 5.85 5.9 5.95 6
ctme 720
```

Appendix C. MESH Tally Input Code for Background Source

```
MAJ Anthony - DTRA TEAMS - added material container to TEAM8 file
C    Cell Cards
1    1  -0.001205  1 -100 #7 #8 #9 #10 #11 #12 #13
                #14 #15 #16 #17 #18   imp:n,p 1 $ air above earth
2    2  -2.74      -5 -100 #3 #4 #6   imp:n,p 1    $ earth
3    3  -7.82      -1 2 3 -4   imp:n,p 1       $ steel pipe
4    1  -0.001205  -1 2 -3     imp:n,p 1       $ air inside hole
5    4  -2.3       -1 5 -100 #3 #4 #6   imp:n,p 1  $ concrete road
6    5  -2.3       -1 2 4 -6   imp:n,p 1       $ concrete pipe
7    3  -7.82      8 -9 10 -11 12 -13   imp:n,p 1   $ steel table top
8    3  -7.82      -8 1 -14  imp:n,p 1     $ table leg 1
9    3  -7.82      -8 1 -15  imp:n,p 1     $ table leg 2
10   3  -7.82      -8 1 -16  imp:n,p 1     $ table leg 3
11   3  -7.82      -8 1 -17  imp:n,p 1     $ table leg 4
12   6  -2.6989    -23 28 19 -24 21 -22  imp:n,p 1  $ back of Al box
13   6  -2.6989    -23 28 25 -20 21 -22  imp:n,p 1  $ front of Al box
14   6  -2.6989    -23 28 24 -25 21 -26  imp:n,p 1  $ left of Al box
15   6  -2.6989    -23 28 24 -25 27 -22  imp:n,p 1  $ right of Al box
16   6  -2.6989    23 -18 19 -20 21 -22  imp:n,p 1  $ top of Al box
17   6  -2.6989    9 -28 19 -20 21 -22  imp:n,p 1  $ bottom of Al box
18   1  -0.001205  -23 24 -25 26 -27 28  imp:n,p 1  $ air inside box
100  0            100         imp:n,p 0       $ void

C    Surface Cards
1    pz  0         $ earth level
2    pz  -365.76   $ bottom of hole, 12' deep
3    cz  7.62      $ inside of steel pipe, 3" radius
4    cz  10.16     $ outside of steel pipe, 4" radius
5    pz  -30.48    $ thickness of road, 12" deep
6    cz  40.64     $ outside of concrete pipe, 12" thick
7    pz  -182.88   $ plane for source
8    pz  100       $ bottom of table
9    pz  105       $ top of table
10   px  -50       $ back of table
11   px  50        $ front of table
12   py  -50       $ left side of table
13   py  50        $ right side of table
14   c/z  -50 -50 2  $ table leg 1, 2cm radius
15   c/z  -50 50 2   $ table leg 2, 2cm radius
16   c/z  50 -50 2   $ table leg 3, 2cm radius
17   c/z  50 50 2    $ table leg 4, 2cm radius
18   pz  125       $ top of container, outside
19   px  -10       $ back of container, outside
```

```
20   px  10       $ front of container, outside
21   py  -10      $ left side of container, outside
22   py  10       $ right side of container, outside
23   pz  124.5    $ top of container, inside
24   px  -9.5     $ back of container, inside
25   px  9.5      $ front of container, inside
26   py  -9.5     $ left side of container, inside
27   py  9.5      $ right side of container, inside
28   pz  105.5    $ bottom of container, inside
100  so  1000     $ edge of void

C    Data Cards
C    Material Cards
m1   06012 1.51e-4  07014 0.784437  08016 0.210750  $ air
     18040 4.671e-3
m2   08016 0.4660  14028 0.2772  13027 0.0813  $ earth
     26000 0.0500  20040 0.0363  11023 0.0283
     19039 0.0259  12024 0.0209  22048 0.0044
     01001 0.0014  15031 0.0012  25055 0.0010
     09019 0.0008  06012 0.0003  16032 0.0005
     23051 0.0001  17035 0.0005  24052 0.0001
     37085 0.0003  29000 0.0001  07014 5.0e-5
m3   06012 0.022831  26000 0.977170  $ steel
m4   01001 0.304245  06012 0.002870  08016 0.498628  $ ordinary concrete
     11023 0.009179  12000 7.17e-4  13027 0.010261
     14000 0.150505  19000 0.007114  20000 0.014882
     26000 0.001599
m5   01001 0.168759  06012 0.001416  08016 0.562522  $ Portland concrete
     11023 0.011838  12000 0.001400  13027 0.021354
     14000 0.204115  19000 0.005656  20000 0.018674
     26000 0.004264
m6   13027 1.0000    $ aluminum
C    Source Cards
mode n p
sdef pos=0 0 -182.88  dir=1  vec=0 0 1  par=1  erg=14  $ beam source
C    Tally Cards
FMESH4:n  geom=cyl  origin=0 0 -365.76  axs=0 0 1  $ mesh tally, p.3-114
     imesh=7.62 10.16 40.64 100  iints=1 1 1 1
     jmesh=-182.88 -30.48 0 365.76  jints=1 1 1 10
     kmesh=1  kints=1
nps  1e4
```

Appendix D. MCNP Tally Results for Gozani Comparison

Iron Code

Energy [MeV]	Surface Current [particles]	Rel. Uncert.	Abs. Uncert.
5.00E-02	6.54E-05	1.32E-01	8.60E-06
1.00E-01	7.10E-04	3.97E-02	2.82E-05
1.50E-01	4.07E-03	1.65E-02	6.72E-05
2.00E-01	6.34E-03	1.32E-02	8.37E-05
2.50E-01	6.84E-03	1.27E-02	8.68E-05
3.00E-01	6.46E-03	1.31E-02	8.47E-05
3.50E-01	5.97E-03	1.36E-02	8.11E-05
4.00E-01	5.70E-03	1.39E-02	7.93E-05
4.50E-01	5.15E-03	1.46E-02	7.51E-05
5.00E-01	4.79E-03	1.52E-02	7.28E-05
5.50E-01	6.45E-03	1.31E-02	8.45E-05
6.00E-01	3.80E-03	1.70E-02	6.46E-05
6.50E-01	3.61E-03	1.74E-02	6.28E-05
7.00E-01	3.36E-03	1.81E-02	6.07E-05
7.50E-01	3.29E-03	1.83E-02	6.02E-05
8.00E-01	3.34E-03	1.81E-02	6.05E-05
8.50E-01	1.33E-02	0.009	1.19E-04
9.00E-01	1.41E-03	0.0281	3.97E-05
9.50E-01	1.40E-03	0.0282	3.95E-05
1.00E+00	1.46E-03	0.0276	4.03E-05
1.05E+00	2.03E-03	0.0233	4.73E-05
1.10E+00	1.31E-03	0.0291	3.81E-05
1.15E+00	1.31E-03	0.0291	3.81E-05
1.20E+00	1.36E-03	0.0286	3.89E-05
1.25E+00	4.41E-03	0.0158	6.96E-05
1.30E+00	8.48E-04	0.0363	3.08E-05
1.35E+00	1.08E-03	0.0322	3.47E-05
1.40E+00	8.71E-04	0.0357	3.11E-05
1.45E+00	1.30E-03	0.029	3.76E-05
1.50E+00	7.41E-04	0.0388	2.88E-05
1.55E+00	8.25E-04	0.0367	3.03E-05
1.60E+00	8.09E-04	0.0371	3.00E-05
1.65E+00	7.16E-04	0.0395	2.83E-05
1.70E+00	9.49E-04	0.0343	3.26E-05
1.75E+00	8.77E-04	0.0357	3.13E-05
1.80E+00	9.56E-04	0.0341	3.26E-05

1.85E+00	2.08E-03	0.0229	4.76E-05
1.90E+00	9.25E-04	0.0347	3.21E-05
1.95E+00	5.97E-04	0.0432	2.58E-05
2.00E+00	5.73E-04	0.0441	2.53E-05
2.05E+00	6.73E-04	0.0407	2.74E-05
2.10E+00	8.75E-04	0.0355	3.11E-05
2.15E+00	1.83E-03	0.0245	4.49E-05
2.20E+00	4.87E-04	0.0478	2.33E-05
2.25E+00	5.15E-04	0.0465	2.40E-05
2.30E+00	1.03E-03	0.0326	3.37E-05
2.35E+00	4.81E-04	0.0482	2.32E-05
2.40E+00	5.78E-04	0.044	2.54E-05
2.45E+00	5.88E-04	0.0436	2.56E-05
2.50E+00	6.26E-04	0.0422	2.64E-05
2.55E+00	9.84E-04	0.0334	3.29E-05
2.60E+00	9.91E-04	0.0334	3.31E-05
2.65E+00	6.71E-04	0.0406	2.72E-05
2.70E+00	4.39E-04	0.0505	2.22E-05
2.75E+00	3.67E-04	0.0553	2.03E-05
2.80E+00	9.96E-04	0.0333	3.32E-05
2.85E+00	3.91E-04	0.0534	2.09E-05
2.90E+00	3.54E-04	0.0564	2.00E-05
2.95E+00	4.02E-04	0.0528	2.12E-05
3.00E+00	7.15E-04	0.0393	2.81E-05
3.05E+00	4.65E-04	0.049	2.28E-05
3.10E+00	3.85E-04	0.054	2.08E-05
3.15E+00	4.03E-04	0.0527	2.12E-05
3.20E+00	4.01E-04	0.0527	2.12E-05
3.25E+00	7.33E-04	0.0389	2.85E-05
3.30E+00	6.16E-04	0.0424	2.61E-05
3.35E+00	3.29E-04	0.0583	1.92E-05
3.40E+00	4.79E-04	0.0482	2.31E-05
3.45E+00	5.36E-04	0.0455	2.44E-05
3.50E+00	4.66E-04	0.0489	2.28E-05
3.55E+00	6.29E-04	0.042	2.64E-05
3.60E+00	5.71E-04	0.0442	2.52E-05
3.65E+00	3.21E-04	0.0589	1.89E-05
3.70E+00	6.30E-04	0.0421	2.65E-05
3.75E+00	2.66E-04	0.065	1.73E-05

3.80E+00	3.49E-04	0.0567	1.98E-05
3.85E+00	4.00E-04	0.0528	2.11E-05
3.90E+00	2.51E-04	0.0666	1.67E-05
3.95E+00	1.96E-04	0.0757	1.48E-05
4.00E+00	1.75E-04	0.0799	1.40E-05
4.05E+00	2.67E-04	0.0647	1.73E-05
4.10E+00	1.83E-04	0.0784	1.43E-05
4.15E+00	7.14E-04	0.0394	2.81E-05
4.20E+00	2.46E-04	0.0675	1.66E-05
4.25E+00	3.12E-04	0.06	1.87E-05
4.30E+00	2.79E-04	0.0633	1.77E-05
4.35E+00	2.38E-04	0.0684	1.63E-05
4.40E+00	2.27E-04	0.0701	1.59E-05
4.45E+00	2.42E-04	0.068	1.64E-05
4.50E+00	2.18E-04	0.0715	1.56E-05
4.55E+00	2.33E-04	0.0691	1.61E-05
4.60E+00	2.24E-04	0.0708	1.59E-05
4.65E+00	2.00E-04	0.0748	1.50E-05
4.70E+00	1.76E-04	0.0796	1.40E-05
4.75E+00	1.75E-04	0.0796	1.40E-05
4.80E+00	1.99E-04	0.0752	1.50E-05
4.85E+00	1.81E-04	0.0789	1.43E-05
4.90E+00	2.21E-04	0.0711	1.57E-05
4.95E+00	2.23E-04	0.0708	1.58E-05
5.00E+00	1.89E-04	0.0772	1.46E-05

Lead Code

Energy [MeV]	Surface Current [particles]	Rel. Uncert.	Abs. Uncert.
5.00E-02	2.73E-05	2.62E-01	7.14E-06
1.00E-01	1.95E-04	8.81E-02	1.71E-05
1.50E-01	4.13E-05	1.90E-01	7.84E-06
2.00E-01	6.05E-05	1.65E-01	9.95E-06
2.50E-01	9.73E-05	1.26E-01	1.23E-05
3.00E-01	1.67E-04	9.51E-02	1.58E-05
3.50E-01	1.81E-04	9.01E-02	1.63E-05
4.00E-01	2.77E-04	7.30E-02	2.02E-05
4.50E-01	3.23E-04	6.84E-02	2.21E-05
5.00E-01	4.86E-04	5.46E-02	2.65E-05
5.50E-01	1.41E-03	3.25E-02	4.59E-05

6.00E-01	5.75E-04	4.96E-02	2.85E-05
6.50E-01	5.02E-04	5.35E-02	2.69E-05
7.00E-01	4.59E-04	5.61E-02	2.57E-05
7.50E-01	4.80E-04	5.50E-02	2.64E-05
8.00E-01	6.59E-04	4.62E-02	3.04E-05
8.50E-01	7.34E-04	0.0438	3.21E-05
9.00E-01	5.93E-04	0.049	2.91E-05
9.50E-01	5.86E-04	0.0498	2.92E-05
1.00E+00	4.56E-04	0.0565	2.57E-05
1.05E+00	3.68E-04	0.0634	2.34E-05
1.10E+00	3.83E-04	0.0621	2.38E-05
1.15E+00	3.93E-04	0.0615	2.42E-05
1.20E+00	3.95E-04	0.0617	2.44E-05
1.25E+00	3.87E-04	0.0626	2.42E-05
1.30E+00	3.92E-04	0.0617	2.42E-05
1.35E+00	3.65E-04	0.0635	2.32E-05
1.40E+00	4.18E-04	0.0598	2.50E-05
1.45E+00	3.99E-04	0.0608	2.42E-05
1.50E+00	3.88E-04	0.0617	2.40E-05
1.55E+00	3.66E-04	0.0634	2.32E-05
1.60E+00	3.53E-04	0.0647	2.28E-05
1.65E+00	3.71E-04	0.0632	2.35E-05
1.70E+00	3.66E-04	0.0635	2.32E-05
1.75E+00	3.53E-04	0.0642	2.27E-05
1.80E+00	3.58E-04	0.064	2.29E-05
1.85E+00	3.01E-04	0.0698	2.10E-05
1.90E+00	2.68E-04	0.0743	1.99E-05
1.95E+00	2.98E-04	0.0708	2.11E-05
2.00E+00	2.57E-04	0.076	1.95E-05
2.05E+00	2.62E-04	0.0751	1.97E-05
2.10E+00	2.69E-04	0.0744	2.00E-05
2.15E+00	2.33E-04	0.0799	1.86E-05
2.20E+00	2.14E-04	0.0836	1.79E-05
2.25E+00	2.15E-04	0.0835	1.79E-05
2.30E+00	2.38E-04	0.0795	1.89E-05
2.35E+00	2.64E-04	0.0752	1.98E-05
2.40E+00	1.93E-04	0.0877	1.69E-05
2.45E+00	3.31E-04	0.067	2.22E-05
2.50E+00	3.87E-04	0.0618	2.39E-05

2.55E+00	6.87E-04	0.0464	3.19E-05
2.60E+00	8.70E-04	0.0411	3.58E-05
2.65E+00	8.25E-04	0.0423	3.49E-05
2.70E+00	6.89E-04	0.0463	3.19E-05
2.75E+00	4.18E-04	0.0595	2.48E-05
2.80E+00	2.62E-04	0.0756	1.98E-05
2.85E+00	1.84E-04	0.0901	1.65E-05
2.90E+00	1.70E-04	0.0942	1.60E-05
2.95E+00	9.44E-05	0.1262	1.19E-05
3.00E+00	9.54E-05	0.126	1.20E-05
3.05E+00	1.10E-04	0.1166	1.28E-05
3.10E+00	1.11E-04	0.1158	1.29E-05
3.15E+00	7.86E-05	0.1378	1.08E-05
3.20E+00	7.47E-05	0.1417	1.06E-05
3.25E+00	5.91E-05	0.1588	9.38E-06
3.30E+00	7.88E-05	0.1378	1.09E-05
3.35E+00	7.21E-05	0.1445	1.04E-05
3.40E+00	6.76E-05	0.1493	1.01E-05
3.45E+00	1.00E-04	0.1224	1.23E-05
3.50E+00	1.11E-04	0.1165	1.29E-05
3.55E+00	1.10E-04	0.1171	1.29E-05
3.60E+00	6.76E-05	0.1493	1.01E-05
3.65E+00	9.54E-05	0.1253	1.20E-05
3.70E+00	1.02E-04	0.1215	1.24E-05
3.75E+00	1.08E-04	0.118	1.27E-05
3.80E+00	9.33E-05	0.1271	1.19E-05
3.85E+00	9.79E-05	0.1235	1.21E-05
3.90E+00	8.78E-05	0.1306	1.15E-05
3.95E+00	9.54E-05	0.1253	1.19E-05
4.00E+00	9.84E-05	0.1234	1.21E-05
4.05E+00	9.28E-05	0.1272	1.18E-05
4.10E+00	9.28E-05	0.1272	1.18E-05
4.15E+00	1.10E-04	0.1172	1.28E-05
4.20E+00	9.18E-05	0.1282	1.18E-05
4.25E+00	8.93E-05	0.1302	1.16E-05
4.30E+00	6.40E-05	0.1529	9.79E-06
4.35E+00	6.55E-05	0.1511	9.90E-06
4.40E+00	3.95E-05	0.1935	7.64E-06
4.45E+00	4.89E-05	0.1747	8.55E-06

4.50E+00	5.15E-05	0.1715	8.83E-06
4.55E+00	4.19E-05	0.1894	7.93E-06
4.60E+00	6.56E-05	0.1511	9.92E-06
4.65E+00	3.18E-05	0.2182	6.93E-06
4.70E+00	4.85E-05	0.1768	8.57E-06
4.75E+00	5.45E-05	0.1667	9.09E-06
4.80E+00	3.64E-05	0.2041	7.42E-06
4.85E+00	3.94E-05	0.1961	7.72E-06
4.90E+00	5.25E-05	0.1693	8.88E-06
4.95E+00	2.11E-05	0.2673	5.65E-06
5.00E+00	4.44E-05	0.1833	8.14E-06

Polyethylene Code

Energy [MeV]	Surface Current [particles]	Rel. Uncert.	Abs. Uncert.
5.00E-02	6.30E-05	1.26E-01	7.94E-06
1.00E-01	7.60E-05	1.15E-01	8.72E-06
1.50E-01	1.13E-04	9.49E-02	1.07E-05
2.00E-01	1.21E-04	9.09E-02	1.10E-05
2.50E-01	1.03E-04	9.85E-02	1.01E-05
3.00E-01	1.66E-04	7.76E-02	1.29E-05
3.50E-01	1.15E-04	9.32E-02	1.07E-05
4.00E-01	1.13E-04	9.41E-02	1.06E-05
4.50E-01	9.70E-05	1.02E-01	9.85E-06
5.00E-01	8.70E-05	1.07E-01	9.33E-06
5.50E-01	1.73E-04	7.60E-02	1.31E-05
6.00E-01	6.50E-05	1.24E-01	8.06E-06
6.50E-01	7.10E-05	1.19E-01	8.43E-06
7.00E-01	4.80E-05	1.44E-01	6.93E-06
7.50E-01	4.90E-05	1.43E-01	7.00E-06
8.00E-01	5.00E-05	1.41E-01	7.07E-06
8.50E-01	5.50E-05	0.1348	7.41E-06
9.00E-01	3.80E-05	0.1622	6.16E-06
9.50E-01	3.80E-05	0.1622	6.16E-06
1.00E+00	3.40E-05	0.1715	5.83E-06
1.05E+00	3.60E-05	0.1667	6.00E-06
1.10E+00	3.60E-05	0.1667	6.00E-06
1.15E+00	3.10E-05	0.1796	5.57E-06
1.20E+00	3.30E-05	0.1741	5.75E-06
1.25E+00	2.40E-05	0.2041	4.90E-06

1.30E+00	3.70E-05	0.1644	6.08E-06
1.35E+00	3.50E-05	0.169	5.92E-06
1.40E+00	2.60E-05	0.1961	5.10E-06
1.45E+00	3.50E-05	0.169	5.92E-06
1.50E+00	3.30E-05	0.1741	5.75E-06
1.55E+00	3.40E-05	0.1715	5.83E-06
1.60E+00	3.10E-05	0.1796	5.57E-06
1.65E+00	2.90E-05	0.1857	5.39E-06
1.70E+00	2.90E-05	0.1857	5.39E-06
1.75E+00	3.30E-05	0.1741	5.75E-06
1.80E+00	2.20E-05	0.2132	4.69E-06
1.85E+00	2.20E-05	0.2132	4.69E-06
1.90E+00	2.70E-05	0.1924	5.19E-06
1.95E+00	2.30E-05	0.2085	4.80E-06
2.00E+00	3.10E-05	0.1796	5.57E-06
2.05E+00	3.30E-05	0.1741	5.75E-06
2.10E+00	2.10E-05	0.2182	4.58E-06
2.15E+00	2.50E-05	0.2	5.00E-06
2.20E+00	3.80E-05	0.1622	6.16E-06
2.25E+00	3.53E-03	0.0173	6.11E-05
2.30E+00	1.50E-05	0.2582	3.87E-06
2.35E+00	9.00E-06	0.3333	3.00E-06
2.40E+00	1.10E-05	0.3015	3.32E-06
2.45E+00	1.10E-05	0.3015	3.32E-06
2.50E+00	1.40E-05	0.2673	3.74E-06
2.55E+00	8.00E-06	0.3536	2.83E-06
2.60E+00	9.00E-06	0.3333	3.00E-06
2.65E+00	1.00E-05	0.3162	3.16E-06
2.70E+00	1.20E-05	0.2887	3.46E-06
2.75E+00	6.00E-06	0.4082	2.45E-06
2.80E+00	1.00E-05	0.3162	3.16E-06
2.85E+00	9.00E-06	0.3333	3.00E-06
2.90E+00	1.30E-05	0.2773	3.60E-06
2.95E+00	1.40E-05	0.2673	3.74E-06
3.00E+00	1.20E-05	0.2887	3.46E-06
3.05E+00	6.00E-06	0.4082	2.45E-06
3.10E+00	8.00E-06	0.3536	2.83E-06
3.15E+00	1.20E-05	0.2887	3.46E-06
3.20E+00	9.00E-06	0.3333	3.00E-06

3.25E+00	1.00E-05	0.3162	3.16E-06
3.30E+00	6.00E-06	0.4082	2.45E-06
3.35E+00	1.30E-05	0.2773	3.60E-06
3.40E+00	1.40E-05	0.2673	3.74E-06
3.45E+00	1.10E-05	0.3015	3.32E-06
3.50E+00	1.30E-05	0.2773	3.60E-06
3.55E+00	1.00E-05	0.3162	3.16E-06
3.60E+00	1.70E-05	0.2425	4.12E-06
3.65E+00	9.00E-06	0.3333	3.00E-06
3.70E+00	1.70E-05	0.2425	4.12E-06
3.75E+00	1.20E-05	0.2887	3.46E-06
3.80E+00	8.00E-06	0.3536	2.83E-06
3.85E+00	1.00E-05	0.3162	3.16E-06
3.90E+00	1.20E-05	0.2887	3.46E-06
3.95E+00	1.00E-05	0.3162	3.16E-06
4.00E+00	9.00E-06	0.3333	3.00E-06
4.05E+00	1.20E-05	0.2887	3.46E-06
4.10E+00	1.00E-05	0.3162	3.16E-06
4.15E+00	7.00E-06	0.378	2.65E-06
4.20E+00	9.00E-06	0.3333	3.00E-06
4.25E+00	8.00E-06	0.3536	2.83E-06
4.30E+00	6.00E-06	0.4082	2.45E-06
4.35E+00	1.10E-05	0.3015	3.32E-06
4.40E+00	5.00E-06	0.4472	2.24E-06
4.45E+00	7.37E-03	0.0117	8.62E-05
4.50E+00	1.00E-06	1	1.00E-06
4.55E+00	0.00E+00	0	0.00E+00
4.60E+00	0.00E+00	0	0.00E+00
4.65E+00	0.00E+00	0	0.00E+00
4.70E+00	0.00E+00	0	0.00E+00
4.75E+00	0.00E+00	0	0.00E+00
4.80E+00	0.00E+00	0	0.00E+00
4.85E+00	0.00E+00	0	0.00E+00
4.90E+00	0.00E+00	0	0.00E+00
4.95E+00	1.00E-05	0.3162	3.16E-06
5.00E+00	0.00E+00	0	0.00E+00

U-235 Code

Energy [MeV]	Surface Current [particles]	Rel. Uncert.	Abs. Uncert.

5.00E-02	0.00E+00	0.00E+00	0.00E+00
1.00E-01	1.42E-05	4.15E-01	5.89E-06
1.50E-01	9.08E-06	4.58E-01	4.16E-06
2.00E-01	2.20E-06	7.10E-01	1.56E-06
2.50E-01	8.83E-06	4.55E-01	4.02E-06
3.00E-01	7.95E-06	5.00E-01	3.98E-06
3.50E-01	9.96E-06	4.47E-01	4.46E-06
4.00E-01	2.48E-05	2.91E-01	7.22E-06
4.50E-01	5.66E-06	7.38E-01	4.17E-06
5.00E-01	1.47E-05	3.70E-01	5.44E-06
5.50E-01	3.00E-05	2.69E-01	8.07E-06
6.00E-01	2.53E-05	2.65E-01	6.70E-06
6.50E-01	2.26E-05	3.36E-01	7.59E-06
7.00E-01	2.57E-05	2.78E-01	7.12E-06
7.50E-01	3.95E-05	2.43E-01	9.59E-06
8.00E-01	1.57E-05	3.91E-01	6.14E-06
8.50E-01	2.02E-05	0.2949	5.95E-06
9.00E-01	1.45E-05	0.3613	5.22E-06
9.50E-01	3.92E-05	0.2581	1.01E-05
1.00E+00	2.72E-05	0.2648	7.22E-06
1.05E+00	1.20E-05	0.3636	4.36E-06
1.10E+00	1.34E-05	0.3951	5.29E-06
1.15E+00	1.49E-05	0.3573	5.32E-06
1.20E+00	4.80E-06	0.5907	2.83E-06
1.25E+00	2.28E-05	0.318	7.25E-06
1.30E+00	1.88E-05	0.3144	5.93E-06
1.35E+00	1.87E-05	0.3201	5.98E-06
1.40E+00	2.03E-05	0.3313	6.74E-06
1.45E+00	9.20E-06	0.4542	4.18E-06
1.50E+00	1.77E-05	0.3236	5.72E-06
1.55E+00	1.34E-05	0.3895	5.22E-06
1.60E+00	9.79E-06	0.4476	4.38E-06
1.65E+00	1.48E-05	0.422	6.26E-06
1.70E+00	6.56E-06	0.5956	3.90E-06
1.75E+00	7.76E-06	0.4602	3.57E-06
1.80E+00	5.28E-06	0.5877	3.10E-06
1.85E+00	1.14E-05	0.4136	4.72E-06
1.90E+00	1.67E-05	0.3934	6.55E-06
1.95E+00	1.76E-05	0.3842	6.77E-06

2.00E+00	1.01E-05	0.4475	4.51E-06
2.05E+00	2.03E-06	1	2.03E-06
2.10E+00	4.01E-06	0.7071	2.84E-06
2.15E+00	5.78E-06	0.507	2.93E-06
2.20E+00	8.34E-06	0.5061	4.22E-06
2.25E+00	7.06E-06	0.5078	3.59E-06
2.30E+00	8.87E-06	0.5381	4.77E-06
2.35E+00	5.68E-06	0.7384	4.19E-06
2.40E+00	4.03E-06	0.7072	2.85E-06
2.45E+00	0.00E+00	0	0.00E+00
2.50E+00	5.74E-06	0.7356	4.22E-06
2.55E+00	1.69E-06	1	1.69E-06
2.60E+00	4.27E-06	0.7602	3.25E-06
2.65E+00	3.01E-06	0.7404	2.23E-06
2.70E+00	1.04E-05	0.5267	5.50E-06
2.75E+00	5.85E-06	0.5786	3.39E-06
2.80E+00	0.00E+00	0	0.00E+00
2.85E+00	0.00E+00	0	0.00E+00
2.90E+00	0.00E+00	0	0.00E+00
2.95E+00	5.75E-06	0.7352	4.23E-06
3.00E+00	0.00E+00	0	0.00E+00
3.05E+00	3.69E-06	1	3.69E-06
3.10E+00	2.62E-06	0.7217	1.89E-06
3.15E+00	2.08E-06	1	2.08E-06
3.20E+00	7.21E-06	0.619	4.46E-06
3.25E+00	0.00E+00	0	0.00E+00
3.30E+00	2.99E-06	0.7448	2.23E-06
3.35E+00	0.00E+00	0	0.00E+00
3.40E+00	1.05E-06	1	1.05E-06
3.45E+00	0.00E+00	0	0.00E+00
3.50E+00	2.08E-06	1	2.08E-06
3.55E+00	0.00E+00	0	0.00E+00
3.60E+00	0.00E+00	0	0.00E+00
3.65E+00	4.19E-06	0.5891	2.47E-06
3.70E+00	7.14E-06	0.6231	4.45E-06
3.75E+00	0.00E+00	0	0.00E+00
3.80E+00	0.00E+00	0	0.00E+00
3.85E+00	1.16E-06	1	1.16E-06
3.90E+00	0.00E+00	0	0.00E+00

3.95E+00	2.00E-06	1	2.00E-06
4.00E+00	1.85E-06	1	1.85E-06
4.05E+00	0.00E+00	0	0.00E+00
4.10E+00	0.00E+00	0	0.00E+00
4.15E+00	0.00E+00	0	0.00E+00
4.20E+00	0.00E+00	0	0.00E+00
4.25E+00	3.54E-06	0.7129	2.52E-06
4.30E+00	0.00E+00	0	0.00E+00
4.35E+00	0.00E+00	0	0.00E+00
4.40E+00	0.00E+00	0	0.00E+00
4.45E+00	0.00E+00	0	0.00E+00
4.50E+00	0.00E+00	0	0.00E+00
4.55E+00	0.00E+00	0	0.00E+00
4.60E+00	0.00E+00	0	0.00E+00
4.65E+00	0.00E+00	0	0.00E+00
4.70E+00	3.69E-06	1	3.69E-06
4.75E+00	0.00E+00	0	0.00E+00
4.80E+00	0.00E+00	0	0.00E+00
4.85E+00	0.00E+00	0	0.00E+00
4.90E+00	0.00E+00	0	0.00E+00
4.95E+00	0.00E+00	0	0.00E+00
5.00E+00	0.00E+00	0	0.00E+00

U-238 Code

Energy [MeV]	Surface Current [particles]	Rel. Uncert.	Abs. Uncert.
5.00E-02	3.94E-05	1.87E-01	7.36E-06
1.00E-01	2.45E-04	7.97E-02	1.95E-05
1.50E-01	1.54E-04	9.88E-02	1.52E-05
2.00E-01	4.55E-05	1.92E-01	8.73E-06
2.50E-01	1.27E-04	1.11E-01	1.41E-05
3.00E-01	1.98E-04	9.16E-02	1.81E-05
3.50E-01	2.01E-04	9.04E-02	1.81E-05
4.00E-01	2.99E-04	7.41E-02	2.21E-05
4.50E-01	3.36E-04	7.11E-02	2.39E-05
5.00E-01	3.54E-04	6.81E-02	2.41E-05
5.50E-01	6.82E-04	4.83E-02	3.29E-05
6.00E-01	4.76E-04	5.80E-02	2.76E-05
6.50E-01	4.68E-04	5.90E-02	2.76E-05
7.00E-01	4.79E-04	5.91E-02	2.83E-05

7.50E-01	4.59E-04	6.09E-02	2.80E-05
8.00E-01	4.08E-04	6.45E-02	2.63E-05
8.50E-01	4.61E-04	0.0611	2.81E-05
9.00E-01	4.38E-04	0.0621	2.72E-05
9.50E-01	4.08E-04	0.0643	2.62E-05
1.00E+00	3.97E-04	0.0654	2.60E-05
1.05E+00	3.51E-04	0.0697	2.45E-05
1.10E+00	3.99E-04	0.0664	2.65E-05
1.15E+00	3.39E-04	0.0702	2.38E-05
1.20E+00	3.94E-04	0.0666	2.62E-05
1.25E+00	3.76E-04	0.0679	2.55E-05
1.30E+00	3.18E-04	0.0732	2.33E-05
1.35E+00	2.77E-04	0.0786	2.18E-05
1.40E+00	2.72E-04	0.08	2.17E-05
1.45E+00	2.99E-04	0.077	2.30E-05
1.50E+00	2.66E-04	0.0784	2.09E-05
1.55E+00	2.19E-04	0.0874	1.92E-05
1.60E+00	2.25E-04	0.0849	1.91E-05
1.65E+00	2.34E-04	0.086	2.01E-05
1.70E+00	2.11E-04	0.0869	1.83E-05
1.75E+00	2.18E-04	0.0854	1.87E-05
1.80E+00	2.12E-04	0.0865	1.84E-05
1.85E+00	1.83E-04	0.0931	1.70E-05
1.90E+00	1.76E-04	0.0967	1.70E-05
1.95E+00	1.88E-04	0.0909	1.71E-05
2.00E+00	1.97E-04	0.0897	1.77E-05
2.05E+00	1.95E-04	0.0889	1.73E-05
2.10E+00	1.61E-04	0.1024	1.65E-05
2.15E+00	1.48E-04	0.1015	1.50E-05
2.20E+00	1.38E-04	0.1072	1.48E-05
2.25E+00	1.49E-04	0.1063	1.59E-05
2.30E+00	1.25E-04	0.1142	1.42E-05
2.35E+00	1.13E-04	0.1165	1.32E-05
2.40E+00	1.03E-04	0.1209	1.24E-05
2.45E+00	1.04E-04	0.1259	1.31E-05
2.50E+00	1.23E-04	0.1169	1.44E-05
2.55E+00	8.38E-05	0.1358	1.14E-05
2.60E+00	6.66E-05	0.1504	1.00E-05
2.65E+00	5.93E-05	0.162	9.60E-06

2.70E+00	8.99E-05	0.1377	1.24E-05
2.75E+00	8.34E-05	0.1391	1.16E-05
2.80E+00	6.28E-05	0.1603	1.01E-05
2.85E+00	7.03E-05	0.1458	1.02E-05
2.90E+00	6.27E-05	0.1658	1.04E-05
2.95E+00	5.29E-05	0.1825	9.66E-06
3.00E+00	4.96E-05	0.1781	8.83E-06
3.05E+00	4.18E-05	0.1961	8.20E-06
3.10E+00	5.30E-05	0.1831	9.71E-06
3.15E+00	3.69E-05	0.2177	8.04E-06
3.20E+00	4.94E-05	0.1944	9.60E-06
3.25E+00	2.32E-05	0.2482	5.76E-06
3.30E+00	3.08E-05	0.2316	7.14E-06
3.35E+00	2.13E-05	0.2737	5.83E-06
3.40E+00	3.11E-05	0.2284	7.10E-06
3.45E+00	4.73E-05	0.1919	9.08E-06
3.50E+00	3.14E-05	0.2291	7.20E-06
3.55E+00	1.11E-05	0.3246	3.61E-06
3.60E+00	3.35E-05	0.2375	7.96E-06
3.65E+00	2.00E-05	0.2627	5.26E-06
3.70E+00	1.53E-05	0.3147	4.80E-06
3.75E+00	7.20E-06	0.3784	2.73E-06
3.80E+00	1.36E-05	0.3739	5.07E-06
3.85E+00	1.20E-05	0.3337	4.01E-06
3.90E+00	1.15E-05	0.3519	4.03E-06
3.95E+00	2.01E-05	0.2534	5.08E-06
4.00E+00	1.96E-05	0.2531	4.95E-06
4.05E+00	2.35E-05	0.2254	5.29E-06
4.10E+00	3.42E-05	0.2036	6.97E-06
4.15E+00	2.05E-05	0.2257	4.63E-06
4.20E+00	1.05E-05	0.3741	3.94E-06
4.25E+00	8.77E-06	0.3883	3.41E-06
4.30E+00	5.59E-06	0.5845	3.27E-06
4.35E+00	7.19E-06	0.5191	3.73E-06
4.40E+00	3.67E-06	0.5963	2.19E-06
4.45E+00	7.30E-06	0.5145	3.76E-06
4.50E+00	7.26E-06	0.5202	3.78E-06
4.55E+00	8.49E-06	0.5032	4.27E-06
4.60E+00	4.83E-06	0.6065	2.93E-06

4.65E+00	6.53E-06	0.5362	3.50E-06
4.70E+00	5.51E-06	0.5122	2.82E-06
4.75E+00	6.97E-06	0.5239	3.65E-06
4.80E+00	7.99E-06	0.5043	4.03E-06
4.85E+00	1.70E-06	1	1.70E-06
4.90E+00	1.77E-06	1	1.77E-06
4.95E+00	2.27E-06	1	2.27E-06
5.00E+00	3.97E-06	0.7135	2.84E-06

Appendix E. Signal to Noise Ratios (SNR) for Gamma Rays Spectra

Iron		
Energy (MeV)	SNR	Abs. Uncert.
0.05	2.24	1.28E+00
0.10	1.02	9.84E-02
0.15	1.13	4.49E-02
0.20	1.39	2.57E-01
0.25	1.29	1.48E-01
0.30	1.40	7.10E-02
0.35	1.33	1.28E-01
0.40	1.45	9.29E-02
0.45	1.32	1.60E-01
0.50	1.15	1.45E-01
0.55	1.27	7.67E-02
0.60	1.43	1.30E-01
0.65	1.43	1.28E-01
0.70	1.59	2.23E-01
0.75	1.53	1.90E-01
0.80	1.40	1.70E-01
0.85	1.95	7.92E-02
0.90	1.12	1.17E-01
0.95	1.52	3.73E-01
1.00	1.28	1.62E-01
1.05	1.09	9.54E-02
1.10	1.22	1.43E-01
1.15	1.50	2.00E-01
1.20	1.40	2.03E-01
1.25	1.69	1.51E-01
1.30	1.18	1.25E-01
1.35	1.43	1.59E-01
1.40	1.45	2.20E-01
1.45	1.33	1.65E-01
1.50	1.68	3.13E-01
1.55	1.80	3.09E-01
1.60	1.22	2.02E-01
1.65	1.12	1.39E-01
1.70	1.25	1.91E-01
1.75	1.07	1.51E-01

Lead		
Energy (MeV)	SNR	Abs. Uncert.
0.05	0.63	1.99E-01
0.10	1.04	9.59E-02
0.15	0.97	3.78E-02
0.20	0.92	4.40E-02
0.25	0.88	8.25E-02
0.30	0.96	5.20E-02
0.35	1.00	1.02E-01
0.40	1.07	7.16E-02
0.45	0.91	1.11E-01
0.50	0.86	1.09E-01
0.55	1.19	9.37E-02
0.60	1.27	1.27E-01
0.65	1.38	1.32E-01
0.70	1.02	1.05E-01
0.75	1.32	1.45E-01
0.80	1.09	1.26E-01
0.85	1.16	5.14E-02
0.90	1.05	1.07E-01
0.95	1.25	3.48E-01
1.00	0.94	1.17E-01
1.05	1.00	9.15E-02
1.10	1.21	1.50E-01
1.15	1.13	1.64E-01
1.20	4.47	2.21E+00
1.25	1.02	9.81E-02
1.30	0.94	9.65E-02
1.35	1.08	1.27E-01
1.40	1.05	1.71E-01
1.45	1.02	1.35E-01
1.50	1.54	3.02E-01
1.55	1.49	2.41E-01
1.60	1.16	1.88E-01
1.65	1.16	1.52E-01
1.70	1.12	1.80E-01
1.75	1.19	1.58E-01

1.80	1.00	9.15E-02
1.85	1.48	1.43E-01
1.90	1.08	1.61E-01
1.95	1.12	1.41E-01
2.00	1.23	2.03E-01
2.05	1.18	1.48E-01
2.10	1.38	1.59E-01
2.15	1.37	1.61E-01
2.20	1.24	2.23E-01
2.25	1.03	3.46E-02
2.30	1.32	1.60E-01
2.35	1.07	2.73E-01
2.40	1.43	2.53E-01
2.45	1.35	2.00E-01
2.50	1.08	2.47E-01
2.55	1.29	1.66E-01
2.60	1.73	2.72E-01
2.65	2.72	8.73E-01
2.70	1.44	3.08E-01
2.75	1.39	2.13E-01
2.80	1.45	1.86E-01
2.85	1.09	1.76E-01
2.90	1.65	3.81E-01
2.95	1.11	2.30E-01
3.00	1.14	2.04E-01
3.05	1.19	1.90E-01
3.10	0.94	1.89E-01
3.15	1.56	3.00E-01
3.20	1.65	4.02E-01
3.25	1.44	2.30E-01
3.30	1.36	2.17E-01
3.35	1.30	2.24E-01
3.40	1.52	2.74E-01
3.45	1.36	2.09E-01
3.50	1.80	3.11E-01
3.55	1.14	6.22E-02
3.60	1.06	1.61E-01
3.65	1.45	2.79E-01
3.70	1.22	1.23E-01
3.75	0.94	2.14E-01

1.80	1.08	1.02E-01
1.85	1.07	1.11E-01
1.90	0.90	1.36E-01
1.95	1.14	1.58E-01
2.00	1.66	3.05E-01
2.05	1.09	1.31E-01
2.10	1.27	1.39E-01
2.15	0.99	1.19E-01
2.20	1.10	2.23E-01
2.25	1.07	3.61E-02
2.30	0.90	1.27E-01
2.35	0.77	1.97E-01
2.40	1.14	2.14E-01
2.45	1.20	1.75E-01
2.50	1.05	2.35E-01
2.55	1.03	1.38E-01
2.60	2.66	8.37E-01
2.65	1.76	3.06E-01
2.70	1.45	3.07E-01
2.75	1.39	2.02E-01
2.80	1.16	1.53E-01
2.85	1.18	1.88E-01
2.90	1.44	3.10E-01
2.95	0.79	1.60E-01
3.00	0.89	1.59E-01
3.05	0.87	1.37E-01
3.10	0.79	1.61E-01
3.15	1.22	2.85E-01
3.20	1.45	3.31E-01
3.25	0.93	1.58E-01
3.30	0.77	1.19E-01
3.35	1.18	2.25E-01
3.40	1.14	2.23E-01
3.45	1.25	1.92E-01
3.50	1.08	1.99E-01
3.55	1.05	5.07E-02
3.60	0.87	1.40E-01
3.65	1.20	2.19E-01
3.70	1.04	1.17E-01
3.75	0.90	1.81E-01

3.80	1.63	4.59E-01
3.85	1.26	2.42E-01
3.90	0.70	1.36E-01
3.95	0.92	1.97E-01
4.00	1.17	2.28E-01
4.05	1.60	3.59E-01
4.10	1.04	2.27E-01
4.15	2.14	3.11E-01
4.20	0.95	1.97E-01
4.25	1.07	2.55E-01
4.30	1.11	2.74E-01
4.35	1.55	4.06E-01
4.40	1.21	2.63E-01
4.45	1.09	1.36E-01
4.50	1.18	2.62E-01
4.55	1.38	3.35E-01
4.60	0.88	2.03E-01
4.65	1.32	3.03E-01
4.70	1.24	2.53E-01
4.75	1.25	2.41E-01
4.80	1.50	3.59E-01
4.85	1.67	5.01E-01
4.90	1.31	2.57E-01
4.95	1.13	4.66E-02
5.00	1.31	3.07E-01
5.05	0.94	2.07E-01
5.10	1.87	4.71E-01
5.15	1.22	2.17E-01
5.20	1.02	2.04E-01
5.25	1.43	4.18E-01
5.30	1.44	3.71E-01
5.35	1.12	2.62E-01
5.40	1.01	1.62E-01
5.45	0.67	1.64E-01
5.50	1.74	4.47E-01
5.55	1.61	2.51E-01
5.60	0.80	1.91E-01
5.65	1.51	4.37E-01
5.70	1.03	1.74E-01
5.75	1.24	2.94E-01

3.80	0.92	2.12E-01
3.85	1.06	2.00E-01
3.90	0.64	1.30E-01
3.95	0.89	1.92E-01
4.00	1.20	2.30E-01
4.05	0.82	1.75E-01
4.10	1.48	3.74E-01
4.15	1.25	2.01E-01
4.20	1.30	2.95E-01
4.25	0.65	1.06E-01
4.30	0.76	2.05E-01
4.35	1.62	5.25E-01
4.40	0.98	2.06E-01
4.45	0.85	1.14E-01
4.50	0.89	2.05E-01
4.55	1.38	3.54E-01
4.60	0.70	1.81E-01
4.65	1.20	3.04E-01
4.70	1.04	2.22E-01
4.75	1.13	2.67E-01
4.80	1.15	2.93E-01
4.85	1.01	2.44E-01
4.90	1.15	2.92E-01
4.95	1.22	5.75E-02
5.00	0.97	2.28E-01
5.05	0.82	2.15E-01
5.10	0.90	2.20E-01
5.15	0.81	1.55E-01
5.20	0.89	1.81E-01
5.25	0.96	2.90E-01
5.30	1.28	3.45E-01
5.35	0.58	1.41E-01
5.40	1.22	2.38E-01
5.45	0.59	1.62E-01
5.50	1.07	2.37E-01
5.55	1.34	2.12E-01
5.60	0.57	1.40E-01
5.65	0.80	1.83E-01
5.70	0.84	1.53E-01
5.75	0.86	2.25E-01

5.80	1.62	3.28E-01
5.85	1.02	3.81E-01
5.90	1.17	2.66E-01
5.95	1.05	1.44E-01
6.00	1.42	3.61E-01

5.80	1.10	1.94E-01
5.85	0.58	1.94E-01
5.90	1.22	2.95E-01
5.95	0.84	9.81E-02
6.00	0.80	2.25E-01

Polyethylene		
Energy (MeV)	**SNR**	**Abs. Uncert.**
0.05	4.43	2.51E+00
0.10	1.20	9.31E-02
0.15	1.21	4.64E-02
0.20	1.16	5.65E-02
0.25	1.77	5.05E-01
0.30	1.21	6.12E-02
0.35	1.08	1.05E-01
0.40	1.25	8.34E-02
0.45	1.22	1.85E-01
0.50	0.97	1.24E-01
0.55	1.09	7.12E-02
0.60	3.39	2.06E+00
0.65	1.19	1.12E-01
0.70	1.16	1.51E-01
0.75	1.10	1.33E-01
0.80	1.08	1.46E-01
0.85	1.05	4.90E-02
0.90	0.90	9.84E-02
0.95	0.81	1.19E-01
1.00	1.07	1.51E-01
1.05	0.94	9.21E-02
1.10	1.23	1.60E-01
1.15	1.21	1.68E-01
1.20	1.26	1.84E-01
1.25	1.05	1.07E-01
1.30	0.93	1.04E-01
1.35	1.03	1.30E-01
1.40	0.99	1.74E-01
1.45	1.02	1.42E-01
1.50	1.40	2.89E-01

U-235		
Energy (MeV)	**SNR**	**Abs. Uncert.**
0.05	0.61	1.92E-01
0.10	0.93	8.13E-02
0.15	0.94	3.77E-02
0.20	0.89	4.87E-02
0.25	0.93	1.14E-01
0.30	0.88	4.45E-02
0.35	0.86	8.60E-02
0.40	1.00	6.68E-02
0.45	1.01	1.52E-01
0.50	0.95	1.51E-01
0.55	1.05	6.60E-02
0.60	1.00	9.33E-02
0.65	0.99	9.18E-02
0.70	0.98	9.99E-02
0.75	0.90	1.01E-01
0.80	1.00	1.22E-01
0.85	0.99	4.42E-02
0.90	0.91	9.49E-02
0.95	0.95	1.43E-01
1.00	0.89	1.24E-01
1.05	0.70	6.62E-02
1.10	1.01	1.17E-01
1.15	1.00	1.33E-01
1.20	1.00	1.38E-01
1.25	1.04	1.09E-01
1.30	0.94	9.48E-02
1.35	1.01	1.18E-01
1.40	0.99	1.46E-01
1.45	1.06	1.40E-01
1.50	1.18	2.37E-01

1.55	1.38	2.34E-01
1.60	0.80	1.27E-01
1.65	1.17	1.54E-01
1.70	0.85	1.50E-01
1.75	1.08	1.49E-01
1.80	0.92	8.93E-02
1.85	1.05	1.20E-01
1.90	1.01	1.62E-01
1.95	0.94	1.29E-01
2.00	1.21	2.30E-01
2.05	1.01	1.38E-01
2.10	1.14	1.32E-01
2.15	0.85	1.09E-01
2.20	1.03	2.01E-01
2.25	2.46	8.99E-02
2.30	1.05	1.78E-01
2.35	0.84	2.20E-01
2.40	1.32	2.89E-01
2.45	0.94	1.55E-01
2.50	0.88	2.16E-01
2.55	0.87	1.21E-01
2.60	1.35	2.44E-01
2.65	1.16	2.16E-01
2.70	1.07	2.53E-01
2.75	1.14	1.92E-01
2.80	1.00	1.26E-01
2.85	1.04	1.72E-01
2.90	1.03	2.48E-01
2.95	0.98	2.03E-01
3.00	0.94	1.80E-01
3.05	0.95	1.56E-01
3.10	0.83	1.68E-01
3.15	1.30	3.10E-01
3.20	1.46	3.05E-01
3.25	0.97	1.81E-01
3.30	1.00	1.81E-01
3.35	1.08	1.98E-01
3.40	1.18	2.23E-01
3.45	1.15	1.79E-01
3.50	1.02	1.93E-01

1.55	1.12	1.99E-01
1.60	0.88	1.51E-01
1.65	0.94	1.18E-01
1.70	0.70	1.13E-01
1.75	0.93	1.34E-01
1.80	0.89	8.56E-02
1.85	0.93	9.48E-02
1.90	0.73	1.22E-01
1.95	0.85	1.13E-01
2.00	0.81	1.32E-01
2.05	1.00	1.24E-01
2.10	1.10	1.31E-01
2.15	0.99	1.26E-01
2.20	0.71	1.35E-01
2.25	0.93	3.03E-02
2.30	0.79	1.07E-01
2.35	1.25	3.40E-01
2.40	0.90	1.67E-01
2.45	0.82	1.22E-01
2.50	1.04	2.36E-01
2.55	0.98	1.31E-01
2.60	1.05	1.73E-01
2.65	0.86	1.56E-01
2.70	1.12	2.49E-01
2.75	1.04	1.61E-01
2.80	1.00	1.20E-01
2.85	0.88	1.43E-01
2.90	1.19	2.74E-01
2.95	0.67	1.35E-01
3.00	0.73	1.37E-01
3.05	0.64	1.09E-01
3.10	0.82	1.60E-01
3.15	0.80	1.60E-01
3.20	1.12	2.22E-01
3.25	0.78	1.36E-01
3.30	1.25	2.16E-01
3.35	1.04	1.86E-01
3.40	1.22	2.29E-01
3.45	0.99	1.44E-01
3.50	0.96	1.72E-01

3.55	1.09	5.53E-02
3.60	0.92	1.91E-01
3.65	1.28	2.86E-01
3.70	0.96	1.01E-01
3.75	0.94	2.08E-01
3.80	0.82	1.81E-01
3.85	0.95	1.91E-01
3.90	0.74	1.56E-01
3.95	0.93	2.09E-01
4.00	0.86	1.30E-01
4.05	1.05	2.39E-01
4.10	1.24	3.20E-01
4.15	1.01	1.66E-01
4.20	0.95	2.42E-01
4.25	0.99	1.87E-01
4.30	1.04	2.65E-01
4.35	1.16	3.36E-01
4.40	0.84	1.69E-01
4.45	5.96	6.25E-01
4.50	1.16	3.03E-01
4.55	0.98	2.24E-01
4.60	0.91	2.30E-01
4.65	1.12	2.98E-01
4.70	1.16	2.32E-01
4.75	0.87	1.66E-01
4.80	1.82	4.86E-01
4.85	1.39	3.03E-01
4.90	0.89	1.82E-01
4.95	1.06	4.38E-02
5.00	0.77	1.72E-01
5.05	0.94	2.66E-01
5.10	1.49	4.17E-01
5.15	1.04	1.93E-01
5.20	1.02	2.11E-01
5.25	1.17	3.58E-01
5.30	1.29	3.61E-01
5.35	0.77	2.01E-01
5.40	0.82	1.36E-01
5.45	0.92	2.33E-01
5.50	0.93	1.74E-01

3.55	1.07	4.88E-02
3.60	0.91	1.34E-01
3.65	1.30	2.63E-01
3.70	1.07	1.08E-01
3.75	0.88	1.93E-01
3.80	0.88	2.05E-01
3.85	0.78	1.51E-01
3.90	0.98	2.21E-01
3.95	0.89	2.08E-01
4.00	1.00	1.58E-01
4.05	0.72	1.54E-01
4.10	0.70	1.41E-01
4.15	1.00	1.51E-01
4.20	0.88	1.93E-01
4.25	1.11	1.99E-01
4.30	0.82	2.06E-01
4.35	0.93	2.51E-01
4.40	1.01	2.02E-01
4.45	0.79	9.41E-02
4.50	0.75	1.78E-01
4.55	0.79	1.74E-01
4.60	0.58	1.40E-01
4.65	0.94	2.35E-01
4.70	1.02	1.97E-01
4.75	0.90	1.58E-01
4.80	1.10	3.28E-01
4.85	1.09	2.36E-01
4.90	1.06	2.29E-01
4.95	0.99	3.85E-02
5.00	0.82	1.99E-01
5.05	0.79	1.71E-01
5.10	1.15	2.72E-01
5.15	1.06	1.92E-01
5.20	0.80	1.60E-01
5.25	0.81	2.48E-01
5.30	1.06	2.88E-01
5.35	0.92	2.31E-01
5.40	1.13	2.05E-01
5.45	0.72	1.79E-01
5.50	1.39	3.16E-01

5.55	1.04	1.69E-01
5.60	0.63	1.55E-01
5.65	1.15	4.03E-01
5.70	0.74	1.36E-01
5.75	0.87	1.85E-01
5.80	1.03	1.94E-01
5.85	0.51	1.70E-01
5.90	1.01	2.39E-01
5.95	1.15	1.49E-01
6.00	0.89	2.60E-01

5.55	0.92	1.26E-01
5.60	0.74	2.03E-01
5.65	0.82	1.76E-01
5.70	0.74	1.92E-01
5.75	0.95	2.26E-01
5.80	0.83	1.42E-01
5.85	1.05	4.06E-01
5.90	1.02	2.69E-01
5.95	0.91	1.08E-01
6.00	0.71	1.98E-01

U-238		
Energy (MeV)	**SNR**	**Abs. Uncert.**
0.05	0.66	1.99E-01
0.10	1.10	1.38E-01
0.15	0.99	3.78E-02
0.20	0.95	4.45E-02
0.25	1.02	1.07E-01
0.30	1.04	5.23E-02
0.35	1.85	6.45E-01
0.40	1.04	7.51E-02
0.45	0.99	1.22E-01
0.50	0.94	1.19E-01
0.55	1.17	6.96E-02
0.60	1.20	1.10E-01
0.65	1.46	1.33E-01
0.70	1.24	1.26E-01
0.75	1.51	1.59E-01
0.80	1.37	1.50E-01
0.85	1.24	8.33E-02
0.90	1.22	1.24E-01
0.95	1.21	1.72E-01
1.00	1.25	1.60E-01
1.05	1.11	9.75E-02
1.10	1.68	2.44E-01
1.15	1.31	1.64E-01
1.20	1.26	1.59E-01
1.25	1.21	1.13E-01

1.30	1.48	2.20E-01
1.35	1.26	1.40E-01
1.40	1.77	2.60E-01
1.45	1.31	1.63E-01
1.50	1.81	3.38E-01
1.55	1.81	2.79E-01
1.60	1.29	2.12E-01
1.65	1.26	1.53E-01
1.70	1.17	1.83E-01
1.75	1.04	1.39E-01
1.80	1.18	1.10E-01
1.85	1.28	1.34E-01
1.90	0.87	1.19E-01
1.95	1.26	1.65E-01
2.00	1.61	2.72E-01
2.05	1.00	1.17E-01
2.10	1.29	1.42E-01
2.15	1.13	1.35E-01
2.20	1.17	2.17E-01
2.25	1.21	3.98E-02
2.30	0.97	1.26E-01
2.35	1.19	2.91E-01
2.40	1.49	2.69E-01
2.45	1.20	1.75E-01
2.50	0.96	2.17E-01
2.55	1.15	1.45E-01
2.60	1.32	2.40E-01
2.65	1.07	1.86E-01
2.70	1.40	3.06E-01
2.75	1.38	2.16E-01
2.80	1.07	1.21E-01
2.85	1.20	1.82E-01
2.90	1.53	3.35E-01
2.95	0.80	1.52E-01
3.00	1.10	2.12E-01
3.05	0.93	1.44E-01
3.10	1.00	1.95E-01
3.15	1.27	2.87E-01
3.20	1.16	2.27E-01
3.25	1.13	1.84E-01

3.30	1.10	1.94E-01
3.35	1.23	2.23E-01
3.40	1.24	2.33E-01
3.45	1.47	2.11E-01
3.50	1.40	2.57E-01
3.55	1.18	5.51E-02
3.60	1.07	2.05E-01
3.65	1.26	2.39E-01
3.70	0.97	9.71E-02
3.75	0.92	2.16E-01
3.80	0.91	1.93E-01
3.85	1.07	2.15E-01
3.90	0.79	1.79E-01
3.95	0.92	1.94E-01
4.00	1.26	2.23E-01
4.05	0.85	1.81E-01
4.10	1.24	2.63E-01
4.15	1.26	1.91E-01
4.20	0.76	1.53E-01
4.25	0.98	1.70E-01
4.30	0.82	1.97E-01
4.35	1.06	2.97E-01
4.40	1.27	3.46E-01
4.45	0.93	1.13E-01
4.50	0.79	1.81E-01
4.55	1.24	3.19E-01
4.60	0.68	1.64E-01
4.65	1.18	3.04E-01
4.70	1.03	1.96E-01
4.75	0.86	1.83E-01
4.80	1.46	3.90E-01
4.85	1.05	2.26E-01
4.90	0.95	1.93E-01
4.95	1.15	4.42E-02
5.00	1.06	2.43E-01
5.05	0.93	2.04E-01
5.10	1.16	2.73E-01
5.15	1.36	3.53E-01
5.20	0.91	1.82E-01
5.25	0.93	2.75E-01

5.30	1.29	2.44E-01
5.35	0.77	1.83E-01
5.40	0.82	1.67E-01
5.45	0.92	1.54E-01
5.50	0.93	2.66E-01
5.55	1.04	1.49E-01
5.60	0.63	2.74E-01
5.65	1.15	1.98E-01
5.70	0.74	1.52E-01
5.75	0.87	2.16E-01
5.80	1.03	1.71E-01
5.85	0.51	2.70E-01
5.90	1.01	1.93E-01
5.95	1.15	1.10E-01
6.00	0.89	1.99E-01

Bibliography

1. Caffrey, A.J., J.D. Cole, R.J. Gehrke, and R.C. Greenwood. "Chemical Warfare Agent and High Explosive Identification by Spectroscopy of Neutron-Induced Gamma Rays". IEEE Transactions On Nuclear Science, Vol. 39, No. 5, October 1992.

2. Chang, J. H. ENDFPLOT-2.0. Korea Atomic Energy Research Institute, http://atom.kaeri.re.kr/cgi-bin/endfplot.pl, 2000.

3. Gozani, Tsahi. "Conventional and Non-Conventional Nuclear Material Signatures". American Institute of Physics 978-0-7354-0633-9, 2009.

4. Gozani, Tsahi, Peter Sawa, and Patrick M. Shea. "Apparatus and Method for Detecting Contraband Using Fast Neutron Activation". United States Patent US005098640A.

5. Knoll, Glenn F. *Radiation Detection and Measurement.* 4th Ed. John Wiley & Sons, Inc., 2010.

6. Krane, Kenneth S. *Introductory Nuclear Physics*. John Wiley & Sons, Inc., 1988.

7. National Nuclear Data Center. n. pag. http://www.nndc.bnl.gov/nudat2/indx_adopted.jsp.

8. Northrop Grumman. "Active Interrogation Experiments: The Examination of 6 High Explosive Compounds Using 14.1 MeV Neutrons. Safety and Environmental Plan." March 2004.

9. Shultis, J. Kenneth and Richard E. Shaw. "Radiation Shielding". American Nuclear Society, 2000.

10. Spitz, Henry, Bingjing Su, Samuel Glover, James Petrosky, and David Smith. "Design of a Novel, Multi-Element Scintillation Detector Exhibiting Improved Energy and Spatial Resolution for Measuring Low Photon Energy Emitting Radioactive Materials", 1 October 2008.

11. Wikipedia: The Free Encyclopedia. n. pag. http://en.wikipedia.org/wiki/Crust_(geology).

12. Wrixon, Anthony D. "New ICRP Recommendations". Journal of Radiological,Protection, 2008.

13. X-5 Monte Carlo Team, “MCNP — A General Monte Carlo N-Particle Transport Code, Version 5, Volume I: Overview and Theory”. LA-UR-03-1987, 2005.

REPORT DOCUMENTATION PAGE

Form Approved
OMB No. 074-0188

1. REPORT DATE *(DD-MM-YYYY)*	2. REPORT TYPE	3. DATES COVERED *(From – To)*
24-03-2011	Master's Thesis	June 2010 – March 2011

TITLE AND SUBTITLE

Background and Source Term Identification In Active Neutron Interrogation Methods

5a. CONTRACT NUMBER

5b. GRANT NUMBER

5c. PROGRAM ELEMENT NUMBER

6. AUTHOR(S)

Anthony, David A., Major, USA

5d. PROJECT NUMBER

5e. TASK NUMBER

5f. WORK UNIT NUMBER

7. PERFORMING ORGANIZATION NAMES(S) AND ADDRESS(S)
Air Force Institute of Technology
Graduate School of Engineering and Management (AFIT/ENP)
2950 Hobson Way, Building 640
WPAFB OH 45433-8865

8. PERFORMING ORGANIZATION REPORT NUMBER

AFIT/GNE/ENP/11-M01

9. SPONSORING/MONITORING AGENCY NAME(S) AND ADDRESS(ES)
Intentionally Left Blank

10. SPONSOR/MONITOR'S ACRONYM(S)

11. SPONSOR/MONITOR'S REPORT NUMBER(S)

12. DISTRIBUTION/AVAILABILITY STATEMENT
APPROVED FOR PUBLIC RELEASE; DISTRIBUTION UNLIMITED.

13. SUPPLEMENTARY NOTES

14. ABSTRACT

The detection and tracking of special nuclear material (SNM) is vitally important in order to know where these materials are and prevent them from being used in a harmful manner. Active neutron interrogation is a sought after method for this since the resulting high energy gamma rays produced by inelastic scattering and neutron capture reactions can pass through denser shielding than natural decay gammas, and their energy spectra are unique to each isotope. Using Monte Carlo N Particle (MCNP) simulations, this research investigated the characterization of gamma ray sources created by active neutron interrogation. Ring detector and mesh tallies within MCNP provide the energy and spatial distributions of gamma rays and neutrons associated with the induced background produced by a 14 MeV D-T neutron generator operated for 10 seconds at the Defense Threat Reduction Agency (DTRA) Technical Evaluation Assessment Monitor Site (TEAMS) at Kirtland AFB, NM. Iron (Fe-56), lead (Pb-207), polyethylene (C_2H_4 —> C-12 & H-1), and uranium (U-235 and U-238) were simulated as the target isotopes. Analysis of their corresponding neutron and gamma ray energy spectra provide the target source term. The resulting signal-to-noise ratios for each target demonstrated that while 6,859 cm^3 of Fe-56, H-1, and C-12 were distinguishable from the neutron induced background radiation, the same size of Pb-207 and U-238 and 1.5 kg of U-235 were not. Therefore, a reduction in the induced background radiation is necessary to accurately identify materials at these sizes or smaller, based upon the simulation.

15. SUBJECT TERMS
Active Neutron Interrogation, Gamma Ray, Monte Carlo N Particle

16. SECURITY CLASSIFICATION OF:			17. LIMITATION OF ABSTRACT	18. NUMBER OF PAGES	19a. NAME OF RESPONSIBLE PERSON
a. REPORT	b. ABSTRACT	c. THIS PAGE			Benjamin Kowash, Maj, USAF ADVISOR
U	U	U	UU	119	19b. TELEPHONE NUMBER *(Include area code)* (937) 255-3636, ext 4571 (Benjamin.kowash@afit.edu)

Standard Form 298 (Rev. 8-98)
Prescribed by ANSI Std. Z39-18